FACULTY
OF APPLIED SCIENCES
UNIVERSITY
OF WEST BOHEMIA

www.KMA.zcu.cz
SINCE 1954

BLENDING BY RATIONAL CANAL AND RINGED SURFACES

Michal Bizzarri

Dissertation thesis
Supervisor: *Doc. RNDr. Miroslav Lávička, Ph.D.*
Plzeň, 2014

FAKULTA
APLIKOVANÝCH VĚD
ZÁPADOČESKÉ
UNIVERZITY
V PLZNI

www.KMA.zcu.cz
SINCE 1954

KONSTRUKCE RACIONÁLNÍCH PŘECHODOVÝCH KANÁLOVÝCH A PRSTENCOVÝCH PLOCH

Michal Bizzarri

Dizertační práce

Školitel: *Doc. RNDr. Miroslav Lávička, Ph.D.*
Plzeň, 2014

Annotation

In this thesis we study rational techniques for computing exact/approximate parameterizations of canal and ringed surfaces. In the first part of the thesis we focus on canal surfaces given implicitly – the designed approach is based on computing approximate topology-based parameterizations of the so called contour curves on the given canal surface. The method can be directly applied on the practical problem of parameterizing implicit blends consisting of parts of canal (or canal-surface-like) surfaces. In the second part of the thesis we study a condition guaranteeing the rationality of the contour curves on canal surfaces given by medial axis transforms. These curves are then used for a computation of rational parameterizations of canal surfaces with Pythagorean normals. Using the contour curves the parameterization algorithm enables us to construct the whole family of rational canal (blending) surfaces sharing the same silhouette at once, which is especially useful for constructing blends satisfying certain constrains, e.g. when avoiding obstacles or bypassing other objects is required. The last part of the thesis is devoted to rational ringed surfaces – we design the algorithm for blending by these surfaces between two ringed surfaces which can be adjusted for constructing blends avoiding obstacles or for constructing general n-way blends between several ringed surfaces.

Keywords

Canal surfaces, ringed surfaces, rational parameterizations, blends, contour curves, critical points, rational offsets, SOS decomposition, PH and MPH curves, PN surfaces, Ferguson's cubic.

Anotace

V této práci studujeme racionální techniky vhodné pro výpočet přesných/přibližných parametrizací kanálových a prstencových ploch. V první části práce se soustředíme na implicitně zadané kanálové plochy – navržený přístup je založen na výpočtu přibližné parametrizace tak zvaných obrysových křivek na zadané kanálové ploše. Tato metoda může být přímo aplikována na praktické problémy parametrizace implicitních přechodových ploch sestávajících z částí kanálových (nebo přibližně kanálových) ploch. V druhé části práce studujeme podmínku zajišťující racionalitu obrysových křivek na kanálových plochách zadaných pomocí střední osy a poloměrové funkce. Tyto křivky jsou poté použity k výpočtu racionální parametrizace kanálových ploch s pythagorejskými normálami. Použití obrysových křivek v algoritmu parametrizace dovoluje v jednom kroku zkonstruovat celou třídu racionálních kanálových (přechodových) ploch, což je speciálně výhodné pro konstruování přechodových ploch splňujících jistá omezení, např. pokud je požadováno, aby se daná plocha vyhnula prekážkám. Poslední část této práce je věnována racionálním prstencovým plochám, pomocí nichž je navržena metoda konstrukce prechodových ploch mezi dvěmi prstensovými plochami. Tato metoda může být použita pro konstrukci přechodových ploch, které se mají vyhnout jistým překážkám nebo pro konstrukci přechodových ploch mezi několika prstencovými plochami.

Klíčová slova

Kanálové plochy, prstencové plochy, racionalní parametrizace, přechodové plochy, obrysové křivky, kritické body, racionální ofsety, SOS dekompozice, PH a MPH křivky, PN plochy, Fergusonova kubika.

Preface

This Ph.D. thesis contains the crucial results of research undertaken at the Department of Mathematics of the University of West Bohemia in Plzeň during my Ph.D. study – we have studied and designed various rational parameterization techniques mostly connected with canal and ringed surfaces. The thesis is based on the selected papers which have been published in (or submitted to) distinguished peer-reviewed archived journals – for a greater clarity, the papers in which the author of the thesis participated are marked by [*] whenever they are cited.

[8*] Bizzarri, M., and Lávička, M. A symbolic-numerical method for computing approximate parameterizations of canal surfaces. *Computer-Aided Design 44*, 9 (2012), 846 – 857.

[9*] Bizzarri, M., and Lávička, M. Parameterizing rational offset canal surfaces via rational contour curves. *Computer-Aided Design 45*, 2 (2013), 342 – 350.

[10*] Bizzarri, M., and Lávička, M. A symbolic-numerical approach to approximate parameterizations of space curves using graphs of critical points. *Journal of Computational and Applied Mathematics 242*, (2013), 107 – 124.

[11*] Bizzarri, M., and Lávička, M. Approximation of implicit blends by canal surfaces of low parameterization degree. In *Mathematical Methods for Curves and Surfaces*, vol. 8177 of *Lecture Notes in Computer Science.* Springer Berlin Heidelberg, 2014, 34 – 48.

[12*] Bizzarri, M., and Lávička, M. On modelling with rational ringed surfaces. Submitted to *Computer-Aided Design*, (2014).

[13*] Bizzarri, M., Lávička, M., and Vršek, J. Canal surfaces with rational contour curves and blends bypassing the obstacles. Submitted to *Computer-Aided Design*, (2014).

The results from the aforementioned papers have been suitably ordered and slightly reformulated to increase the compactness and the readability of the entire thesis. The

paper [10*] deals with the problem of computing approximate topology-based parameterizations of real spatial algebraic curves using their graphs of critical points. The algorithm from [10*] is then used in the papers [8*] and [11*] where the methods for computing approximate parameterizations of implicitly defined canal surfaces are designed. The next two papers [9*] and [13*] are devoted to the canal surfaces with rational contour curves. These curves are then used for the computation of rational parameterizations of adaptive blending surfaces (avoiding obstacles, bypassing other objects, etc.) providing rational offsets. Finally, the modelling with rational ringed surfaces is thoroughly studied in [12*].

All the presented papers are the common work of me and my supervisor doc. RNDr. Miroslav Lávička, Ph.D. I would like to express my sincere thanks to Miroslav for his friendly and professional guidance and for his constant support.

My special thanks belong to my brother RNDr. Jan Vršek, Ph.D. who cooperated with me on several problems and, among others, significantly contributed to paper [13*].

I also want to express my deep gratitude to my family, my girlfriend Klára and my close friends for their encouragement, inspiration and permanent support during the study and during writing of this thesis.

I hereby declare that this doctoral thesis is my own work based on the selected crucial results which were obtained during my research and my Ph.D. study in the years 2010–2014 at the Department of Mathematics.

Plzeň, March 17, 2014, ...

Contents

Chapter 1

Introduction

Exploring the history of geometric modelling in industrial and related applications such as Computer Aided Design and Manufacturing (CAD and CAM), Geometric Modelling, Computational Geometry, Robotics, Image Processing, Computer Graphics, etc., we can see that rational techniques and rational representations were at the very foundation. When computers allowed machining of 3D shapes, a necessity to define a computer-compatible description of those objects appeared. The most promising representation was soon identified to be the parametric one since parametric descriptions enable to generate points on curves and surfaces and they are also suitable e.g. for surface plotting, computing transformations, determining offsets, computing curvatures or shading and colouring, for curve-curve and surface-surface intersection problems, cf. e.g. [29, 31]. Of course the most important parameterizations (among all) are those that can be described with the help of polynomials or rational functions since these descriptions can be easily included into standard CAD systems (e.g. milling cutters, cutting machines, etc.). Hence a major breakthrough in geometric modeling was brought about the theory of polynomial Bézier and B-spline curves and surfaces, combined later with their rational counterparts, see [29, 31].

Unfortunately, not every geometric object (curve, surfaces, volume) can be described using rational parameterizations – see [84] for more details. We recall that for algebraic curves and surfaces, various symbolic computation based techniques can be found – see e.g. [78, 82, 89, 91, 92] for an exact parameterization of curves, and [1, 68, 79–81, 87] for surfaces. However, these techniques are often algorithmically very difficult. And, as mentioned above, they cannot deal with all algebraic curves and surfaces, since an exact rational parameterization does not exist in the generic case. Approximate techniques, which generate a parameterization within a certain region of interest, are then necessary to avoid these problems.

This thesis is devoted to one of the most important classes of technical surfaces, namely to canal and ringed surfaces. Ringed surfaces are generated by sweeping a circle with variable radius – which is contained in a plane with a possibly non-constant normal vector – along a directrix curve, see [45]. By using circles in the normal plane of the directrix one obtains *normal ringed surfaces*. Special cases include *Darboux cyclides*

(see [23,26]) which can carry up to six families of real circles, see also [5,15,54,72,88]. Ringed surfaces are well suited e.g. for designing pipe structures in plant modeling, cf. [14,16]. A special method for computing the intersection of two ringed surfaces is described in [41].

The class of ringed surfaces contains a special subclass of canal surfaces that are obtained as the envelopes of a one-parameter family of spheres, see e.g. [28]. Special cases include *pipe surfaces* (obtained for spheres of constant radius) and *surfaces of revolution* (generated by spheres whose centers are located on a given line). Canal surfaces are (generally non-normal) ringed surfaces. *Dupin cyclides* – which can be defined as the envelopes of all spheres touching three given spheres – form probably the most studied family of canal surfaces [52,71,85].

It was proved in [59, 68] that any canal surface with a rational spine curve (which is the curve formed by the centers of the moving spheres) and a rational radius function admits a rational parameterization. An algorithm for generating rational parameterizations of canal surfaces was presented in [57]. Analogous result was proven also for normal ringed surfaces – in particular a normal ringed surface with rational directrix and a rational radius function is rational, see [59]. In this thesis we will extend this result for an arbitrary ringed surface with rational directrix, rational normal vector field and radius function equal to the square root of some non-negative rational function.

The canal surfaces have been studied more thoroughly than the ringed surfaces and one can find many applications in CAD based on canal surfaces. Let us recall, for instance, the operation of blending which is one of the most important operations in Computer-Aided (Geometric) Design. The main purpose of this operation is to generate one or more surfaces that create a smooth joint between the given shapes. Blending surfaces are necessary for rounding edges and corners of mechanical parts, or for smooth connection of separated objects, see e.g. [30,44] and references therein. Canal surfaces are often used as blending surfaces between two given surfaces [4]. However not for all input shapes (ending with circular profiles), the canal surfaces are suitable as blending primitives. We recall e.g. the case when oblique cones shall be blended – then the ringed surfaces find their straightforward application.

This thesis, where the new methods for computing exact and approximate parameterizations of canal and ringed surfaces are presented, is divided into three main parts. The first part is devoted to the case when canal surfaces are not given by their spine curves and radius functions but implicitly e.g. as a result of some blending technique. In particular we show, how approximate parameterizations of implicitly given canal surfaces can be computed. Important contributions for blending by implicitly given surfaces can be found in [42,43,73]. Several methods for constructing implicit blends were thoroughly investigated in [38–40, 94]. In addition, as our approach yields 'only' approximate parameterizations, it can also be used for blends not being canal surfaces exactly but only approximately. For overview of several blending techniques (including implicit ones) see [4].

In the second part of this thesis we turn our attention to canal surfaces defined by their spine curves and radius functions. In particular we study a condition guaranteeing

that a given canal surface has rational contour curves. These curves are then used for a computation of rational parameterization providing rational offsets, i.e., it is PN parameterization, for more details about PN surfaces see [32,58,66,67,70,76]. These parameterizations find their application especially when the canal surfaces (e.g. blends consisting of parts of canal surfaces) shall be machined by milling cutter. To document a practical usefulness of the presented approach, we design simple direct algorithms for computing rational offset blends between two canal surfaces based on the contour method. Using the contour curves the parameterization algorithm requires only one MPH approximation/SOS decomposition for the whole family of rational canal (blending) surfaces sharing the same silhouette, which is especially useful for constructing blends satisfying certain constrains, e.g. when avoiding obstacles or bypassing other objects is required.

In the last part of the thesis we deal with the question of the rationality of ringed surfaces – in particular we show which ringed surface are rational and how their rational parameterizations can be computed. Then we design a blending method based on interpolation by Pythagorean curves in plane and show how this method can be modified to satisfy some constraints, e.g. to avoid obstacles or bypass other objects. Another modification of the method enables to construct n-way blending surfaces between n ringed surfaces. We also design a method for approximating the implicitly given blends by rational ring surfaces based on approximation of contour curves.

The remainder of this thesis is organized as follows. Chapter 2 summarizes some basic definitions and notions necessary for right understanding of the thesis. Chapter 3 is devoted to the method of approximating implicitly given blends by canal surfaces. In Chapter 4 we study canal surfaces with rational contour curves which are then used for constructing blends satisfying certain constrains. Chapter 5 deals with the blending by rational ringed surfaces and in Chapter 6 we conclude the thesis.

Chapter 2

Preliminaries

This chapter serves as a survey of basic definitions and notions about particular topics from algebraic geometry and geometric modelling which will be used in this thesis. It is divided into six sections – the first one is devoted to the introduction to the theory of algebraic curves. The second section summarizes some fundamental facts about Pythagorean hodograph curves and surfaces with Pythagorean normal vector fields. In the third and fourth section we recall some basic notions concerning canal and ringed surfaces, respectively. In the fifth section one can find several algorithms concerning approximate parameterizations of algebraic curves and the last one recalls some basic facts about the problem of decomposing polynomials into sum of squares.

2.1 Algebraic curves and surfaces

We start with short recalling necessary fundamental properties of algebraic curves and surfaces, as special cases of algebraic varieties, which are then used in the following text. More details can be found e.g. in [17, 37, 82, 84, 91, 92]. Throughout this thesis, let $\mathbb{R}$ and $\mathbb{C}$ be the fields of real and complex numbers, respectively.

An *affine algebraic variety* $\mathcal{V}$ in $\mathbb{C}^n$ is defined as the set of all points satisfying the system of polynomial equations $f_1(x_1,\dots,x_n) = \dots = f_k(x_1,\dots,x_n) = 0$, i.e.,

$$\mathcal{V} = \left\{(a_1,\dots,a_n)^\top \in \mathbb{C}^n \mid f_i(a_1,\dots,a_n) = 0 \text{ for all } i = 1,\dots,k\right\}. \tag{2.1}$$

The polynomials $f_1,\dots,f_k \in \mathbb{C}[x_1,\dots,x_n]$ are called *defining polynomials* of the variety $\mathcal{V}$. The *dimension* of $\mathcal{V}$ is the transcendence degree over $\mathbb{C}$ of the function field $\mathbb{C}(\mathcal{V})$ of all rational functions on $\mathcal{V}$, with values in $\mathbb{C}$, see [84].

Remark 2.1. Motivated by consequent applications, for the purpose of this thesis we focus only on varieties (curves/surfaces) given as the complete intersection of hyper-

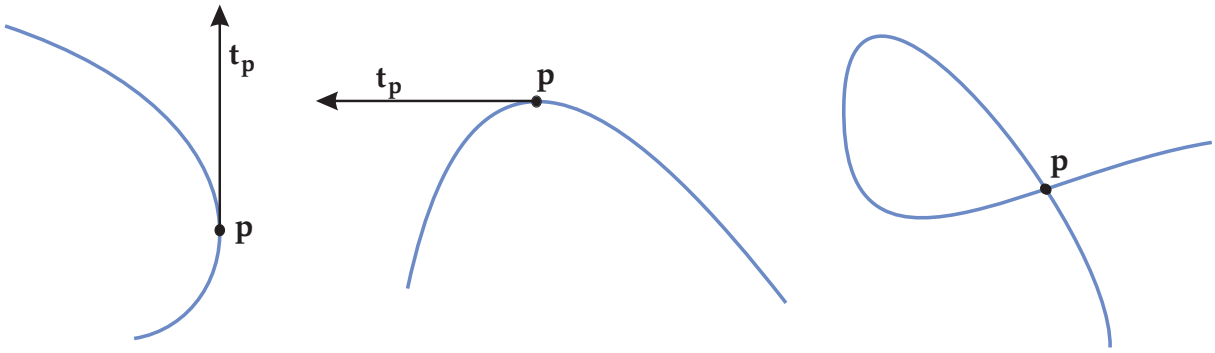

Figure 2.1: An x-critical point (left), a y-critical point (middle) and a singular point (right).

surfaces. We recall that a variety $\mathcal{V}$ is considered as the so-called *complete intersection* of k hypersurfaces if the ideal of $\mathcal{V}$ is generated by exactly $n-k$ elements, see e.g. [24, 37, 86] for more details. Moreover, the ideal theory is also very suitable when defining the degree and irreducibility of algebraic varieties – essentially, the degree of $\mathcal{V}$ is $d_1 \cdots d_k$, where $d_1, \ldots, d_k$ are the algebraic degrees of $f_1, \ldots, f_k$, respectively and $\mathcal{V}$ is *irreducible* if and only if the ideal of $\mathcal{V}$ is a prime ideal.

In what follows we will focus only on algebraic planar and spatial curves, i.e., the algebraic varieties of dimension 1 in $\mathbb{C}^2$ and $\mathbb{C}^3$, respectively and on algebraic surfaces, i.e., the algebraic varieties of dimension 2 in $\mathbb{C}^3$. An *affine planar algebraic curve* $\mathcal{D}$ is the set of zeros of a polynomial in two variables, i.e.,

$$\mathcal{D} = \{(a_1, a_2)^\top \in \mathbb{C}^2 \mid f(a_1, a_2) = 0\}. \tag{2.2}$$

An *affine spatial algebraic curve* $\mathcal{C}$ is defined as the set all solutions of a system of two polynomial equations, i.e.,

$$\mathcal{C} = \{(a_1, a_2, a_3)^\top \in \mathbb{C}^3 \mid f(a_1, a_2, a_3) = g(a_1, a_2, a_3) = 0\}. \tag{2.3}$$

Finally, an *affine algebraic surface* $\mathcal{S}$ is the set of zeros of a polynomial in three variables, i.e.,

$$\mathcal{S} = \{(a_1, a_2, a_3)^\top \in \mathbb{C}^3 \mid f(a_1, a_2, a_3) = 0\}. \tag{2.4}$$

For the purpose of computing approximate parameterizations of algebraic curves, which is a necessary part of the algorithms presented in Chapter 3, we introduce a special points on curves which reflect the change of the shape w.r.t. a given direction.

Definition 2.2. A point $\mathbf{p}$ on algebraic curve $\mathcal{C}$ at which $\mathcal{C}$ possesses the tangent vector $\mathbf{t_p}$ is called a *critical point* w.r.t. the vector (direction) $\mathbf{v}$ if

$$\mathbf{t_p} \cdot \mathbf{v} = 0, \tag{2.5}$$

where '$\cdot$' denotes the standard Euclidean inner product. Points which are critical w.r.t. all directions are called *singular points*.

The critical points on planar curves w.r.t. the directions of the coordinate axes are shown in Figure 2.1.

Remark 2.3. By the definition of the critical points on curves all lines and planar curves in the space would consist of critical points only. However, the critical points were introduced in order to indicate a change of the curve shape with respect to a given direction. Hence, when the whole curve (or its whole component) consists solely of such points these points will not be considered as critical in what follows.

Let $\mathcal{V}$ be a variety of dimension d over a field $\mathbb{C}$. Then $\mathcal{V}$ is said to be *unirational*, or *parametric*, if there exists a rational map $\mathcal{P} : \mathbb{C}^d \to \mathcal{V}$ such that $\mathcal{P}(\mathbb{C}^d)$ is dense in $\mathcal{V}$. We speak about a (*rational*) *parameterization* $\mathcal{P}(t_1,\dots,t_d)$ of $\mathcal{V}$. Furthermore, if $\mathcal{P}$ defines a birational map then $\mathcal{V}$ is called *rational*, and we say that $\mathcal{P}(t_1,\dots,t_d)$ is a *proper parameterization*. By a Riemann's theorem, an irreducible planar curve has a parametrization iff it has a proper parametrization iff its genus is zero, i.e., iff the following relation holds

$$\frac{1}{2}(d-1)(d-2) = \sum_{i=1}^{n} \delta_{\mathbf{p}_i}, \tag{2.6}$$

where d is the degree of $\mathcal{C}$ and $\mathbf{p}_1,\dots,\mathbf{p}_n$ are the singular points of the so called *associated projective curve* $\mathcal{C}^*$ (the curve in the projective space defined by the homogenization $F(x,y,z)$ of the defining polynomial $f(x,y)$ of $\mathcal{C}$) possessing the delta invariants $\delta_{\mathbf{p}_1},\dots,\delta_{\mathbf{p}_n}$, respectively – for more details see [84, 91]. Hence, for planar curves the notions of rationality and unirationality are equivalent for any field.

For every irreducible spatial curve $\mathcal{C}$ there always exists a birational transformation between the points of $\mathcal{C}$ and the points of a certain irreducible planar curve $\mathcal{D}$, see for instance [91]. Hence, the rationality problem of the spatial curve $\mathcal{C}$ is equivalent to the rationality problem of the corresponding planar curve $\mathcal{D}$ – i.e., $\mathcal{C}$ can be rationally parameterized if and only if its birationally projected image $\mathcal{D}$ fulfils the condition (2.6).

In the surface case, the theory differs as Castelnuovo's theorem holds only for algebraically closed fields of characteristic zero. By this theorem, a surface has a parametrization iff it has a proper parametrization iff the arithmetical genus p_a and the second plurigenus P_2 are both zero (see [84] for definitions of these notions).

2.2 Curves with Pythagorean hodographs and surfaces with Pythagorean normals

In this section the fundamental properties of Pythagorean hodograph curves in Euclidean and Minkowski plane/space and surfaces with Pythagorean normal vector fields will be recalled.

Given a regular C^1 parametric curve $\mathbf{x}(t) = (x_1(t), x_2(t))^\top$, the *offset* of $\mathbf{x}(t)$ is the set of all points in $\mathbb{R}^2$ that lie at a perpendicular distance δ from $\mathbf{x}(t)$. For the sake of brevity

we omit the dependence on parameter t whenever no confusion is likely to arise. The two branches of the offset (i.e., inner and outer one-sided offsets) are given by

$$\mathbf{x}_\delta^\pm(t) = \mathbf{x} \pm \delta\,\mathbf{n}, \qquad \mathbf{n} = \frac{\mathbf{x}'^\perp}{\|\mathbf{x}'\|}, \tag{2.7}$$

where $\|\mathbf{x}'\| = \sqrt{\left(x_1'\right)^2 + \left(x_2'\right)^2}$ and $\mathbf{x}'^\perp = (-x_2', x_1')^\top$.

A study of offset rationality led to the class of planar *Pythagorean hodograph* (PH) curves. These curves are defined as rational curves $\mathbf{x} = (x_1, x_2)^\top$ fulfilling the distinguishing condition

$$\mathbf{x}' \cdot \mathbf{x}' = (x_1')^2 + (x_2')^2 = \sigma^2, \tag{2.8}$$

where σ is a rational function. Since the rationality of a δ-offset curve $\mathbf{x}_\delta^\pm$ of a rational curve only depends on the rationality of the unit normal field $\mathbf{n}$, cf. (2.7), planar PH curves possess (piece-wise) rational offsets.

Pythagorean hodograph curves were originally introduced in [33] as *planar polynomial* curves. It was proved [33, 55] that the coordinates of hodographs of polynomial PH curves and σ form the following Pythagorean triples

$$\begin{aligned} x_1' &= m\left(k^2 - l^2\right), \\ x_2' &= 2mkl, \\ \sigma &= m\left(k^2 + l^2\right), \end{aligned} \tag{2.9}$$

where $k, l, m \in \mathbb{R}[t]$ are any non-zero polynomials and k, l are relatively prime.

A generalization of polynomial PH curves to rational ones was introduced and studied in [70]. This approach uses the dual representation of a planar curve considered as an envelope of its tangents

$$T(t) : \mathbf{n} \cdot \mathbf{x} - h = 0, \qquad h \in \mathbb{R}(t). \tag{2.10}$$

In order to guarantee the rationality of (2.7), the unit normal field $\mathbf{n}$ must rationally parameterize the unit circle $\mathcal{S}^1$. Hence, there must exist relatively prime polynomials k, l such that

$$\mathbf{n}(t) = \left(\frac{2kl}{k^2 + l^2}, \frac{k^2 - l^2}{k^2 + l^2}\right)^\top. \tag{2.11}$$

In addition, to simplify further computations we set $g = h(k^2 + l^2)$, i.e., the dual representation of any arbitrary PH curve is

$$\left(2kl, k^2 - l^2\right)^\top \cdot \mathbf{x} - g = 0. \tag{2.12}$$

Consequently, a parametric representation of all planar rational PH curves is obtained as the envelope of their tangents given by (2.12) in the form

$$\mathbf{x}(t) = \left(= \frac{2(ll' - kk')g + (k^2 - l^2)g'}{2(k^2 + l^2)(kl' - k'l)}, \frac{(k'l + kl')g - klg'}{(k^2 + l^2)(kl' - k'l)}\right)^\top. \tag{2.13}$$

Furthermore, the representation of offsets can be easily obtained by translating the tangents by a distance δ, i.e., it is sufficient to replace $g = h(k^2+l^2)$ by $g = (h\pm\delta)(k^2+l^2)$ in (2.13).

Analogously for the surface case, consider a regular C^1 surface $\mathbf{x} : \mathbb{R}^2 \to \mathbb{R}^3$ given by a rational parameterization $\mathbf{x}$. The *δ-offset* of $\mathbf{x}$ is the set of all points in $\mathbb{R}^3$ that lie at a distance δ from $\mathbf{x}$. The two branches of the offset are given by

$$\mathbf{x}_\delta^\pm(u,v) = \mathbf{x} \pm \delta\,\mathbf{n}, \qquad \mathbf{n} = \frac{\mathbf{x}_u \times \mathbf{x}_v}{\|\mathbf{x}_u \times \mathbf{x}_v\|}, \tag{2.14}$$

where $\mathbf{x}_u$ and $\mathbf{x}_v$ are the partial derivatives with respect to u and v, respectively.

A study of offset rationality for surfaces led to the class of *surfaces with Pythagorean normal vector fields*, introduced in [70], distinguished by the condition (the so called *PN property*)

$$\|\mathbf{x}_u \times \mathbf{x}_v\|^2 = \sigma^2, \tag{2.15}$$

where σ is a rational function. In addition, it can be proved that $\sigma^2 = EG - F^2$, where E, F, G are the coefficients of the first fundamental form, and thus the PN condition (2.15) shows that the PN surfaces in $\mathbb{R}^3$ are simultaneously the surfaces with *Pythagorean area elements*.

In what follows, we will consider only non-developable PN surfaces. Such surfaces $\mathbf{x}$ can be obtained as the envelope of a two-parametric set of the associated tangent planes

$$T(u,v): \quad \mathbf{n}\cdot\mathbf{x} - h = 0, \tag{2.16}$$

where $h(u,v)$ is a rational function and $\mathbf{n}$ is a rational parameterization of the unit sphere $\mathcal{S}^2$, cf. [70],

$$\mathbf{n}(u,v) = \left(\frac{2km}{k^2+l^2+m^2}, \frac{2lm}{k^2+l^2+m^2}, \frac{k^2+l^2-m^2}{k^2+l^2+m^2}\right)^\top, \tag{2.17}$$

with k, l, m fulfilling the condition $\gcd(k,l,m) = 1$. A parametric representation of an arbitrary non-developable PN surface can be then obtained from the system of equations $T = 0$, $T_u = 0$, $T_v = 0$ (where T_x denote the partial derivative of T w.r.t. x) using Cramer's rule – see formula (3.3) in [70]. Furthermore, the representation of offsets can be again easily obtained by translating the tangent planes by a distance δ, i.e., it is sufficient to replace h by $h \pm \delta$ in (2.16).

Consider a planar domain $\Omega \subset \mathbb{R}^2$ and the family of all inscribed discs in Ω partially ordered with respect to inclusion. An inscribed disc is called maximal if it is not contained in any other inscribed disc. Then the *medial axis* $\mathrm{MA}(\Omega)$ is the locus of all centers $(x_1, x_2)^\top$ of maximal inscribed discs and the *medial axis transform* $\mathrm{MAT}(\Omega)$ is obtained by appending the corresponding disc radii r to the medial axis, i.e., MAT consists of points $\overline{\mathbf{x}} = (x_1, x_2, r)^\top$.

For a C^1 segment $\overline{\mathbf{x}} = (x_1, x_2, r)^\top$ of $\mathrm{MAT}(\Omega)$ we can compute the corresponding boundary of Ω from the envelope formula, cf. [21, 62], in the form

$$\mathbf{x}_r^\pm(t) = \begin{pmatrix} x_1 \\ x_2 \end{pmatrix} - \frac{r}{x_1'^2 + x_2'^2}\left[r'\begin{pmatrix} x_1' \\ x_2' \end{pmatrix} \pm \sqrt{x_1'^2 + x_2'^2 - r'^2}\begin{pmatrix} -x_2' \\ x_1' \end{pmatrix}\right]. \tag{2.18}$$

A study of rationality of envelopes (2.18) led to the class of *Minkowski Pythagorean hodograph* (MPH) curves introduced in [62]. MPH curves are defined as rational curves $\overline{\mathbf{x}} = (x_1, x_2, r)^\top$ in three-dimensional space fulfilling the condition

$$x_1'^2 + x_2'^2 - r'^2 = \sigma^2, \tag{2.19}$$

where $\sigma \in \mathbb{R}(t)$. The PH condition (2.8) is now fulfilled with respect to the inner product

$$\langle \mathbf{u}, \mathbf{v} \rangle = u_1 v_1 + u_2 v_2 - u_3 v_3. \tag{2.20}$$

A three-dimensional real affine space along with the indefinite bilinear form (2.20) is called *Minkowski space* and denoted $\mathbb{R}^{2,1}$. We recall that the *squared norm* of a vector $\mathbf{u} \in \mathbb{R}^{2,1}$ with respect to the indefinite *Minkowski inner product* (2.20), can be positive, negative or zero. Hence, we distinguish three types of vectors: a vector $\mathbf{u}$ is called *space-like* if $\langle \mathbf{u}, \mathbf{u} \rangle > 0$, *time-like* if $\langle \mathbf{u}, \mathbf{u} \rangle < 0$, and *light-like* (or *isotropic*) if $\langle \mathbf{u}, \mathbf{u} \rangle = 0$. Considering their tangent vectors we analogously speak about space-, light-, or time-like curves.

Now, we recall the result from [49] that any rational MPH curve $\overline{\mathbf{x}}$ in $\mathbb{R}^{2,1}$ can be constructed starting from an (associated) planar rational PH curve $\mathbf{y}$ in $\mathbb{R}^2$ and a rational function r in the form

$$\overline{\mathbf{x}}(t) = (y_1 + r n_1, y_2 + r n_2, r)^\top, \tag{2.21}$$

where $\mathbf{n} = (n_1, n_2)^\top = \mathbf{y}'^{\perp}/\sigma$.

Using (2.21) and (2.13), we can show that a curve $\overline{\mathbf{x}} \in \mathbb{R}^{2,1}$ is an MPH curve if and only if there exist two polynomials k, l and two rational functions q, r such that

$$\overline{\mathbf{x}} = \frac{1}{2(k^2+l^2)(kl'-k'l)} \begin{pmatrix} 2(ll'-kk')g + (k^2-l^2)g' \\ 2(k'l+kl')g - 2klg' \\ 0 \end{pmatrix} + \frac{r}{k^2+l^2} \begin{pmatrix} 2kl \\ k^2-l^2 \\ k^2+l^2 \end{pmatrix}. \tag{2.22}$$

Obviously, *polynomial* MPH curves form a proper subset of the set of rational MPH curves described by (2.22). It turns out that we can efficiently adapt the approach for relating planar rational and polynomial PH curves used in [35] and show that any polynomial MPH curve in $\mathbb{R}^{2,1}$ can be obtained using (2.22) by setting

$$\begin{aligned} g(t) &= 2kl \int (km-ln)\,\mathrm{d}t - (k^2-l^2) \int (kn+lm)\,\mathrm{d}t - (k^2+l^2) \int (lm-kn)\,\mathrm{d}t, \\ r(t) &= \int (lm-kn)\,\mathrm{d}t, \end{aligned} \tag{2.23}$$

where k, l, m, n are arbitrary polynomials. Substituting (2.23) into (2.22) we obtain an alternative to the original formula for polynomial MPH curves presented in [62]

$$x_1' = km - ln, \quad x_2' = -kn - lm, \quad r' = -kn + lm, \quad \varrho = km + ln. \tag{2.24}$$

A prominent role is played by polynomial MPH curves given by a polynomial (associated) PH curve $\mathbf{y} \subset \mathbb{R}^2$ and a polynomial r. Recalling [50], these curves have the form

$$\mathbf{x}(t) = (y_1 + p y_2', y_2 - p y_1', p\sigma)^\top, \tag{2.25}$$

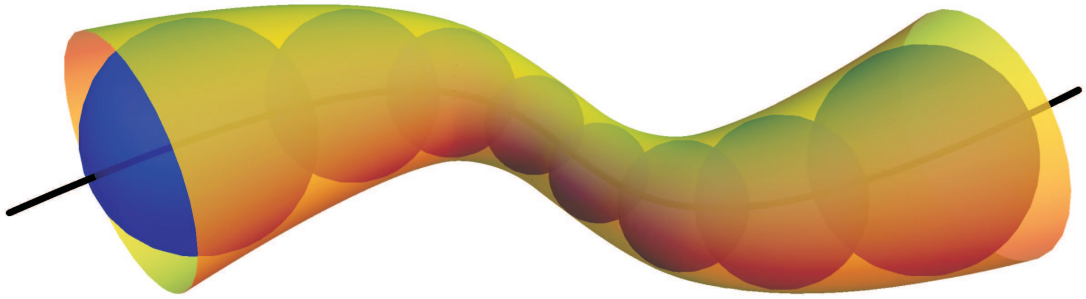

Figure 2.2: An envelope (yellow) of one-parameter family of spheres (blue) – a canal surface.

where y_1', y_2', σ are given by (2.9) and p is an arbitrary polynomial. In addition, let $\mathbf{y}$ be a polynomial PH curve of degree d_1, and d_2 is the degree of p then it holds

$$\deg(\overline{\mathbf{x}}) = d_1 + d_2 - 1. \tag{2.26}$$

2.3 Canal surfaces and contour curves

A *canal surface* $\mathcal{S}$ is the envelope of a 1-parameter family of spheres F whose centers trace a curve $\mathbf{m}$ in $\mathbb{R}^3$ and possess radii r (see Figure 2.2), i.e.,

$$F(t) : \|\mathbf{x} - \mathbf{m}(t)\|^2 - r(t)^2 = 0, \quad t \in I, \tag{2.27}$$

where $\mathbf{x} = (x, y, z)^\top$. The curve $\mathbf{m}$ is called the *spine curve* and r the *radius function* of $\mathcal{S}$. For constant r we obtain a *pipe surface*. The defining equations for the canal surface $\mathcal{S}$ are

$$F(t) = 0, \quad F'(t) = 0, \tag{2.28}$$

where F' is the derivative of F with respect to t. After eliminating the parameter t from (2.28) one can get the corresponding implicit equation $f(\mathbf{x}) = 0$ of $\mathcal{S}$. The linear equation $F' = 0$ describes the plane with the normal vector $\mathbf{m}'$, i.e., perpendicular to the spine curve $\mathbf{m}$. Thus the canal surface $\mathcal{S}$ contains a one parameter set of the so called *characteristic circles* $F \cap F'$, see Figure 2.3 (left), and hence canal surfaces belong to the so called *ringed surfaces*, see Chapter 5. It can be proved that the envelope (i.e. the canal surface) is real iff the condition

$$\|\mathbf{m}'(t)\|^2 - r'^2(t) \geq 0 \tag{2.29}$$

is fulfilled for all $t \in I$.

By appending the corresponding sphere radii r to the points of the spine curve we obtain the *medial axis transform* MAT, i.e., the curve $\overline{\mathbf{m}}$. For the sake of clarity, we identify the canal surface $\mathcal{S} \subset \mathbb{R}^3$ with its medial axis transform $\overline{\mathbf{m}} = (\mathbf{m}, r)^\top \subset \mathbb{R}^{3,1}$, see [62, 68], where $\mathbb{R}^{3,1}$ is the 4-dimensional *Minkowski space* serving as the natural ambient space for MATs of canal surfaces, cf. (2.27).

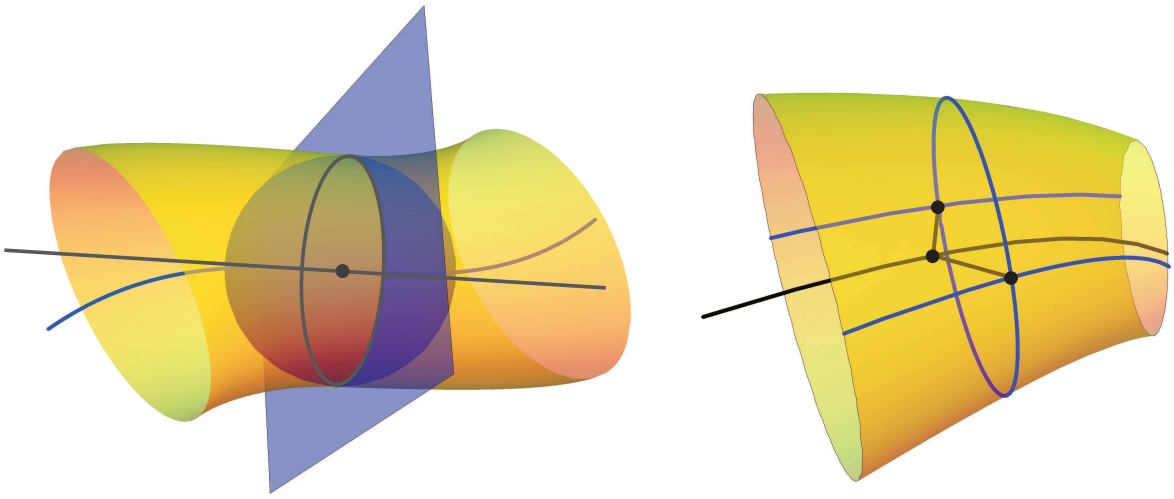

Figure 2.3: A characteristic circle (black) of a canal surface, left and associated foot points on contour curves, right.

As proved in [57, 68], any canal surface given by a rational MAT possesses a rational parameterization. A method which uses MPH representation and Lorentzian geometry to parameterize canal surfaces was presented in [19, 20]. Nevertheless, it must be emphasized that the computation of rational parameterizations of canal surfaces is still a challenging problem, which is equivalent to the SOS (sum of squares) problem for non-negative polynomials. And in addition, we have to be aware of another important issue. There exist rational canal surfaces with non-rational MATs, i.e., r is a square root of a rational function, see [64].

In this thesis we compute the rational parameterization of a given canal surface by rotating one curve $\mathbf{c}(t)$ on it (different from the characteristic circles) around the tangents of the spine curve $\mathbf{m}(t)$. Thus the parameterization of $\mathcal{S}$ will be in the form

$$\mathbf{s}(t,u) = \mathbf{m}(t) + \frac{(\varphi(u) + \mathbf{m}'(t)) \star (\mathbf{c}(t) - \mathbf{m}(t)) \star (\varphi(u) - \mathbf{m}'(t))}{(\varphi(u) + \mathbf{m}'(t)) \star (\varphi(u) - \mathbf{m}'(t))}, \tag{2.30}$$

where $\varphi(u)$ is a rational function, the sums $\varphi(u) \pm \mathbf{m}'(t)$ of scalars and vectors are considered as quaternions, and $\star$ is the operation of quaternion multiplication

$$(a + \mathbf{a}) \star (b + \mathbf{b}) = ab - \mathbf{a} \cdot \mathbf{b} + a\mathbf{b} + b\mathbf{a} + \mathbf{a} \times \mathbf{b}, \tag{2.31}$$

see [2, 36] for more details about quaternions. For any $t = t_0$ the rational function $\varphi(u)$ determines a rational parameterization of the associated characteristic circle. Any rational choice of $\varphi(u)$ yields the rational parameterization of a canal surface – for the sake simplicity we choose $\varphi(u) = u$ for the low rational degree of $\mathbf{s}(t,u)$ in u, and $\varphi(u) = 2u/(1-u^2)$ for a relatively uniform distribution of the t-parameter lines (clearly, the given generating curve $\mathbf{c}(t)$ is determined by zero rotation angle, i.e., by the choice $u = 1$).

Let us emphasize that when using the spine curve and another curve for computing the rational parameterization of $\mathcal{S}$, we have to guarantee that their parameterizations

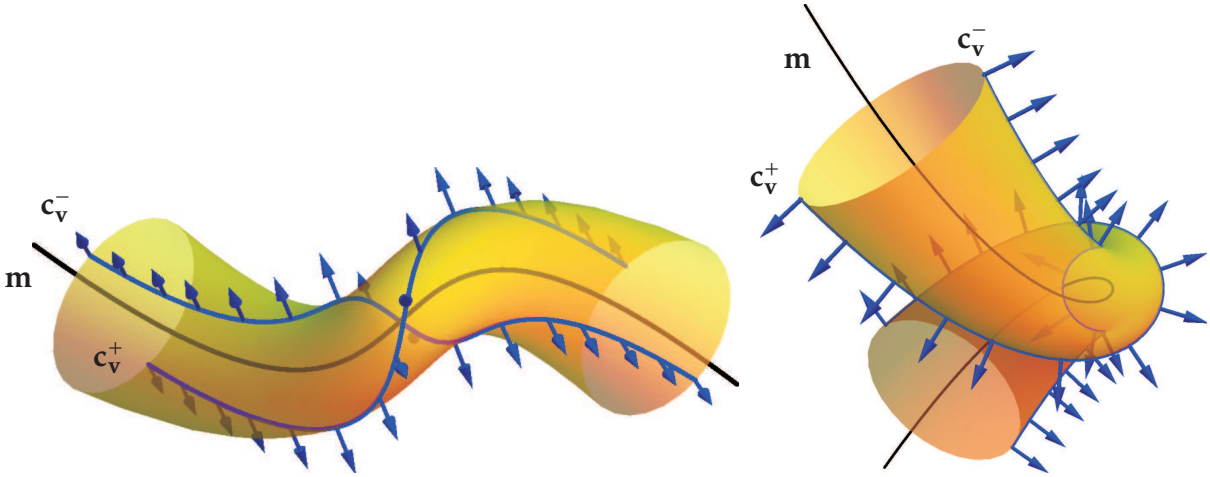

Figure 2.4: The two branches $\mathbf{c}_\mathbf{v}^\pm$ of a contour curve (blue) on a canal surface $\mathcal{S}$ (yellow) with the spine curve $\mathbf{m}$ (black).

are closely related. We say that the curve $\mathbf{c}$ *corresponds in parameter* with the given curve $\mathbf{m}$ in the interval I if it holds

$$\mathbf{c}'(t) \cdot (\mathbf{c}(t) - \mathbf{m}(t)) = 0, \quad \text{for all } t \in I. \tag{2.32}$$

Hence, considering the spine curve $\mathbf{m}$ and one curve $\mathbf{c}$ on a given canal surface $\mathcal{S}$ which are corresponding in parameter we have ensured that the point $\mathbf{c}(t_0)$ lies at the characteristic circle of $\mathcal{S}$ corresponding to the sphere centered at $\mathbf{m}(t_0)$ and with the radius $r(t_0)$, for all $t_0 \in I$.

By analogy we can define a correspondence in parameter for two arbitrary curves $\mathbf{c}_1$ and $\mathbf{c}_2$ (different from the characteristic circles) on a canal surface $\mathcal{S}$. We say that $\mathbf{c}_1$ and $\mathbf{c}_2$ *correspond in parameter* in the interval I if the points $\mathbf{c}_1(t_0)$ and $\mathbf{c}_2(t_0)$ lie on the same characteristic circle of $\mathcal{S}$ for all $t_0 \in I$. The points $\mathbf{c}_1(t_0)$ and $\mathbf{c}_2(t_0)$ are then called *the associated foot points*, see Figure 2.3 (right).

A prominent role among all curves on a given canal surface is played by the so called contour curves which e.g. enable to construct the whole family of rational canal surfaces sharing the same silhouette, as we will see.

Definition 2.4. *A* contour curve $\mathcal{C}_\mathbf{v}$ *w.r.t. the vector* $\mathbf{v}$ *of the canal surface* $\mathcal{S}$ *is a curve on* $\mathcal{S}$ *different from its characteristic circles and consisting of all the points at which the normals of* $\mathcal{S}$ *are orthogonal to* $\mathbf{v}$.

A contour curve $\mathcal{C}_\mathbf{v}$ w.r.t. the vector $\mathbf{v}$ corresponds to the *silhouette* of the given canal surface when projecting it to the plane with the normal vector $\mathbf{v}$, see Figure 2.4. Without loss of generality, we may assume in what follows that $\mathbf{v}$ is a unit vector.

Contour and spine curves are related with the valuable property – in particular for a contour curve $\mathbf{c}_\mathbf{v}$ w.r.t. the vector $\mathbf{v}$ on a canal surface with the spine curve $\mathbf{m}$ ($\mathbf{c}_\mathbf{v}$ and $\mathbf{m}$ correspond in parameter in I) the following equality holds:

$$(\mathbf{c}_\mathbf{v} - \mathbf{m}) \cdot \mathbf{v} = 0, \quad \text{for all } t \in I. \tag{2.33}$$

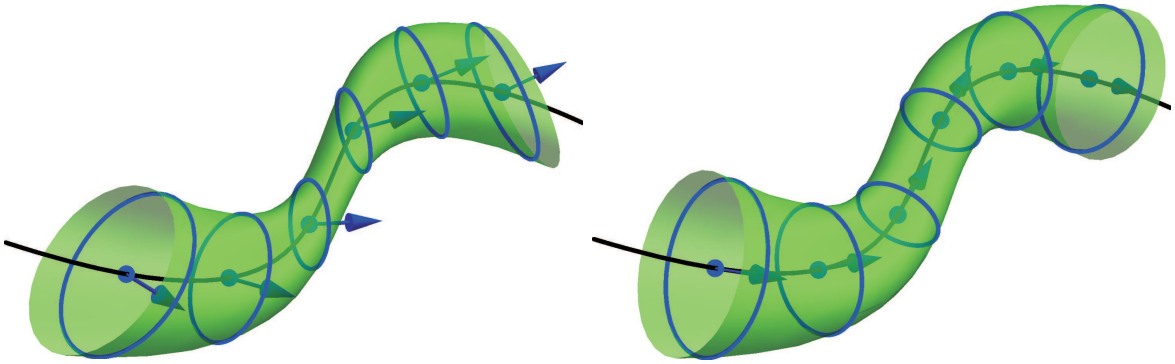

Figure 2.5: An arbitrary (left) and normal (right) ringed surface (green) with a directrix (black), vectors corresponding to the orientation function (blue) and sweeping circles (blue).

This follows from the fact that the normal lines of a canal surface are actually the normal lines of the corresponding spheres and normal lines at the points of the contour curve are perpendicular to the given direction.

When a canal surface is given by its implicit equation $f(\mathbf{x}) = 0$ then the contour curve w.r.t. the vector $\mathbf{v}$ is determined as the complete intersection of two algebraic surfaces defined by the polynomials

$$f(\mathbf{x}) \quad \text{and} \quad f_{\mathbf{v}}(\mathbf{x}) = \nabla f(\mathbf{x}) \cdot \mathbf{v}, \tag{2.34}$$

where ∇f stands for the gradient of f.

2.4 Ringed surfaces

A *ringed surface* $\mathcal{R}$, see Figure 2.5, is a surface generated by sweeping a circle centered at a curve $\mathbf{d}$, called the *directrix*, lying in a plane with the prescribed normal vector $\mathbf{n}$, called the *orientation function*, and possessing a radius described by the *radius function* ρ. We will shortly write $\mathcal{R} : (\mathbf{d}, \mathbf{n}, \rho)$. When $\mathbf{n} \times \mathbf{d}' = \mathbf{o}$ (i.e., the orientation function describes the field of the directrix tangent's directions) we speak about the *normal ringed surfaces*, see Figure 2.5, right.

Since all canal surfaces, cf. Section 2.3, contain 1-parameter family of circles (characteristic circles) they constitute a special subclass of the ringed surfaces – in particular every canal surface is a ringed surfaces with

$$\mathbf{d} = \mathbf{m} - \frac{rr'}{\|\mathbf{m}'\|^2}\mathbf{m}', \quad \mathbf{n} = \mathbf{m}', \quad \rho = \frac{r\sqrt{\|\mathbf{m}'\|^2 - r'^2}}{\|\mathbf{m}'\|}. \tag{2.35}$$

On the other hand a ringed surface is a canal surface iff

$$((\mathbf{n} \cdot \mathbf{d}')\,\mathbf{d}' + (\rho\rho')\,\mathbf{n}') \times \mathbf{n} \equiv \mathbf{o}, \tag{2.36}$$

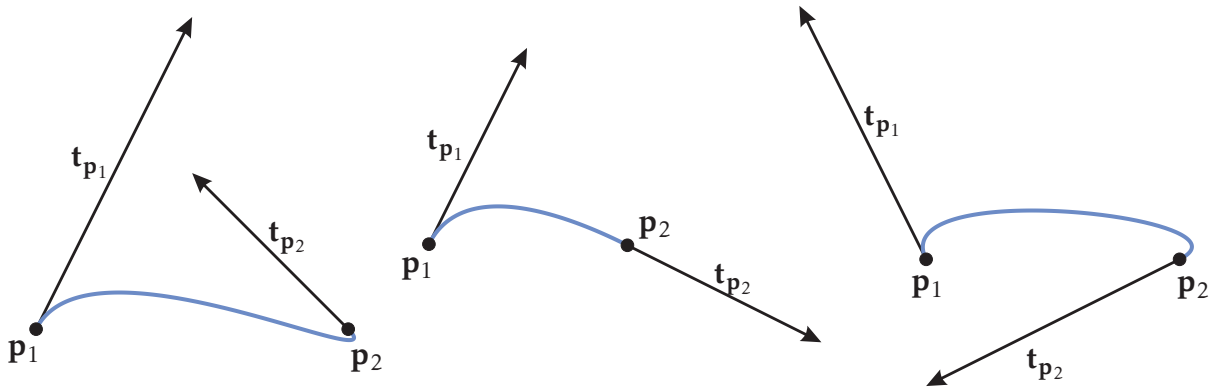

Figure 2.6: Ferguson's cubics for different initial data.

see [5], where also a close relation of ringed/canal surfaces to Darboux cyclides is investigated.

A parameterization $\mathbf{s}(t,u)$ of the ringed surface $\mathcal{R}$ can be obtained analogously as a parameterization of canal surfaces, see (2.30), by rotating the points of a (suitably chosen) curve $\mathbf{c}(t)$ on $\mathcal{R}$ (different from any of the sweeping circles) around the corresponding line element $\Big(\mathbf{d}(t),\mathbf{n}(t)\Big)$, i.e., we arrive at

$$\mathbf{s}(t,u)=\mathbf{d}(t)+\frac{(\varphi(u)+\mathbf{n}(t))\star(\mathbf{c}(t)-\mathbf{d}(t))\star(\varphi(u)-\mathbf{n}(t))}{(\varphi(u)+\mathbf{n}(t))\star(\varphi(u)-\mathbf{n}(t))}. \tag{2.37}$$

Hence the problem of computing a rational parameterization of $\mathcal{R}$ is reduced to the problem of finding a rational curve $\mathbf{c}\subset\mathcal{R}$. All such curves (except from the sweeping circles) can be written in the form

$$\mathbf{c}=\mathbf{d}+\rho\frac{\mathbf{n}^{\perp}}{\|\mathbf{n}^{\perp}\|}, \tag{2.38}$$

where $\mathbf{n}^{\perp}$ is a certain vector field perpendicular to the vector field $\mathbf{n}$.

Remark 2.5. Contour curves of ringed surfaces can be defined analogously as contour curves of canal surfaces, cf. Definition 2.4, and for a ringed surface implicitly defined by a polynomial $f(\mathbf{x})$, the contour curve w.r.t. the vector $\mathbf{v}$ is also given by (2.34).

2.5 Approximate parameterization techniques

In this thesis we introduce some algorithms which are based on parameterizing certain planar/spatial algebraic curves. The approximate parameterization of the curve $\mathcal{C}$ will be computed by approximating particular arcs of $\mathcal{C}$ by suitable segments of a chosen polynomial/rational curve. For the sake of simplicity, we use the so called *Ferguson's cubic*. However, an arbitrary – and at any time replaceable – suitable free-form curve can be used instead.

The Ferguson's cubic is determined by the two points $\mathbf{p}_1$ and $\mathbf{p}_2$ and by the tangent vectors $\mathbf{t}_{\mathbf{p}_1}$ and $\mathbf{t}_{\mathbf{p}_2}$ at these points, see Figure 2.6, and it is given by the formula

$$\mathbf{f}(t) = F_1\,\mathbf{p}_1 + F_2\,\mathbf{p}_2 + F_3\,\mathbf{t}_{\mathbf{p}_1} + F_4\,\mathbf{t}_{\mathbf{p}_2}, \quad t \in [0,1], \tag{2.39}$$

where

$$F_1 = 2t^3 - 3t^2 + 1, \quad F_2 = -2t^3 + 3t^2, \quad F_3 = t^3 - 2t^2 + t, \quad F_4 = t^3 - t^2. \tag{2.40}$$

The deviation of the planar parametric curve $\mathbf{c}(t)$, $t \in I$ from the curve given by the implicit equation $h = 0$ can be measured by the following integral

$$\int_I \frac{h^2(\mathbf{c}(t))}{\|\nabla h(\mathbf{c}(t))\|^2}\,\mathrm{d}t \tag{2.41}$$

and by analogy the deviation of the spatial curve $\mathbf{c}(t)$, $t \in I$ from the one given by the implicit equation $f = g = 0$ can be computed by

$$\int_I \left(\frac{f^2(\mathbf{c}(t))}{\|\nabla f(\mathbf{c}(t))\|^2} + \frac{g^2(\mathbf{c}(t))}{\|\nabla g(\mathbf{c}(t))\|^2} \right) \mathrm{d}t. \tag{2.42}$$

For the sake of completeness the deviation of the parametric surface $\mathbf{s}(t,u)$, $t \in I$, $u \in J$ from the surface defined by polynomial f can be measured by

$$\int_J \left(\int_I \frac{f^2(\mathbf{s}(t,u))}{\|\nabla f(\mathbf{s}(t,u))\|^2}\,\mathrm{d}t \right) \mathrm{d}u. \tag{2.43}$$

Furthermore we formulate the problem of approximate parameterization as an optimization process – hence e.g. the classical Newton's method for computing the roots of a system of non-linear equations can be used, see for instance [25, 63, 75].

Let us consider a system of non-linear equations

$$\mathbf{F}(\mathbf{x}) = \mathbf{0}, \tag{2.44}$$

where $\mathbf{F}(\mathbf{x})$ is a given vector-function of the vector argument $\mathbf{x} = (x_1, x_2, \ldots, x_n)^\top$. Newton's method is based on the linearization of the function $\mathbf{F}(\mathbf{x})$. The iteration process can be shortly written in the form

$$\mathbf{x}^{(i+1)} = \mathbf{x}^{(i)} - \frac{\mathbf{F}(\mathbf{x}^{(i)})}{\mathbf{F}'(\mathbf{x}^{(i)})} = \mathbf{x}^{(i)} - \mathbf{J}^{-1}(\mathbf{x}^{(i)})\mathbf{F}(\mathbf{x}^{(i)}), \quad i = 0, 1, 2, \ldots, \tag{2.45}$$

where $\mathbf{J}(\mathbf{x})$ is the Jacobian of $\mathbf{F}(\mathbf{x})$. A remarkable property of the Newton's method is its quadratic convergence. On the other hand, to ensure any convergence at all, the initial value $\mathbf{x}_0$ must be chosen sufficiently close to the (yet unknown) root $\widehat{\mathbf{x}}$, see e.g. [75].

2.6 Sum of squares decomposition

The sum of squares (SOS) problem is closely connected with solving polynomial equations, for more details see e.g. [22, 61]. A polynomial τ over reals is said to be *positive semidefinite* (PSD), or *positive definite* (PD) if $\tau(t) \geq 0$, or $\tau(t) > 0$ for all $t \in \mathbb{R}$. We say that τ is a sum of squares if the degree of τ is even and it can be written as a sum of squares of other polynomials. It is obvious that SOS decomposition of τ implies its nonnegativity. However, the converse is not true in general – the construction of PSD polynomials which are not sums of squares was first described by Hilbert in 1888.

For the sake of brevity, we recall only elementary notions dealing with the univariate polynomials where the situation becomes much easier than in the general case. It can be shown that every PSD univariate polynomial is a sum of *just two* squares. In this section we show how the decomposition of a polynomial $\tau \in \mathbb{R}[t]$ can be computed, i.e., we want to find two polynomials $f, g \in \mathbb{R}[t]$ such that

$$\tau = f^2 + g^2. \tag{2.46}$$

Let us recall that a real polynomial in one variable is PSD iff its leading coefficient is positive and its roots are either complex in conjugate pairs or real with even multiplicity. Of course, the SOS decomposition (2.46) is by no mean unique; for an arbitrary φ the polynomials

$$f_\varphi = \cos\varphi\, f - \sin\varphi\, g \quad \text{and} \quad g_\varphi = \cos\varphi\, g + \sin\varphi\, f \tag{2.47}$$

solve the problem as well, i.e., formula (2.47) generates an equivalence class of decompositions. For a polynomial τ of degree $2n$, there exist 2^{n-1} non-equivalent classes of decompositions, see [57]. Hence in order to obtain all possible decompositions we have to compute 2^{n-1} particular non-equivalent decompositions and use formula (2.47) to generate all of them.

Of course, it is not easy to get the initial decomposition (f, g), because we are not able to compute the exact roots, in general. And another limitation appears when we want to work only with polynomials with rational coefficients, when the SOS decomposition may include more than two squares. Nonetheless, in this thesis we are going to decompose quadratic and quartic polynomials, only, and thus the computation of a SOS decomposition can be achieved symbolically. In particular we can obtain a decomposition (2.46) with the help of the roots of τ which can be computed using the discriminant for quadratic τ and the so called Ferrari's formulas for quartic τ.

Example 2.6. If τ is a quadratic PSD polynomial, we can write its factorization as follows

$$\tau(t) = \lambda(t - \alpha - \beta i)(t - \alpha + \beta i), \tag{2.48}$$

where $\alpha, \beta \in \mathbb{R}$ and $\lambda \in \mathbb{R}^+$. Then there exists only one equivalence class of the decomposition generated e.g. by

$$f(t) = \sqrt{\lambda}(t - \alpha), \quad g = \sqrt{\lambda}\beta. \tag{2.49}$$

Example 2.7. For a quartic PSD polynomial

$$\tau(t) = \lambda(t-\alpha-\beta i)(t-\alpha+\beta i)(t-\gamma-\delta i)(t-\gamma+\delta i), \tag{2.50}$$

where $\alpha, \beta, \gamma, \delta \in \mathbb{R}$ and $\lambda \in \mathbb{R}^+$ we use the Fibonacci's identities

$$(a^2+b^2)(c^2+d^2) = (ac \pm bd)^2 + (ad \mp bc)^2 \tag{2.51}$$

and obtain two non-equivalent decompositions in the form

$$f_{1,2}(t) = \sqrt{\lambda}\,(\delta(t-\alpha) \pm \beta(t-\gamma)), \quad g_{1,2}(t) = \sqrt{\lambda}\,((t-\alpha)(t-\gamma) \mp \beta\delta). \tag{2.52}$$

Chapter 3

Approximate parameterization of implicitly given canal surfaces

In this chapter, we present two methods (Sections 3.3 and 3.4) for the computation of approximate rational parameterizations of implicitly given canal surfaces. Both methods are based on computing approximate parameterizations of contour curves on a given canal surface which is performed by constructing their graphs of critical points (cf. Section 3.2) and afterwards replacing its edges by a suitable free-form curve. More precisely the method described in Section 3.3 starts with computing approximate parameterizations of the both branches of the z-contour curve of the given canal surface. From these parameterizations an approximation of its spine curve is reconstructed and afterwards its approximate parameterization is computed. The improvement of the method producing the parameterization having the lower rational degree is introduced in Section 3.4. The main idea of the improved method is based on computing the parameterizations (corresponding in parameter) of three different contour curves and from them we reconstruct the spine curve with the same degree as the approximated contour curves. Both methods are mainly suitable for implicit blend surfaces of the canal-surface-type. The papers in which the author of the thesis participated and which contain the author's main contribution to this topic are – [8], [11*], [10*], [13*].*

3.1 Motivation - implicit blends

Let us consider two canal (ringed) surfaces $\mathcal{R}_1$ and $\mathcal{R}_2$ (e.g. cones or cylinders of revolution) implicitly defined by polynomials f_1 and f_2, and bounded by planes $\mathcal{P}_1$ and $\mathcal{P}_2$ defined by f_{10} and f_{20}, respectively. Then in [39] the implicit blending surface $\mathcal{B}$ between $\mathcal{R}_1$ and $\mathcal{R}_2$ (and joining $\mathcal{R}_1$ and $\mathcal{R}_2$ in $\mathcal{P}_1$ and $\mathcal{P}_2$, respectively) is constructed

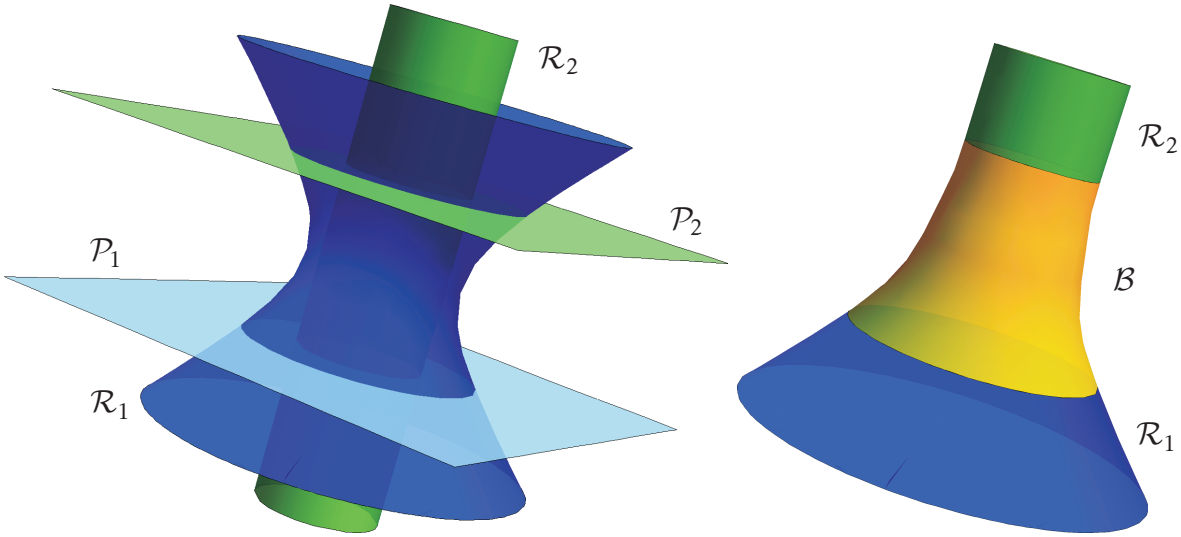

Figure 3.1: A Hyperboloid of one sheet (blue) and a cylinder (green), both bounded by planes (light blue and light green), left and the implicit blend (yellow) between these surfaces, right.

and defined by the polynomial

$$f = f_1(1-\lambda)f_{20}^{n+1} - f_2\lambda f_{10}^{n+1}, \tag{3.1}$$

where $\lambda \in (0,1)$ and $n \in \mathbb{N}$, see Figure 3.1. Now the problem can be formulated as follows: How the approximation of this implicitly given blending surface can be computed? In this chapter we solve this problem by approximating the given blending surface by a suitable rational canal surface.

3.2 Graphs of critical points of spatial curves

This section is devoted to the special graphs of spatial algebraic curves reflecting their shape and topology. Constructing such graphs is especially useful when approximating these curves.

The construction starts with computing the critical points of a given spatial curve $\mathcal{C}$ w.r.t. the chosen basis vectors of $\mathbb{R}^3$ – we use the standard (canonical) basis, i.e.

$$\mathbf{e}_1 = (1,0,0)^\top, \quad \mathbf{e}_2 = (0,1,0)^\top, \quad \mathbf{e}_3 = (0,0,1)^\top. \tag{3.2}$$

Then we connect the critical points appropriately by line segments such that each line segment corresponds to some real part of $\mathcal{C}$. Such an arrangement of line segments is called a *graph of critical points* of $\mathcal{C}$ and is denoted by $G(\mathcal{C})$. It is beyond the scope of this thesis to go into details, so we recall only basic steps – for more details see [10*]. We only recall that for curves with non-complicated topology (which are assumed in

our approach as we deal with curves on canal surfaces playing a role in technical applications, e.g. in blending) the graph of critical points is topologically equivalent to the given curve.

The construction of the graph of critical points $G(\mathcal{C})$ of a spatial algebraic curve $\mathcal{C}$ implicitly defined by polynomials f and g proceeds in computing all the x-, y- and z-critical points (the critical points w.r.t. $\mathbf{e}_1$, $\mathbf{e}_2$ and $\mathbf{e}_3$, respectively) of $\mathcal{C}$, projecting $\mathcal{C}$ to the plane $z = 0$ ($\pi_z : \mathcal{C} \mapsto \pi_z(\mathcal{C})$) and constructing the planar critical graph $G(\pi_z(\mathcal{C}))$ which contains the projections of all the critical points of $\mathcal{C}$ as its vertices, and finally lifting its edges back to space, see Algorithm 1.

Algorithm 1 Construction of the graph of critical points

INPUT: A spatial curve $\mathcal{C}$ defined by the polynomials f and g and a set $\mathfrak{M}$ of some prescribed points on $\mathcal{C}$.

1: Compute the x-coordinates $x_1 < \ldots < x_k$ of x-, y- and z-critical points of $\mathcal{C}$, of the singular points of $\pi_z(\mathcal{C})$ obtained only by the projection π_z and of points from $\mathfrak{M}$;
2: For every x_i, compute the real roots of $h(x_i, y)$: $y_{i,1} < y_{i,2} < \ldots < y_{i,s}$, where $h = \mathrm{Res}_z(f, g)$;
3: For all points $(x_i, y_{i,j})^\top$ compute the number of left and right branches going from these points;
4: Connect the points $(x_i, y_{i,j})^\top$ with the points $(x_{i+1}, y_{i+1,j})^\top$ appropriately;
5: Delete such singular points of $\pi_z(\mathcal{C})$ which are not the projections of the singular points of $\mathcal{C}$, see [10*];
6: Delete all vertices of $G(\pi_z(\mathcal{C}))$ which are not the projections of critical points or points from the set $\mathfrak{M}$;
7: Lift the edges of $G(\pi_z(\mathcal{C}))$ to the space and hence obtain $G(\mathcal{C})$;

OUTPUT: The graph $G(\mathcal{C})$ of critical points of $\mathcal{C}$ having its critical points and the points from the set $\mathfrak{M}$ as its vertices.

Remark 3.1. For later use, we need $G(\mathcal{C})$ to contain some additional points as its vertices, thus we introduce the set $\mathfrak{M}$, which enables us to prescribe the vertices of the constructed graph. Hence, the graph will contain only the points from $\mathfrak{M}$ and the critical points of $\mathcal{C}$.

In Algorithm 1 we require $G(\mathcal{C})$ to contain the critical points of $\mathcal{C}$ as its vertices. The x-critical points of $\mathcal{C}$ satisfy the condition

$$f_y g_z - f_z g_y = 0. \tag{3.3}$$

First, we compute the real roots $x_1 < x_2 < \ldots < x_k$ of

$$\mathrm{Res}_y\left(\mathrm{Res}_z(f, g), \frac{\partial \mathrm{Res}_z(f, g)}{\partial y}\right), \tag{3.4}$$

where $\mathrm{Res}_x(f, g)$ denotes the resultant of the polynomials f and g with respect to x. The computation of the roots of polynomials in one variable is a numerically well

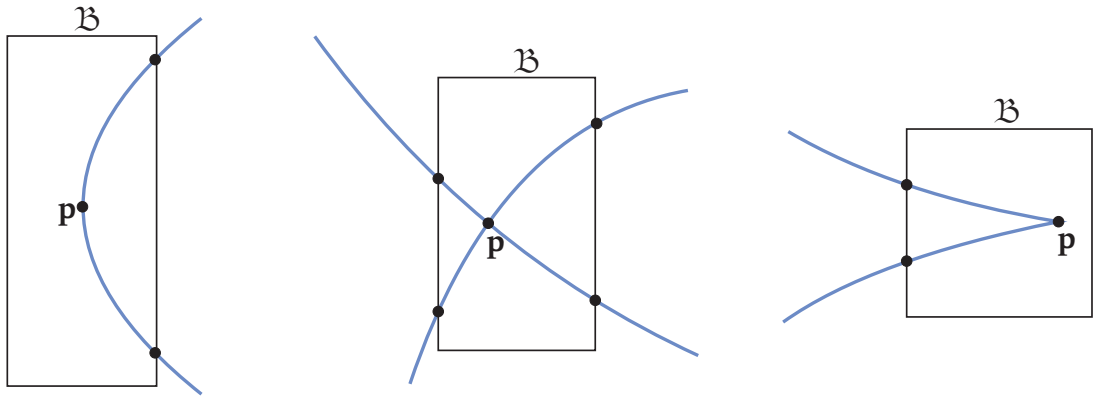

Figure 3.2: Construction of bounding boxes at the critical points.

handled problem. Now, for every root x_i we compute all the associated real roots $y_{i,1} < y_{i,2} < \ldots < y_{i,s_i}$ of

$$\gcd\left(\mathrm{Res}_z(f,g)(x_i,y), \frac{\partial \mathrm{Res}_z(f,g)}{\partial y}(x_i,y)\right). \tag{3.5}$$

Note that if the coordinates x_i are approximate numbers we may need to compute the approximate greatest common divisors, see for instance [74]. Finally, we compute the corresponding z-coordinates of x-critical points by solving the equation (again based on computing the approximate gcd, in general)

$$\gcd\Big(f(x_i,y_{i,j},z), g(x_i,y_{i,j},z)\Big) = 0. \tag{3.6}$$

It is guaranteed (we recall the space general position from [10*]) that exactly one real root $z_{i,j}$ is obtained for each $(x_i,y_{i,j})^\top$. Hence, we arrive at all x-critical points $(x_i,y_{i,j},z_{i,j})^\top$. Analogously, we compute the y- and z-critical points of $\mathcal{C}$. Let us emphasize that the singular points of $\mathcal{C}$ are simultaneously x-, y- and z-critical.

Remark 3.2. Let us note that extra factors may arise during the process of resultant computation. Hence, it must be verified that all obtained points fulfil the conditions for critical points of $\mathcal{C}$.

We also need to compute the number of the left and right branches going from a particular point $\mathbf{p}$ (Step 3 in Algorithm 1) on the planar curve $\pi_z(\mathcal{C})$. This can be done by the following method: We enclose $\mathbf{p}$ by a small box $\mathfrak{B}$ such that the curve $\pi_z(\mathcal{C})$ does not intersect the box $\mathfrak{B}$ in the bottom and in the top and, moreover, there exists exactly one intersection point (the point $\mathbf{p}$) of the vertical line going through the point $\mathbf{p}$ with the curve $\pi_z(\mathcal{C})$ in the box, see Figure 3.2. Then the number of the right and left intersection points yields the number of half-branches to the right and to the left at $\mathbf{p}$, respectively, cf. [18] for more details of this technique.

Finally, we show how the vertices of $G(\pi_z(\mathcal{C}))$ can be connected. We write the sequence R_i of vertices $(x_i,y_{i,j})^\top$ where each vertex occurs as many times as it has half-branches to the right, and the sequence L_{i+1} of vertices $(x_{i+1},y_{i+1,j})^\top$ where each vertex again

occurs as many times as it has half-branches to the left, for particular i. Then, the m-th vertex from R_i is connected with the m-th vertex from L_{i+1}. Note that the way how to connect the vertices by edges is uniquely determined since any incorrect connecting vertices lead to at least one intersection of two edges at a non-critical point.

3.3 Algorithm of approximation

In this section we summarize the method for computing an approximate parameterization of the canal surface $\mathcal{S}$ defined by the polynomial f, for more detail see [8*]. The method starts with constructing the graph of critical points $G(\mathcal{C}) = G(\mathcal{C}_1) \cup G(\mathcal{C}_2)$ of both branches of the z-contour curve $\mathcal{C} = \mathcal{C}_1 \cup \mathcal{C}_2$ and consequently replacing the edges of $G(\mathcal{C})$ by the arcs of Ferguson's cubic – this step is formulated as an optimization process.

Since we require that the parameterizations of $\mathcal{C}_1$ and $\mathcal{C}_2$ correspond in parameter we have to add all corresponding foot points of all the critical points of $\mathcal{C}$ to the set of vertices of $G(\mathcal{C})$. Hence the both branches of $G(\mathcal{C})$ will possess the same number of the vertices and moreover the corresponding vertices will be the associated foot points.

Let $\mathbf{p} = (p_1, p_2, p_3)^\top \in \mathcal{C}_1$, then by formula (2.33) the corresponding foot point $\mathbf{q} \in \mathcal{C}_2$ possesses the same z-coordinate p_3 as $\mathbf{p}$ has. Hence we arrive at the points $\mathbf{q}_1, \ldots, \mathbf{q}_s$ by cutting the curve $\mathcal{C}$ with the plane $z = p_3$; in particular we solve the system of nonlinear equations

$$f = f_z = z - p_3 = 0. \tag{3.7}$$

Now, we have to choose the right point $\mathbf{q} = \mathbf{q}_i$ from the set of points $\mathbf{q}_1, \ldots, \mathbf{q}_s$. This can be easily checked as the normal lines of $\mathcal{S}$ at the points $\mathbf{p}$ and $\mathbf{q}$ have to intersect in the point $\mathbf{m}$ such that $\|\mathbf{p} - \mathbf{m}\| = \|\mathbf{q} - \mathbf{m}\|$.

Thus firstly we parameterize $\mathcal{C}_1$ such that for each edge $e_i \in G(\mathcal{C}_1)$ (joining points $\mathbf{p}_i$ and $\mathbf{p}_{i+1}$) we construct the Ferguson's cubic $\mathbf{f}_i(t, \alpha_i^1, \alpha_i^2)$ going from $\mathbf{p}_i$ to $\mathbf{p}_{i+1}$ and possessing the tangent vectors $\alpha_i^1 \mathbf{t}_{\mathbf{p}_i}$ and $\alpha_i^2 \mathbf{t}_{\mathbf{p}_{i+1}}$ at these points. Then we minimize the objective function

$$\Phi_i(\alpha_i^1, \alpha_i^2) = \int_0^1 \left(\frac{f^2(\mathbf{f}_i(t, \alpha_i^1, \alpha_i^2))}{\|\nabla f(\mathbf{f}_i(t, \alpha_i^1, \alpha_i^2))\|^2} + \frac{f_z^2(\mathbf{f}_i(t, \alpha_i^1, \alpha_i^2))}{\|\nabla f_z(\mathbf{f}_i(t, \alpha_i^1, \alpha_i^2))\|^2} \right) \mathrm{d}t \tag{3.8}$$

to get the particular lengths of the tangent vectors $\mathbf{t}_{\mathbf{p}_i}$ and $\mathbf{t}_{\mathbf{p}_{i+1}}$ and substitute them to $\mathbf{f}_i(t, \alpha_i^1, \alpha_i^2)$. In order to minimize objective function (3.8) we used the Newton's iteration process (see [8*]) since it allows us to handle the integral, however any other optimization method could be used instead – for example it is acceptable to use Newton-Cotes integration formulas to dispose of the integral and afterwards minimize the function by an arbitrary optimization method.

Then we compute the approximate parameterization of the second branch $\mathcal{C}_2$ of the z-contour curve but only in the plane xy again by replacing the edges of the projected graph of critical points $\pi_z(\mathcal{C}_2)$ by Ferguson's cubic with free parameters (the

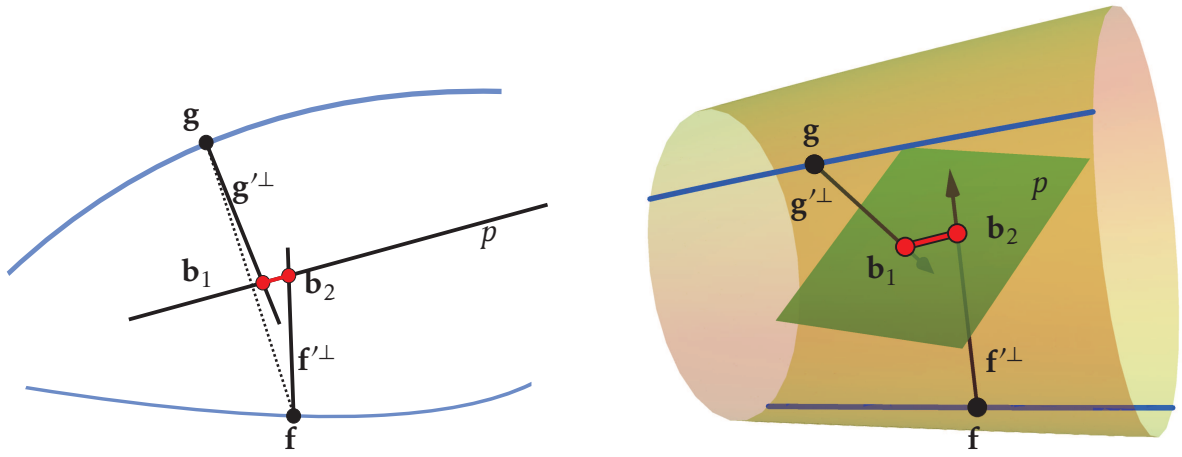

Figure 3.3: Curves approximately corresponding in parameter – in the plane xy, left and in the space (on a canal surface), right.

lengths of the tangent vectors) and minimize the objective function, which now should measure the deviance of the planar parametric curve from $\pi_z(\mathcal{C}_2)$ (given implicitly by $h = Res_z(f, f_z)$) and moreover the deviance of the correspondence in parameter with the projected parametric curve $\pi_z(\mathbf{f})$.

According to Preliminaries, the deviance of $\mathbf{g}$ from $h = 0$ is measured using (2.41), i.e.,

$$\Phi_1(\beta^1, \beta^2) = \int_0^1 \left(\frac{h^2(\mathbf{g}(t, \beta^1, \beta^2))}{\|\nabla h(\mathbf{g}(t, \beta^1, \beta^2))\|^2} \right) \mathrm{d}t. \tag{3.9}$$

Next we define a suitable function which measures the deviance of the correspondence in parameter of two planar parametric curves $\mathbf{f}$ and $\mathbf{g}$ as follows. Let $\mathbf{b}_1$ and $\mathbf{b}_2$ be the intersection points (curves) of the axis p of the segment $\mathbf{fg}$ with the normal lines of $\mathbf{f}$ and $\mathbf{g}$, respectively. Then $\mathbf{f}$ and $\mathbf{g}$ correspond in parameter if $\mathbf{b}_1(t) = \mathbf{b}_2(t)$ for all $t \in [0,1]$ and the deviance of the approximate correspondence in parameter corresponds to the distance between $\mathbf{b}_1$ and $\mathbf{b}_2$ (see Figure 3.3, left), i.e.,

$$\Phi_2(\beta^1, \beta^2) = \int_0^1 \|\mathbf{b}_1(t, \beta^1, \beta^2) - \mathbf{b}_2(t, \beta^1, \beta^2)\|^2 \, \mathrm{d}t, \tag{3.10}$$

where

$$\mathbf{b}_1(t) = \mathbf{g} + \frac{\|\mathbf{f} - \mathbf{g}\|^2}{2(\mathbf{f} - \mathbf{g}) \cdot \mathbf{g}'^{\perp}} \mathbf{g}'^{\perp}, \quad \text{and} \quad \mathbf{b}_2(t) = \mathbf{f} + \frac{\|\mathbf{f} - \mathbf{g}\|^2}{2(\mathbf{f} - \mathbf{g}) \cdot \mathbf{f}'^{\perp}} \mathbf{f}'^{\perp}. \tag{3.11}$$

Thus, let us recall, that we replace the edges $l_i \in \pi_z(G(\mathcal{C}_2))$ (joining points $\pi_z(\mathbf{q}_i)$ and $\pi_z(\mathbf{q}_{i+1})$) by Ferguson's cubic $\pi_z(\mathbf{g}_i)(t, \beta_i^1, \beta_i^2)$ going from $\pi_z(\mathbf{q}_i)$ to $\pi_z(\mathbf{q}_{i+1})$ and possessing the tangent vectors $\beta_i^1 \pi_z(\mathbf{t}_{\mathbf{q}_i})$ and $\beta_i^2 \pi_z(\mathbf{t}_{\mathbf{q}_{i+1}})$ at these points and minimize the objective function

$$\Phi_i(\beta_i^1, \beta_i^2) = \Phi_i^1(\beta_i^1, \beta_i^2) + w \Phi_i^2(\beta_i^1, \beta_i^2), \tag{3.12}$$

where w is a suitably chosen weigh and Φ_i^1 and Φ_i^2 correspond to objective functions (3.9) and (3.10). The minimizing process could be again achieved e.g. by Newton's iteration process.

Finally, we reconstruct the spine curve $\mathbf{m}$ of $\mathcal{S}$ by lifting the approximation

$$\mathbf{b}(t) = \frac{\mathbf{b}_1 + \mathbf{b}_2}{2}. \tag{3.13}$$

of the bisector curve of $\pi_z(\mathbf{f})$ and $\pi_z(\mathbf{g})$ to the space. From property (2.33) the spine curve and the z-contour curve possess the same third coordinate.

Then rotating $\mathbf{f}$ around the tangents of $\mathbf{m}$ yields the parameterization of a given canal surface. The whole method is summarized in Algorithm 2.

Algorithm 2 Approximate parameterization of implicitly defined canal surface.

INPUT: Defining polynomial f of a canal surface $\mathcal{S}$.

1: Construct a graph of critical points $G(\mathcal{C})$ of the z-contour curve having as vertices its critical points and their associated foot points – it consists of two paths $G(\mathcal{C}_1) : \mathbf{p}_1, \dots, \mathbf{p}_k$ and $G(\mathcal{C}_2) : \mathbf{q}_1, \dots, \mathbf{q}_k$;
2: **for** each $i \in \{1, \dots, k-1\}$ **do**
3: Compute the approximate parameterization $\mathbf{f}_i$ of the particular part of $\mathcal{C}_1$ between the points $\mathbf{p}_i$ and $\mathbf{p}_{i+1}$;
4: Compute the approximate parameterization $\pi_z(\mathbf{g}_i)$ of the particular part of the projected curve $\pi_z(\mathcal{C}_2)$ between the points $\pi_z(\mathbf{q}_i)$ and $\pi_z(\mathbf{q}_{i+1})$ approximately corresponding in parameter with $\pi_z(\mathbf{f}_i)$;
5: Compute the bisector $\mathbf{b}_i$ of $\pi_z(\mathbf{f}_i)$ and $\pi_z(\mathbf{g}_i)$ and reconstruct the approximate parameterization $\mathbf{m}_i := (b_i^1, b_i^2, f_i^3)^\top$ of the spine curve of $\mathcal{S}$;
6: Rotate $\mathbf{f}_i$ around the tangents of $\mathbf{m}_i$ - obtain parameterization $\mathbf{s}_i$;
7: **end for**

OUTPUT: The piecewise approximate parameterization $\mathbf{s}_1(t,u), \dots, \mathbf{s}_k(t,u)$ of $\mathcal{S}$.

Remark 3.3. We recall that the deviance of the approximately parameterized surface $\mathbf{s}(t,u)$ from the implicitly given surface given by polynomial f can be computed by integral (2.43) and when needed Algorithm 2 can be adjusted to perform adaptive refinement in order to increase the accuracy. In particular we can divide the edges of the graph of critical points to increase the number of arcs of Ferguson's cubics, for more details see [8*].

Let us note that when we approximate a canal surface $\mathcal{S}$, e.g. some blending surface, we are interested only in some prescribed part of $\mathcal{S}$ bounded e.g. by planes $\mathcal{P}_i$. Hence we slightly modify the construction of the graph of critical points of the contour curves to achieve this – i.e., we consider only the critical points in the corresponding region interest and add all the intersections of $\mathcal{C}$ with the planes $\mathcal{P}_i$ to the set of the vertices of $G(\mathcal{C})$.

Example 3.4. We compute the approximate parameterization of the canal surface $\mathcal{B}$ (see Fig 3.4, left), obtained by formula (3.1) (for $\lambda = 1/4$ and $n = 2$) as an implicit blending surface between the cone $f_1 = -x^2 + 2x + y^2 + z^2 - 4$ and the cylinder $f_2 = y^2 + z^2 - 2$ bounded by the planes $f_{10} = x + 2$ and $f_{20} = x - 2$, respectively. Hence $\mathcal{B}$ is defined by the following polynomial

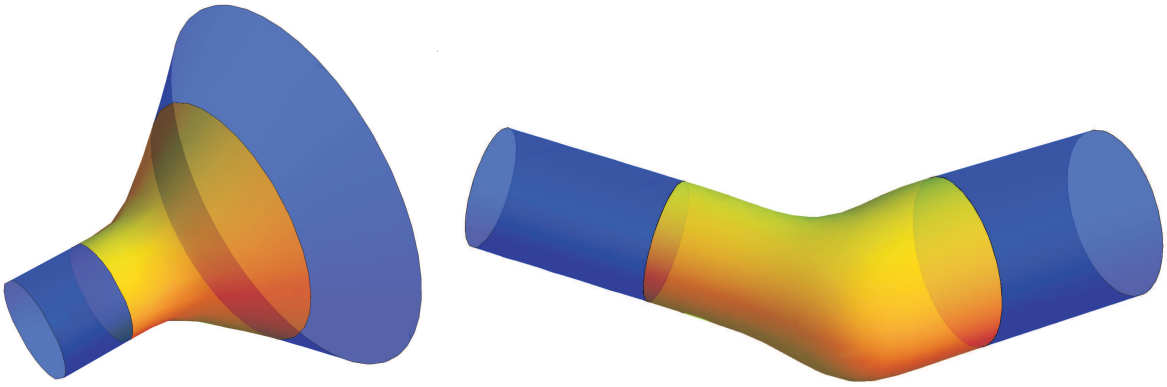

Figure 3.4: Implicit blending surface (yellow) between two canal surfaces (blue), left from Example 3.4 and right from Example 3.5.

$$\begin{aligned} f = \; & -3x^5 + 24x^4 + 2x^3y^2 + 2x^3z^2 - 82x^3 - 24x^2y^2 - 24x^2z^2 + 180x^2 + 24xy^2 + 24xz^2 - \\ & 168x - 32y^2 - 32z^2 + 112. \end{aligned}$$

No critical points are on the contour curve, hence the approximate parameterization of f will be composed of only one part. The error of the approximation measured by integral (2.43) is less then $2.1 \cdot 10^{-4}$.

Example 3.5. We approximate the implicit blending surface (see Figure 3.4, right) given by the polynomial

$$\begin{aligned} f = \; & -7\sqrt{2}x^5 + 14\sqrt{2}x^4z - 42\sqrt{2}x^4 - 14\sqrt{2}x^3y^2 + 3x^3y^2 - 7\sqrt{2}x^3z^2 + 3x^3z^2 + 84\sqrt{2}x^3z - \\ & 70\sqrt{2}x^3 - 6x^3 + 9x^2y^2z - 111\sqrt{2}x^2y^2 + 9x^2z^3 - 69\sqrt{2}x^2z^2 + 168\sqrt{2}x^2z - 18x^2z + \\ & 82\sqrt{2}x^2 + 9xy^2z^2 - 54\sqrt{2}xy^2z - 168\sqrt{2}xy^2 + 162xy^2 + 9xz^4 - 54\sqrt{2}xz^3 - 84\sqrt{2}xz^2 + \\ & 144xz^2 + 220\sqrt{2}xz + 168\sqrt{2}x - 324x + 3y^2z^3 - 27\sqrt{2}y^2z^2 + 162y^2z - 274\sqrt{2}y^2 + \\ & 3z^5 - 27\sqrt{2}z^4 + 156z^3 - 164\sqrt{2}z^2 - 324z + 436\sqrt{2}. \end{aligned}$$

This surface was again obtained by by formula (3.1) (for $\lambda = 7/10$ and $n = 2$) as a blending surface between two implicitly given cylinders

$$f_1 = y^2 + z^2 - 2, \quad \text{and} \quad f_2 = x^2 - 2xz + 2y^2 + z^2 - 2, \tag{3.14}$$

bounded by the planes

$$f_{10} = x + 2, \quad \text{and} \quad f_{20} = x + z - 3\sqrt{2}. \tag{3.15}$$

Although the shape of the computed blend f looks like a canal surface it is not exactly surface of this type. Anyway, we may still use our method – now for approximating the blend by a canal surface. The contour curve contains 4 critical and 4 boundary points: 4 on the first branch and 4 (being simultaneously the foot points) on the second branch. Hence the approximation of the blending surface will be composed of three parts. The error of the approximation measured by integral (2.43) is less then $1.8 \cdot 10^{-2}$.

Remark 3.6. In Example 3.5, we applied our method on the implicit blend f which was not exactly a canal surface. In these cases it is necessary to measure how a given surface differs from an exact canal surface. This could be achieved e.g. by considering two contour curves with respect to two different directions (not only the direction perpendicular to the xy plane), constructing the approximations of the spine curve for both directions and measure the Hausdorff distance between these two curves. If the error (distance between the approximations of the spine curve) is acceptable (i.e., less than some prescribed ε) we can use Algorithm 2. An alternative approach is to compute the approximate parameterization of the implicit surface and subsequently check whether the error is less than a chosen ε.

3.4 Algorithm of low degree approximation

A drawback of the method presented in the previous section lies in the fact that it produces parameterizations with the high rational bidegree. This is caused by the quality of the reconstructed spine curve which is rational of degree seven. In this section, we introduce the method from [11*] yielding the polynomial cubic approximations (corresponding in parameter) of contour and spine curves which will be consequently used for computing an approximate parameterization of a given canal surface having the rational degree $[7,4]$ in t and $[2,2]$ in u.

The idea of the method is based on property (2.33). In particular the parameterizations $\mathbf{c}_x = (c_x^1, c_x^2, c_x^3)^\top$, $\mathbf{c}_y = (c_y^1, c_y^2, c_y^3)^\top$ and $\mathbf{c}_z = (c_z^1, c_z^2, c_z^3)^\top$ (corresponding in parameter) of the contour curves $\mathcal{C}_x, \mathcal{C}_y$ and $\mathcal{C}_z$ are computed and afterwards the parametric description of the spine curve is derived in the form

$$\mathbf{m}(t) = \left(c_x^1, c_y^2, c_z^3\right)^\top. \tag{3.16}$$

Thus the problem of computing the approximation $\mathbf{m}$ of the spine curve of a given canal surface is reduced to the problem of computing approximate parameterizations of the particular branches of contour curves, e.g. $\mathcal{C}_x^+, \mathcal{C}_y^+$ and $\mathcal{C}_z^+$. Moreover $\mathbf{m}$ is polynomial if $\mathbf{c}_x^+, \mathbf{c}_y^+$ and $\mathbf{c}_z^+$ are polynomial and it has the degree which is equal to the maximum of the degrees of c_x^1, c_y^2, c_z^3.

A limitation of this method and the method presented in the previous section lies in the fact that they are not independent of the coordinate system – i.e. when a canal surface is in a special position this methods (designed in [8*] and [11*]) may lead to some difficulties, see Example 3.7. These problems can be easily avoided considering the contour curves w.r.t. a general viewpoint. Hence according to [13*] instead of considering contour curves w.r.t. the directions of the coordinate axes we consider the contour curves w.r.t. the three linearly independent vectors and using them we reconstruct the spine curve. More precisely, we compute the parameterizations $\mathbf{c}_{\mathbf{v}_1}$, $\mathbf{c}_{\mathbf{v}_2}$ and $\mathbf{c}_{\mathbf{v}_3}$ (corresponding in parameter) of three different contour curves on $\mathcal{S}$ w.r.t. the linearly independent vectors $\mathbf{v}_1$, $\mathbf{v}_2$ and $\mathbf{v}_3$, respectively. Then the spine curve

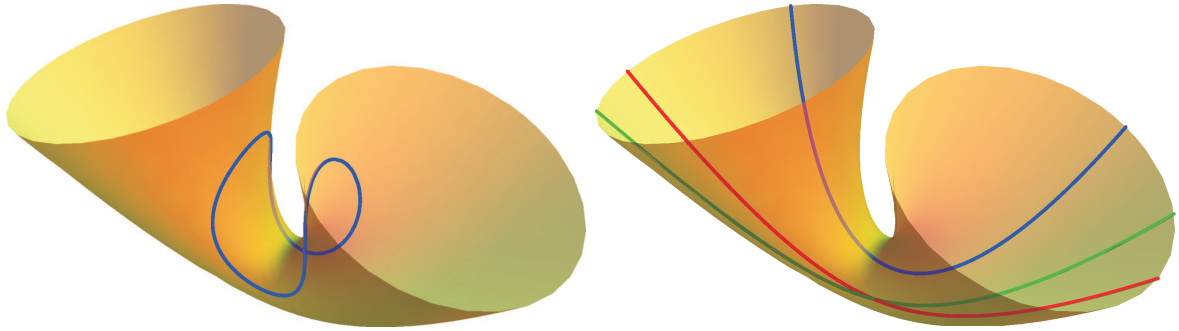

Figure 3.5: The z-contour curve (left) and three different contour curves w.r.t. the general viewpoints on the canal surface (right) from Example 3.7.

possesses the parameterization

$$\mathbf{m} = \begin{pmatrix} \mathbf{v}_1 \\ \mathbf{v}_2 \\ \mathbf{v}_3 \end{pmatrix}^{-1} \cdot \begin{pmatrix} \mathbf{v}_1^\top \cdot \mathbf{c}_{\mathbf{v}_1} \\ \mathbf{v}_2^\top \cdot \mathbf{c}_{\mathbf{v}_2} \\ \mathbf{v}_3^\top \cdot \mathbf{c}_{\mathbf{v}_3} \end{pmatrix}. \tag{3.17}$$

In this case '$\cdot$' denotes the matrix product.

Example 3.7. Let us consider the canal surface $\mathcal{S}$ implicitly given by the polynomial

$$\begin{aligned} f = \; & 2304x^6 + 6912x^4y^2 + 768x^4z^2 + 4608x^4z - 1296x^4 + 6912x^2y^4 + 1536x^2y^2z^2 - \\ & 4608x^2y^2z + 2592x^2y^2 - 1280x^2z^4 + 3072x^2z^3 + 1632x^2z^2 - 1440x^2z + 216x^2 + \\ & 2304y^6 + 768y^4z^2 - 9216y^4z - 1296y^4 - 1280y^2z^4 - 8704y^2z^3 + 4512y^2z^2 + 288y^2z - \\ & 216y^2 + 256z^6 - 1536z^5 + 2672z^4 - 1056z^3 - 24z^2 + 72z - 9. \end{aligned}$$

We want to compute an approximate parameterization of $\mathcal{S}$ in some prescribed bounding box $\mathfrak{B}$. The methods based on the contour curves w.r.t. the directions of the coordinate axes cannot be applied as the z-contour curve $\mathcal{C}_z$ lying in $\mathfrak{B}$ is closed and thus cannot be used for parameterizing the whole part of $\mathcal{S}$ in $\mathfrak{B}$, see Figure 3.5 (left). An easy way to overcome this problem is considering other three viewpoints, see Figure 3.5 (right).

We proceed analogously as in the previous section. First we construct the graphs of the critical points $G(\mathcal{C}_{\mathbf{v}_1}), G(\mathcal{C}_{\mathbf{v}_2})$ and $G(\mathcal{C}_{\mathbf{v}_3})$ of the contour curves $\mathcal{C}_{\mathbf{v}_1}, \mathcal{C}_{\mathbf{v}_2}$ and $\mathcal{C}_{\mathbf{v}_3}$, respectively, such that each graph will contain the critical points of the corresponding contour curve and the foot points associated with the critical points of the two other contour curves as its vertices. The algorithm for constructing the graphs of critical points having in addition some prescribed points as its vertices is described in Section 3.2. In what follows it is sufficient to use only one branch from each constructed graph of critical points – in particular, we will use $G(\mathcal{C}^+_{\mathbf{v}_1}), G(\mathcal{C}^+_{\mathbf{v}_2})$ and $G(\mathcal{C}^+_{\mathbf{v}_3})$.

Since the considered contour curves are related to canal surfaces originating in technical applications (i.e., with non-complicated topology), the individual graphs are the paths only. Thus, we can consider that $G(\mathcal{C}^+_{\mathbf{v}_1})$ is composed of the path $\mathbf{p}_1, \ldots, \mathbf{p}_k$, $G(\mathcal{C}^+_{\mathbf{v}_2})$

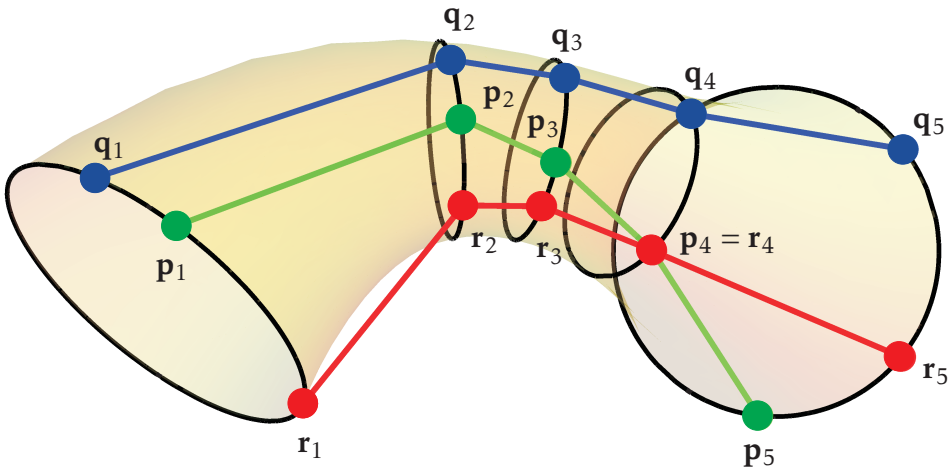

Figure 3.6: One branch from each constructed graph of critical points of contour curves.

of the path $\mathbf{q}_1,\dots,\mathbf{q}_k$, and $G(\mathcal{C}^+_{\mathbf{v}_3})$ of the path $\mathbf{r}_1,\dots,\mathbf{r}_k$ and being simultaneously satisfied that $\mathbf{p}_i,\mathbf{q}_i$ and $\mathbf{r}_i$ are the associated foot points, see Figure 3.6 for a particular example of the constructed graphs of critical points.

Remark 3.8. When reducing the graphs $G(\mathcal{C}_{\mathbf{v}_i})$, $i=1,2,3$, to $G(\mathcal{C}^+_{\mathbf{v}_i})$, it is convenient to omit from our further considerations the vertices which appeared in $G(\mathcal{C}_{\mathbf{v}_i})$ as the foot points associated to the critical points of $\mathcal{C}^-_{\mathbf{v}_i}$.

Our goal is to replace the edges $\mathbf{p}_i,\mathbf{p}_{i+1}\in G(\mathcal{C}^+_{\mathbf{v}_1})$, $\mathbf{q}_i,\mathbf{q}_{i+1}\in G(\mathcal{C}^+_{\mathbf{v}_2})$ and $\mathbf{r}_i,\mathbf{r}_{i+1}\in G(\mathcal{C}^+_{\mathbf{v}_3})$ by suitable Ferguson's cubics $\mathbf{f}_i$, $\mathbf{g}_i$ and $\mathbf{h}_i$, respectively, such that $\mathbf{f}_i$ is an approximate parameterization of the corresponding segment of $\mathcal{C}^+_{\mathbf{v}_1}$, $\mathbf{g}_i$ of $\mathcal{C}^+_{\mathbf{v}_2}$, $\mathbf{h}_i$ of $\mathcal{C}^+_{\mathbf{v}_3}$ and $\mathbf{f}_i$, $\mathbf{g}_i$ and $\mathbf{h}_i$ approximately correspond in parameter. This step will be formulated as an optimization process – when interpolating points $\mathbf{p}_i$, $\mathbf{p}_{i+1}$ and normalized tangent vectors $\mathbf{t}_{\mathbf{p}_i}$, $\mathbf{t}_{\mathbf{p}_{i+1}}$ at these points. We set the lengths of the tangent vectors at $\mathbf{p}_i$, $\mathbf{p}_{i+1}$ as free parameters α^1_i and α^2_i. By analogy we obtain parameter β^1_i,β^2_i and γ^1_i,γ^2_i. Now, we need to find such particular values of $\alpha^1_i,\alpha^2_i,\beta^1_i,\beta^2_i,\gamma^1_i,\gamma^2_i$ that the corresponding parameterizations will approximate the contour curves and simultaneously be approximately corresponding in parameter.

As a function which measures the deviation of the approximate parameterization $\mathbf{f}(t)$, $t\in[0,1]$ from their exact implicit representation $f=g=0$ we use the function (2.42), i.e.,

$$\Phi(f,g,\mathbf{f})=\int_0^1\left(\frac{f^2(\mathbf{f}(t)}{\|\nabla f(\mathbf{f}(t)\|^2}+\frac{g^2(\mathbf{f}(t)}{\|\nabla g(\mathbf{f}(t)\|^2}\right)\mathrm{d}t. \tag{3.18}$$

For our purposes, we construct

$$\Phi_1(\alpha_1,\alpha_2)=\Phi(f,f_{\mathbf{v}_1},\mathbf{f}),\quad \Phi_2(\beta_1,\beta_2)=\Phi(f,f_{\mathbf{v}_2},\mathbf{g}),\quad \Phi_3(\gamma_1,\gamma_2)=\Phi(f,f_{\mathbf{v}_3},\mathbf{h}), \tag{3.19}$$

In addition, we need a function measuring the deviance of the correspondence in parameter of the parameterizations $\mathbf{f}$, $\mathbf{g}$ and $\mathbf{h}$. The function responsible for the deviance

of the correspondence in parameter of the curves $\mathbf{f}$ and $\mathbf{g}$ lying on a canal surface $\mathcal{S}$ defined by the polynomial f will be taken as the distance of the intersection points of the normal lines of $\mathcal{S}$ at $\mathbf{f}$ and $\mathbf{g}$ with the bisector plane of $\mathbf{f}$ and $\mathbf{g}$ (see Figure 3.3, right), i.e.,

$$\Psi(\mathbf{f},\mathbf{g},f) = \int_0^1 \|\mathbf{b}_1 - \mathbf{b}_2\|^2 \,\mathrm{d}t, \tag{3.20}$$

where

$$\mathbf{b}_1 = \mathbf{f} + \frac{\|\mathbf{f}-\mathbf{g}\|^2}{2(\mathbf{g}-\mathbf{f})\cdot\nabla f(\mathbf{f})}\nabla f(\mathbf{f}) \quad \text{and} \quad \mathbf{b}_2 = \mathbf{g} + \frac{\|\mathbf{f}-\mathbf{g}\|^2}{2(\mathbf{f}-\mathbf{g})\cdot\nabla f(\mathbf{g})}\nabla f(\mathbf{g}). \tag{3.21}$$

Thus we arrive at two further objective functions:

$$\Psi_1(\alpha_1,\alpha_2,\beta_1,\beta_2) = \Psi(\mathbf{f},\mathbf{g},f), \quad \Psi_2(\alpha_1,\alpha_2,\gamma_1,\gamma_2) = \Psi(\mathbf{f},\mathbf{h},f). \tag{3.22}$$

To sum up, the global objective function will be of the form

$$\Upsilon(\alpha_i^1,\alpha_i^2,\beta_i^1,\beta_i^2,\gamma_i^1,\gamma_i^2) = (\Phi_1+\Phi_2+\Phi_3) + w(\Psi_1+\Psi_2) \tag{3.23}$$

for some weight w (in all presented examples we have chosen $w = 1$). In order to minimize Υ we used the Newton's iteration process. The whole method for computing approximate parameterizations of implicitly given canal surfaces is summarized in Algorithm 3.

Algorithm 3 Approximate parameterization of implicitly defined canal surface.

INPUT: Defining polynomial f of a canal surface $\mathcal{S}$.

1: Choose three linearly independent vectors $\mathbf{v}_1, \mathbf{v}_2, \mathbf{v}_3$;
2: Construct graphs $G(\mathcal{C}_{\mathbf{v}_1})$, $G(\mathcal{C}_{\mathbf{v}_2})$ and $G(\mathcal{C}_{\mathbf{v}_3})$ of critical points having the critical and its associated foot points of the contour curves $\mathcal{C}_{\mathbf{v}_1}$, $\mathcal{C}_{\mathbf{v}_2}$ and $\mathcal{C}_{\mathbf{v}_3}$ as its vertices;
3: Reduce the computed graphs to $G(\mathcal{C}^+_{\mathbf{v}_1})$, $G(\mathcal{C}^+_{\mathbf{v}_2})$ and $G(\mathcal{C}^+_{\mathbf{v}_3})$ only, i.e., consider the graphs reflecting only one of the two branches for each contour curve. Each graph is composed of $k-1$ edges (k vertices);
4: **for** each $i = 1, \dots, k-1$ **do**
5: Construct Ferguson's cubic $\mathbf{f}_i(t, \alpha_i^1, \alpha_i^2)$ matching the points $\mathbf{p}_i, \mathbf{p}_{i+1}$ (the vertices of the i-th edge of $G(\mathcal{C}^+_{\mathbf{v}_1})$) and the tangent vectors $\alpha_i^1 \mathbf{t}_{\mathbf{p}_i}, \alpha_i^2 \mathbf{t}_{\mathbf{p}_{i+1}}$;
6: Construct Ferguson's cubic $\mathbf{g}_i(t, \beta_i^1, \beta_i^2)$ matching the points $\mathbf{q}_i, \mathbf{q}_{i+1}$ (the vertices of the i-th edge of $G(\mathcal{C}^+_{\mathbf{v}_2})$) and the tangent vectors $\beta_i^1 \mathbf{t}_{\mathbf{q}_i}, \beta_i^2 \mathbf{t}_{\mathbf{q}_{i+1}}$;
7: Construct Ferguson's cubic $\mathbf{h}_i(t, \gamma_i^1, \gamma_i^2)$ matching the points $\mathbf{r}_i, \mathbf{r}_{i+1}$ (the vertices of the i-th edge of $G(\mathcal{C}^+_{\mathbf{v}_3})$) and the tangent vectors $\gamma_i^1 \mathbf{t}_{\mathbf{r}_i}, \gamma_i^2 \mathbf{t}_{\mathbf{r}_{i+1}}$;
8: Minimize the objective function $\Upsilon(\alpha_i^1, \alpha_i^2, \beta_i^1, \beta_i^2, \gamma_i^1, \gamma_i^2)$ to get the particular lengths of the tangent vectors $\mathbf{t}_{\mathbf{p}_i}, \mathbf{t}_{\mathbf{p}_{i+1}}, \mathbf{t}_{\mathbf{q}_i}, \mathbf{t}_{\mathbf{q}_{i+1}}, \mathbf{t}_{\mathbf{r}_i}, \mathbf{t}_{\mathbf{r}_{i+1}}$ – obtain the cubics $\mathbf{f}_i, \mathbf{g}_i$ and $\mathbf{h}_i$ approximating the contour curves;
9: Reconstruct the approximation of the spine curve of $\mathcal{S}$ from $\mathbf{f}_i, \mathbf{g}_i$ and $\mathbf{h}_i$, cf. (3.17);
10: Rotate $\mathbf{f}_i$ around the tangents of $\mathbf{m}_i$ – this yields the approximate parameterization $\mathbf{s}_i(t, u)$ of the corresponding part of $\mathcal{S}$;
11: **end for**

OUTPUT: The piecewise approximate parameterization $\mathbf{s}_1(t, u), \dots, \mathbf{s}_{k-1}(t, u)$.

Remark 3.9. Instead of minimizing the objective function $\Upsilon(\alpha_i^1, \alpha_i^2, \beta_i^1, \beta_i^2, \gamma_i^1, \gamma_i^2)$, one can firstly compute an approximate parameterization $\mathbf{f}$ of $\mathcal{C}^+_{\mathbf{v}_1}$ and then construct two new objective functions considering the other contour curves $\mathcal{C}^+_{\mathbf{v}_2}$ and $\mathcal{C}^+_{\mathbf{v}_3}$. Thus, we have altogether three objective functions, the first one is

$$\Upsilon_1(\alpha_1, \alpha_2) = \Phi(f, f_{\mathbf{v}_1}, \mathbf{f}). \tag{3.24}$$

Hence after minimizing $\Upsilon_1(\alpha_1, \alpha_2)$ the approximation $\mathbf{f}(t) = \mathbf{f}(t, \alpha_1, \alpha_2)$ of $\mathcal{C}^+_{\mathbf{v}_1}$ is computed and we formulate another two objective functions concerning $\mathcal{C}^+_y$ and $\mathcal{C}^+_z$:

$$\Upsilon_2(\beta_1, \beta_2) = \Phi(f, f_{\mathbf{v}_2}, \mathbf{g}) + \Psi(\mathbf{f}, \mathbf{g}, f), \tag{3.25}$$

and

$$\Upsilon_3(\gamma_1, \gamma_2) = \Phi(f, f_{\mathbf{v}_3}, \mathbf{h}) + \Psi(\mathbf{f}, \mathbf{h}, f). \tag{3.26}$$

The objective functions Υ_1, Υ_2 and Υ_3 can be minimized separately, which is less complicated since we minimize (integrate/evaluate) less complicated functions having only two variables. On the other hand when computing the "fixed" parameterization $\mathbf{f}$ first, the error is slightly bigger – our tests have shown that the error rises approximately ten times when using the simplified approach.

Remark 3.10. The deviance of the approximation $\mathbf{s}_i(t,u)$ from the implicitly given surface defined by a polynomial f can be again computed by integral (2.43) and when needed Algorithm 3 can be easily modified to perform the adaptive refinement similarly to the method presented in [8*]. It is enough to increase the number of the edges of the constructed graphs when needed.

The most difficult part of Algorithm 3 consists in step 2. Firstly, the critical points of the contour curves have to be computed and secondly, for each critical point the associated foot points have to be found. Let us consider that the point $\mathbf{p}_1 \in \mathcal{C}^+_{\mathbf{v}_1}$ is known. We shall find points $\mathbf{p}_2 \in \mathcal{C}^-_{\mathbf{v}_1}$, $\mathbf{q}_1, \mathbf{q}_2 \in \mathcal{C}_{\mathbf{v}_2}$ and $\mathbf{r}_1, \mathbf{r}_2 \in \mathcal{C}_{\mathbf{v}_3}$ such that $\mathbf{p}_1, \mathbf{p}_2, \mathbf{q}_1, \mathbf{q}_2, \mathbf{r}_1, \mathbf{r}_2$ are the associated foot points, i.e., they lie on the same characteristic circle.

Clearly, from property (2.33) the associated foot point $\mathbf{p}_2 \in \mathcal{C}^-_{\mathbf{v}_1}$ lies in the plane going through $\mathbf{p}_1$ and having the normal vector equal to $\mathbf{v}_1$. Thus we arrive at the points $\mathbf{p}_2^1, \ldots, \mathbf{p}_2^s$ by intersecting the curve $\mathcal{C}_{\mathbf{v}_1}$ with that plane, i.e. we solve the system of non-linear equations

$$f(\mathbf{x}) = 0, \quad f_{\mathbf{v}_1}(\mathbf{x}) = 0, \quad \mathbf{v}_1 \cdot (\mathbf{x} - \mathbf{p}_1) = 0. \tag{3.27}$$

Now, we have to choose the right point $\mathbf{p}_2 = \mathbf{p}_2^i$ from the set of points $\mathbf{p}_2^1, \ldots, \mathbf{p}_2^s$. For this we use the fact that the normal lines of $\mathcal{S}$ at the points $\mathbf{p}_1$ and $\mathbf{p}_2$ have to intersect at the point $\mathbf{m}$ such that $\|\mathbf{p}_1 - \mathbf{m}\| = \|\mathbf{p}_2 - \mathbf{m}\|$.

Thus, we have the points $\mathbf{p}_1 \in \mathcal{C}^+_{\mathbf{v}_1}$ and $\mathbf{p}_2 \in \mathcal{C}^-_{\mathbf{v}_1}$, i.e., the points lying on the same characteristic circle. By cutting the remaining critical curves $\mathcal{C}_{\mathbf{v}_2}$ and $\mathcal{C}_{\mathbf{v}_3}$ by the planes $\mathbf{v}_2 \cdot (\mathbf{x} - \mathbf{m}) = 0$ and $\mathbf{v}_3 \cdot (\mathbf{x} - \mathbf{m}) = 0$ (where $\mathbf{m}$ is the intersection point of the normal lines of $\mathcal{S}$ at the points $\mathbf{p}_1$ and $\mathbf{p}_2$) we arrive at the associated foot points $\mathbf{q}_1, \mathbf{q}_2 \in \mathcal{C}_y$ and $\mathbf{r}_1, \mathbf{r}_2 \in \mathcal{C}_z$, respectively. Finally, as in the previous step the "right" points need to be chosen as the points having the same distance from $\mathbf{m}$ as $\mathbf{p}_1$ and $\mathbf{p}_2$ have and all six lie in the same plane.

As in the previous method we deal with the canal surface given only in some prescribed area of interest, hence we have to consider the boundary points in the algorithm.

Proposition 3.11. *Algorithm 3 yields a G^1 continuous rational parameterization of the maximal rational degree $[7,4]$ in t and $[2,2]$ in u.*

Proof. In Algorithm 3, the parameterizations of contour curves are polynomial G^1 continuous parameterizations of degree 3 in t; so is the parameterization of the spine curve, cf. (3.17). Hence, using (2.30) we arrive at a G^1 continuous parameterization of the canal surface having the maximal rational degree $[7,4]$ in t. The rational degree of the parameterization in u depends on the choice of the rational function $\varphi(u)$; the choice $\varphi(u) = u$ leads to the rational degree $[2,2]$ in u. □

Example 3.12. Let us consider the following cubic polynomial parameterizations of the contour curves:

$$\mathbf{c}_x^+ = \mathbf{c}_z^- = (t^3, 0, t)^\top \quad \text{and} \quad \mathbf{c}_y^- = (t^3, t, 0)^\top. \tag{3.28}$$

Then the parameterization of the spine curve (using (3.16)) is of the form

$$\mathbf{m} = (t^3, t, t)^\top. \tag{3.29}$$

It is easy to certify that formula 2.32 is fulfilled, i.e., the parameterizations $\mathbf{c}_x^+$, $\mathbf{c}_y^-$ and $\mathbf{c}_z^-$ are corresponding in parameter with $\mathbf{m}$ (and hence also mutually). Rotating $\mathbf{c}_x^+$ around the tangents of $\mathbf{m}$ (using formula (2.30)) yields the following rational parameterization of the corresponding canal surface

$$\mathbf{s}(t,u) = \left(\frac{9t^7 + t^3\left(u^2-4\right) + 2tu}{9t^4+u^2+2}, \frac{2\left(9t^5+t\right)}{9t^4+u^2+2}, \frac{t\left(u-3t^2\right)^2}{9t^4+u^2+2} \right)^\top \tag{3.30}$$

having bidegree $(7,2)$.

Example 3.13. We parameterize the implicit canal surface $\mathcal{S}$ given by the polynomial

$$\begin{aligned} f = \; & 16x^6 + 48x^4y^2 + 16x^4z^2 - 160x^4z - 32x^4 - 288x^3yz - 288x^3y + 288x^3z + 288x^3 + \\ & 48x^2y^4 + 32x^2y^2z^2 - 104x^2y^2z - 280x^2y^2 + 144x^2yz + 1008x^2y - 128x^2z^3 + 480x^2z^2 - \\ & 168x^2z - 776x^2 - 288xy^3z + 360xy^3 + 288xy^2z + 72xy^2 - 256xyz^3 + 384xyz^2 + \\ & 672xyz - 1480xy + 256xz^3 - 384xz^2 - 672xz + 1048x + 16y^6 + 16y^4z^2 + 56y^4z - \\ & 59y^4 + 144y^3z - 180y^3 + 64y^2z^3 + 192y^2z^2 - 672y^2z + 334y^2 + 128yz^3 - 192yz^2 - \\ & 336yz + 524y + 256z^4 - 704z^3 + 240z^2 + 808z - 635 \end{aligned}$$

in the region bounded by the planes

$$\mathcal{P}_1 : \; 8x + 4y - 12z + 57 = 0 \quad \text{and} \quad \mathcal{P}_2 : \; 8x + 4y + 4z - 11 = 0. \tag{3.31}$$

In particular, we are interested in the part of $\mathcal{S}$ in the region fulfilling $\mathcal{P}_1 > 0$ and $\mathcal{P}_2 < 0$, see Figure 3.7 (left). First, we determine the contour curves w.r.t. the standard basis vectors (3.2), i.e., the curves defined by $f = f_x = 0$, $f = f_y = 0$ and $f = f_z = 0$. The next step is to compute the critical and bounding points of those curves, and to each of those points compute the associated foot points (the points lying on the same characteristic circles and on the other two contour curves). Then we construct the graph having those computed points as vertices and choose only one branch from each contour curve. Deleting redundant points (foot points corresponding to the critical points on the second, not chosen, branches of the contour curves) yields the graph of critical points. In this particular example the graph of critical points is composed of the following three paths:

$$\begin{aligned} G(\mathcal{C}_x^+) &= \left(\left(-3, 1, \frac{9}{4}\right)^\top, \left(-1, 1, \frac{1}{4}\right)^\top, (0,1,0)^\top, \left(1, 1, \frac{1}{4}\right)^\top \right); \\ G\left(\mathcal{C}_y^+\right) &= \left(\left(\frac{-34-15\sqrt{3}}{13}, -\frac{3}{2}, \frac{87-40\sqrt{3}}{52} \right)^\top, \left(-1, -\frac{1}{2}, -\frac{5}{4}\right)^\top, \right. \\ &\quad \left. \left(\frac{1}{2}, 0, -\frac{\sqrt{3}}{2}\right)^\top, \left(\frac{7}{5}, \frac{1}{2}, -\frac{1}{20}\right)^\top \right); \\ G(\mathcal{C}_z^+) &= \left(\left(-1, -3, \frac{9}{4}\right)^\top, \left(\frac{1}{5}, -\frac{7}{5}, \frac{1}{4}\right)^\top, \left(\frac{4}{5}, -\frac{3}{5}, 0\right)^\top, \left(\frac{7}{5}, \frac{1}{5}, \frac{1}{4}\right)^\top \right). \end{aligned}$$

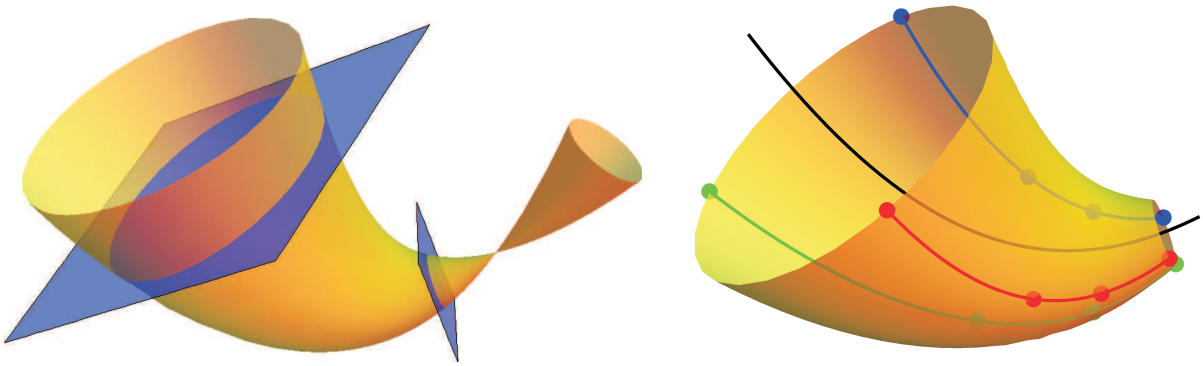

Figure 3.7: Implicitly given canal surface (yellow) together with the bounding planes (blue), left and the parameterized part of a implicitly given canal surface together with the spine and contour curves and the bounding, critical and its associated foot points, right from Example 3.13.

Next we compute the parameterizations **f**, **g** and **h** of the chosen branches of the contour curves such that we replace the edges of the corresponding graph of critical points by Ferguson's cubics and minimize the objective functions (3.23). Finally, we reconstruct the approximation **m** of the spine curve and by rotation of the one of the contour curves, e.g. **f** around the tangents of the spine curve **m** we obtain an approximate parameterization of the canal surface in the given region. The parameterized part of the canal surface with the contour and spine curves and the vertices of the graph of critical points is shown in Figure 3.7 (right). The error of the approximation, measured by integral (2.43), is less than $6 \cdot 10^{-5}$.

Chapter 4

Rational canal surfaces with rational contour curves

In this chapter, we will study a condition which guarantees that a given canal surface has rational contour curves. These curves are then used for a computation of rational parameterizations providing rational offsets. To document a practical usefulness of the presented approach, we design simple direct algorithms for computing rational offset blends between two canal surfaces based on the contour method. A main advantage of the designed blending technique is its simplicity and especially its usefulness for constructing blends satisfying certain constrains, e.g. when avoiding obstacles or bypassing other objects is required. Compared to other methods our approach needs only one SOS decomposition or MPH interpolation for the whole family of rational canal surfaces sharing the same silhouette, see Figure 4.1. The papers in which the author of the thesis participated and which contain the author's main contribution to this topic are – [9], [13*].*

4.1 Motivation – parameterizations derived from rational curves on canal surfaces

Let us assume that the spine curve and one curve (corresponding in parameter with the spine curve) on the canal surface are given. We have to emphasize one important fact, i.e., it is not generally guaranteed that the obtained rational parameterization fulfills the PN condition. As known, all surfaces of revolution are canal surfaces – the next simple example demonstrates a situation when a rational parameterization of a canal surface does not fulfill the PN condition.

Example 4.1. Let us consider two lines given by the parametric equations

$$\mathbf{m}(t) = (t, 0, t)^\top \quad \text{and} \quad \mathbf{c}(t) = (t, 1, 1)^\top, \quad t \in \mathbb{R} \tag{4.1}$$

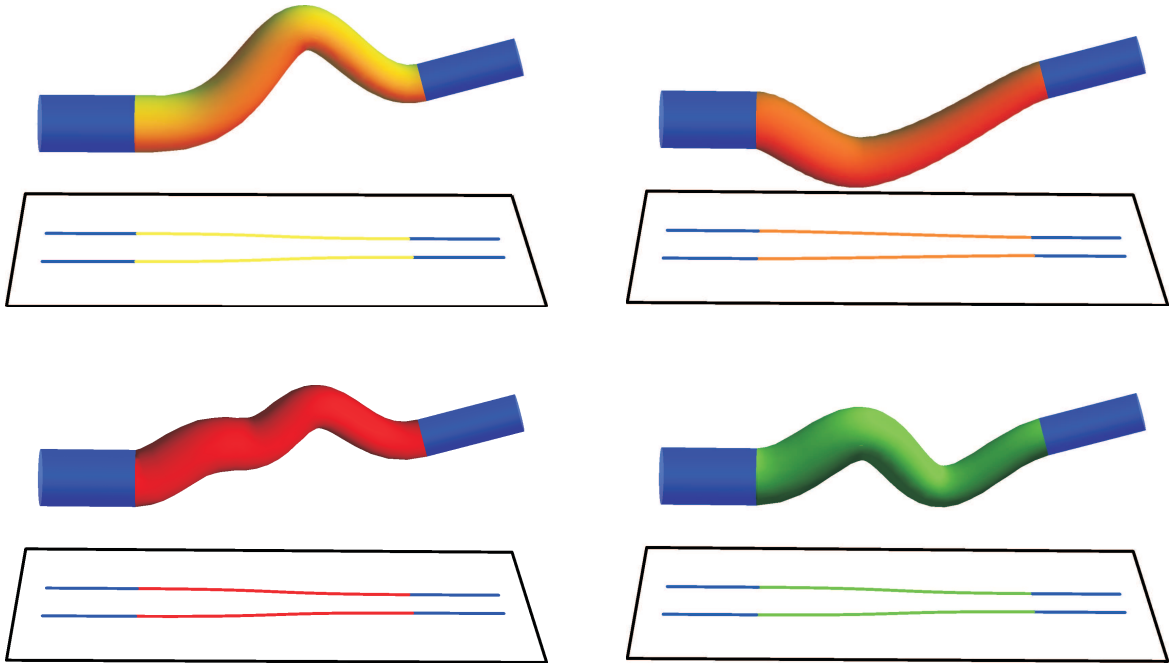

Figure 4.1: Adaptive blend surface(s) (yellow, orange, red, green) between two cylinders (blue) sharing the same silhouette w.r.t. a prescribed projection.

such that $\mathbf{c}$ corresponds in parameter with $\mathbf{m}$ since

$$(\mathbf{m}-\mathbf{c})^{\top}\cdot\mathbf{c}' = (0,-1,-1+t)\cdot(1,0,0)^{\top} = 0. \tag{4.2}$$

In this chapter we multiply vectors and matrices and hence for the sake of clarity '$\cdot$' will be taken only as the matrix product. Rotating $\mathbf{c}$ around the tangents of $\mathbf{m}$ yields the following parameterization of the canal surface:

$$\mathbf{s}(t,u) = \left(\frac{tu^2-2u+2}{u^2+2}, \frac{2(t-1)u+u^2-2}{u^2+2}, \frac{2t+u^2+2u}{u^2+2}\right)^{\top}. \tag{4.3}$$

Although $\mathbf{s}(t,u)$ obtained by formula (2.30) is rational it is not PN since the corresponding area element

$$\sigma(t,u)^2 = \frac{4\left(t^2-2t+2\right)}{\left(u^2+2\right)^2} \tag{4.4}$$

is not a perfect square, i.e., the PN condition is not satisfied.

It is a well-known fact that all canal surfaces with rational MATs are PN surfaces (i.e., surfaces with rational offsets) – this can be easily justified by realizing that the δ-offsets to any rational canal surface $(\mathbf{m},r)^{\top}$ are again rational canal surfaces given by rational $(\mathbf{m},r\pm\delta)^{\top}$. So the question reads why the rational parameterization of the canal surface from Example 4.1 is not PN. Firstly, we compute the corresponding MAT

$$\overline{\mathbf{m}}(t) = \left(t,0,t,\sqrt{t^2-2t+2}\right)^{\top}. \tag{4.5}$$

We can see that this MAT is non-rational; in particular the spine curve is rational but the radius function is not. We will investigate this observation in more detail.

As the vector $\mathbf{n} = \mathbf{c} - \mathbf{m}$ is a normal vector of the canal surface $\mathcal{S}$ at the point $\mathbf{s}(t,1)$ then the unit normal vector field of $\mathcal{S}$ can be easily computed by rotating

$$\frac{\mathbf{c}-\mathbf{m}}{\|\mathbf{c}-\mathbf{m}\|} \tag{4.6}$$

around the tangents of $\mathbf{m}$ using (2.30). Furthermore, assuming that $\|\mathbf{c}-\mathbf{m}\|$ (which is nothing else than r) is a rational function we can compute the rational unit normal vector field of $\mathcal{S}$, and thus the corresponding parameterization $\mathbf{s}(t,u)$ of the canal surface $\mathcal{S}$ (obtained by formula (2.30)) is PN. To sum up, rational parameterizations of canal surfaces obtained by (2.30) such that the spine curve is rational but the radius function is non-rational do not satisfy the PN condition.

To reformulate this PN condition problem, if a rational MAT $\overline{\mathbf{m}} = (\mathbf{m}, r)^{\top}$ is given then we have to find a rational curve $\mathbf{f}$ on the unit sphere (see (4.6)) such that the corresponding curve $\mathbf{c} = \mathbf{m} + r\mathbf{f}$ on the canal surface corresponds in parameter with $\mathbf{m}$. This can be equivalently written as

$$\mathbf{f}^{\top} \cdot \mathbf{m}' + r' \equiv 0, \tag{4.7}$$

which is a equation solved in [59, 68]. Considering the explicit formula for all rational curves $\mathbf{f}$ on the unit sphere (see [27])

$$\mathbf{f}(t) = \left(\frac{2(p_0p_1 - p_2p_3)}{p_0^2+p_1^2+p_2^2+p_3^2}, \frac{2(p_0p_2 + p_1p_3)}{p_0^2+p_1^2+p_2^2+p_3^2}, \frac{p_1^2+p_2^2-p_0^2-p_3^2}{p_0^2+p_1^2+p_2^2+p_3^2} \right)^{\top}, \tag{4.8}$$

where $p_0(t), p_1(t), p_2(t), p_3(t) \in \mathbb{R}[t]$, we arrive at the condition

$$\begin{aligned} 2(p_0p_1 - p_2p_3)\,m_1' + 2(p_0p_2 + p_1p_3)\,m_2' + \\ + \left(p_1^2+p_2^2-p_0^2-p_3^2\right)m_3' + \left(p_0^2+p_1^2+p_2^2+p_3^2\right)r' = 0. \end{aligned} \tag{4.9}$$

Nevertheless the choice of the polynomials p_0, p_1, p_2, p_3 such that condition (4.9) is satisfied is a non-trivial problem. We will discuss it for some purposely selected curves in Section 4.2.1.

4.2 Rational contour curves on canal surfaces

It was shown in the previous section that the rationality of a curve $\mathbf{c} \subset \mathcal{S}$ corresponding in parameter with a rational spine curve $\mathbf{m}$ does not have to guarantee the PN property of the parameterization $\mathbf{s}$ of the obtained canal surface $\mathcal{S}$. Now, we will study contour curves on $\mathcal{S}$ with the property that if they are rational then $\mathbf{s}$ is a PN parameterization.

4.2.1 Rational contour curves w.r.t. the directions of the coordinate axes

According to formula (2.18) the parameterizations of the branches of the contour curve w.r.t. the coordinate vector $\mathbf{e}_3 = (0,0,1)^\top$ (z-contour curve) corresponding in parameter with $\mathbf{m}$ are of the form

$$\mathbf{c}_z^{\pm}(t) = \mathbf{m} - r\frac{r'\overset{\triangledown}{\mathbf{m}}' \pm \overset{\triangledown}{\mathbf{m}}'^{\perp}\sqrt{\|\overset{\triangledown}{\mathbf{m}}'\|^2 - r'^2}}{\|\overset{\triangledown}{\mathbf{m}}'\|^2}, \tag{4.10}$$

where $\overset{\triangledown}{\mathbf{m}}' = (m_1', m_2', 0)^\top$ and $\overset{\triangledown}{\mathbf{m}}'^{\perp} = (-m_2', m_1', 0)^\top$. By analogy we can define x- and y-contour curves, i.e., contour curves w.r.t. $\mathbf{e}_1 = (1,0,0)^\top$ and $\mathbf{e}_2 = (0,1,0)^\top$, respectively.

It follows from (4.10) that for $(m_1, m_2, r)^\top$ being an MPH curve in $\mathbb{R}^{2,1}$ the branches $\mathbf{c}_z^{\pm}$ of the z-contour curve corresponding in parameter with $\mathbf{m}$ are rational curves. Moreover since the corresponding normal vectors are

$$\mathbf{n}^{\pm}(t,1) = \frac{\mathbf{c}_z^{\pm} - \mathbf{m}}{\|\mathbf{c}_z^{\pm} - \mathbf{m}\|} = -\frac{r'\overset{\triangledown}{\mathbf{m}}' \pm \overset{\triangledown}{\mathbf{m}}'^{\perp}\sqrt{\|\overset{\triangledown}{\mathbf{m}}'\|^2 - r'^2}}{\|\overset{\triangledown}{\mathbf{m}}'\|^2}, \tag{4.11}$$

the parameterization of the canal surface computed by rotating the points of the $\mathbf{c}_z$ around the tangents of $\mathbf{m}$ is PN.

Our further considerations are motivated by the ideas from [49] (see Lemma 5) where the interplay between spatial MPH curves and planar PH curves is thoroughly investigated. Before we continue we introduce, for the sake of clarity, some projections which relate MAT of $\mathcal{S}$ with several other curves. For the given medial axis transform $\overline{\mathbf{m}} = (m_1, m_2, m_3, r)^\top \subset \mathbb{R}^{3,1}$, the spine curve is $\mathbf{m} = (m_1, m_2, m_3)^\top \subset \mathbb{R}^3$ and $\mathbf{c}^{\pm} = (c_1^{\pm}, c_2^{\pm}, m_3)^\top \subset \mathbb{R}^3$ is the associated contour curve corresponding in parameter. The resulting canal surface $\mathcal{S}$ is obtained as the envelope by the mapping γ_1, which is the well-known cyclographic mapping $\mathbb{R}^{3,1} \to \mathbb{R}^3$ studied e.g. in the context of Laguerre geometry, see [69, 71]. Projecting the curves $\mathbf{m}, \mathbf{c}^{\pm}$ to plane $\mathbb{R}^2$ by the mapping π_2 we obtain the curves $\widehat{\mathbf{m}} = (m_1, m_2)^\top$ and $\widehat{\mathbf{c}}^{\pm} = (c_1^{\pm}, c_2^{\pm})^\top$. Finally, MAT of the the planar domain bounded by $\widehat{\mathbf{c}}^{\pm}$ will be denoted by $\widetilde{\mathbf{m}} = (m_1, m_2, r)^\top \subset \mathbb{R}^{2,1}$ (conversely, $\widehat{\mathbf{c}}^{\pm}$ are obtained from $\widetilde{\mathbf{m}}$ as envelopes via the cyclographic mapping $\gamma_2 : \mathbb{R}^{2,1} \to \mathbb{R}^2$). For the sake of completeness we introduce the mapping π_1 sending $\overline{\mathbf{m}} \subset \mathbb{R}^{3,1}$ to $\widetilde{\mathbf{m}} \subset \mathbb{R}^{2,1}$. See Figure 4.2 for all relations.

As proved in [49], $\widetilde{\mathbf{m}} \subset \mathbb{R}^{2,1}$ is an MPH curve iff the associated $\widehat{\mathbf{c}}^{\pm} \subset \mathbb{R}^2$ is a PH curve. Hence we immediately arrive at

Proposition 4.2. *The parameterization* $\mathbf{s}$ *of the canal surface* $\mathcal{S}$ *defined by the medial axis transform* $\overline{\mathbf{m}}$ *and obtained by rotating the points of e.g.* $\mathbf{c}^+$ *around the tangents of* $\mathbf{m}$ *is PN if* $\widehat{\mathbf{c}}^+$ *is a planar PH curve.*

Remark 4.3. When a polynomial MAT is given such that it holds

$$\widetilde{\mathbf{m}}(t) = \left(\int (ln - km)\,\mathrm{d}t, \int (kn + lm)\,\mathrm{d}t, \int (lm - kn)\,\mathrm{d}t\right)^\top, \tag{4.12}$$

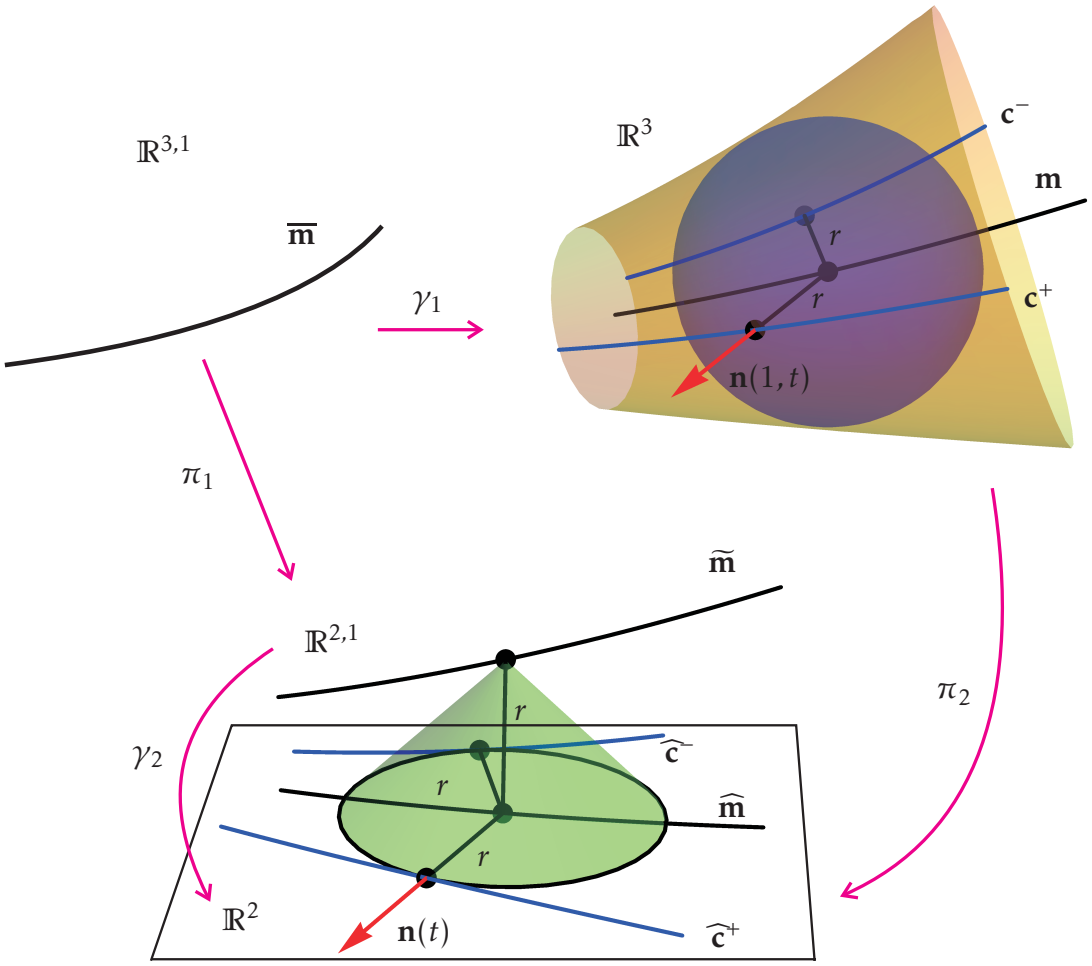

Figure 4.2: Demonstration of the rationality of unit normal vector field of a given canal surface.

cf. (2.24), then the substitution

$$p_0 = k, \quad p_1 = l, \quad p_2 = k, \quad p_3 = -l \tag{4.13}$$

into formula (4.8) leads to the corresponding rational z-contour curve $\mathbf{c} = \mathbf{m} + r\mathbf{f}$.

Example 4.4. Let us consider the medial axis transform

$$\overline{\mathbf{m}}(t) = \left(-3t^2, -3t + t^3, t, 3t + t^3\right)^{\top}. \tag{4.14}$$

One can easily show that $\widetilde{\mathbf{m}}(t) = \left(-3t^2, -3t + t^3, 3t + t^3\right)^{\top}$ is a spatial MPH curve, and the associated curve

$$\widehat{\mathbf{c}}^+(t) = \left(-\frac{t^2\left(t^2-3\right)}{t^2+1}, -\frac{4t^3}{t^2+1}\right)^{\top} \tag{4.15}$$

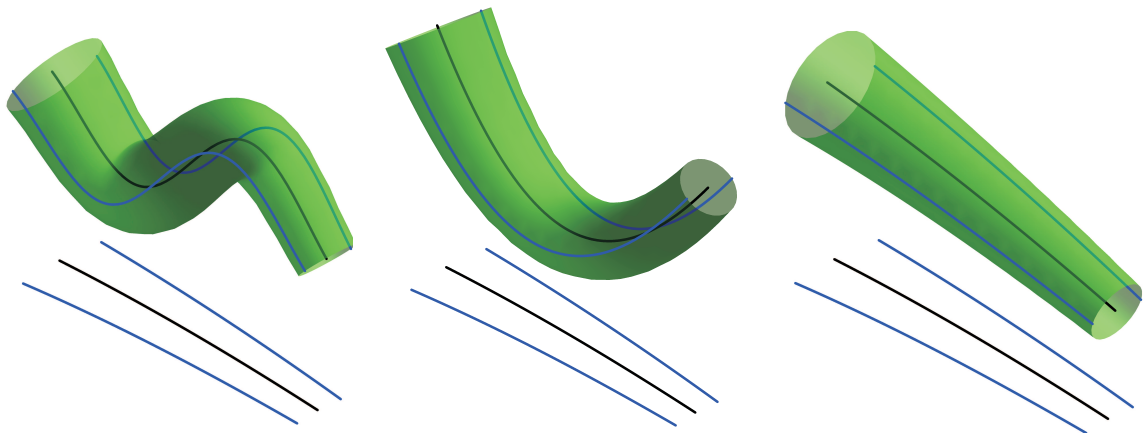

Figure 4.3: Three canal surfaces with PN parameterizations computed for the MATs having the same first two coordinates m_1, m_2 and the radius function r but different in the third coordinate m_3.

is a planar PH curve. Rotating the corresponding contour curve $\mathbf{c}^+$ along the tangents of $\mathbf{m}$ yields the canal surface with the the area element in the form

$$\sigma^2(t,u) = \left(\frac{2t\left(t^2+3\right)\left(3t^4+12t^3u+18t^2+36tu-u^2-10\right)}{\left(9t^4+18t^2+u^2+10\right)^2} \right)^2, \tag{4.16}$$

i.e., $\mathbf{s}(t,u)$ is a PN parameterization.

The previous observation (combined with the approach from [49]) suggests a simple modeling technique with PN canal surfaces. It is enough to construct a certain planar PH curve, i.e., $\widehat{\mathbf{c}}^+$, and then to choose two rational functions r and m_3 to obtain a suitable canal surface described by a rational offset parameterization. This offers a sufficient flexibility for modeling purposes. Figure 4.3 shows three canal surfaces with PN parameterizations sharing the same $\widetilde{\mathbf{m}} \subset \mathbb{R}^{2,1}$ (and thus also $\widehat{\mathbf{c}}^{\pm} \subset \mathbb{R}^2$) but differing in m_3.

Of course, a special role among all canal surfaces (especially because of application purposes) is played by those having the polynomial MATs. The approach from [50] shows how to get polynomial $\widetilde{\mathbf{m}}$ from polynomial $\widehat{\mathbf{c}}^{\pm}$, see (2.25). Hence, we obtain that any polynomial MAT in $\mathbb{R}^{3,1}$ of a canal surface $\mathcal{S}$ which gives a polynomial contour curve with respect to the xy-plane can be expressed in the form

$$\overline{\mathbf{m}} = \left(\int m(k^2-l^2)\,\mathrm{d}t + 2pmkl, \int 2mkl\,\mathrm{d}t - pm(k^2-l^2), q, pm(k^2+l^2) \right)^{\top}, \tag{4.17}$$

where $k(l), l(t), m(t), p(t), q(t)$ are arbitrary non-zero polynomials such that $k(t), l(t)$ are relatively prime, cf. (2.25) and (2.9).

The canal surfaces obtained from polynomial MATs in the form (4.17) by rotating the points of the associated polynomial contour curve along the corresponding tangents of

the spine curve are rational PN surfaces with the rational degree

$$(\max\{3d_1+3d_2-5,3d_3-2\},\max\{2d_1+2d_2-4,2d_3-2\}) \text{ in } t \quad \text{and} \quad (2,2) \text{ in } u, \tag{4.18}$$

where d_1 is the degree of the polynomial PH curve $\widehat{\mathbf{c}^+}$, d_2 is the degree of the polynomial p and d_3 is the degree of the polynomial q.

Remark 4.5. When a polynomial MAT is given by (4.17), then the substitution

$$p_0=-l, \quad p_1=k, \quad p_2=l, \quad p_3=k, \tag{4.19}$$

into formula (4.8) leads to the corresponding polynomial contour curve $\mathbf{c}=\mathbf{m}+r\mathbf{f}$.

Example 4.6. Let us consider the contour curve

$$\mathbf{c}^+(t)=\left(3t+3t^2,3t^2+2t^3,1\right)^\top. \tag{4.20}$$

It can be obtained by appending $q=1$ as the z-coordinate to the PH curve gained from formula (2.9) by setting $k=t+1$, $l=t$ and $m=3$. Then by choosing e.g. $p=1-t$ into (4.17) we arrive at the polynomial MAT

$$\overline{\mathbf{m}}(t)=\left(9t+3t^2-6t^3,-3-3t+9t^2+2t^3,1,3+3t-6t^3\right)^\top. \tag{4.21}$$

Rotating $\mathbf{c}^+$ along the tangents of $\mathbf{m}$ yields the PN parameterization of the canal surface.

Example 4.7. Let us consider a canal surface defined by the following quintic MAT

$$\mathbf{m}(t)=\Big(\frac{1}{225}\left(-24t^5+65t^3+15t^2-150t\right),\frac{1}{225}\left(-57t^5-80t^3-105t^2-75t\right),\\ \frac{1}{90}\left(6t^5+10t^3-15t^2+60t\right),\frac{1}{30}\left(-6t^5+10t^3+15t^2\right)\Big)^\top, \tag{4.22}$$

we arrive at the conclusion that the contour curves w.r.t. the axis directions are not rational since

$$m_i'^2+m_j'^2-r'^2\neq\sigma^2 \tag{4.23}$$

for any $i,j\in\{1,2,3\}$, $i\neq j$. However when considering contour curves w.r.t. a general vector (not only the directions of the coordinate axes) we can obtain a rational contour curve, see Example 4.10 in the following section.

4.2.2 Rational contour curves w.r.t. a general direction

In this section we generalize the condition for the rationality of the contour curves w.r.t. a general vector. For computing the parameterizations $\mathbf{c}_\mathbf{v}^\pm$ of the both branches of the contour curve $\mathcal{C}_\mathbf{v}$ w.r.t. the general vector $\mathbf{v}$ on the canal surface given by its MAT, we orthogonally project the spine curve $\mathbf{m}$ to a plane $\nu_\mathbf{v}$ going through the origin and having the normal vector $\mathbf{v}$. Then we compute the parameterization of the projection of the contour curve and lift it back.

The orthogonal projection $\pi_{\mathbf{v}} : \mathbb{R}^3 \to \nu_{\mathbf{v}}$ is realized as follows:

$$\pi_{\mathbf{v}}(\mathbf{m}) = \mathbf{m} - (\mathbf{m}^\top \cdot \mathbf{v})\mathbf{v}. \tag{4.24}$$

According to (4.10) the contour curve w.r.t. the vector $\mathbf{v}$ possesses the following parameterization

$$\mathbf{c}_{\mathbf{v}}^{\pm} = \mathbf{m} - r\frac{r'\,\pi_{\mathbf{v}}(\mathbf{m})' \pm (\pi_{\mathbf{v}}(\mathbf{m})' \times \mathbf{v})\sqrt{\|\pi_{\mathbf{v}}(\mathbf{m})'\|^2 - r'^2}}{\|\pi_{\mathbf{v}}(\mathbf{m})'\|^2}. \tag{4.25}$$

After some simplifications we obtain

$$\mathbf{c}_{\mathbf{v}}^{\pm} = \mathbf{m} - r\,\frac{r'(\mathbf{m}' - \mathbf{v}(\mathbf{m}'^\top \cdot \mathbf{v})) \pm (\mathbf{m}' \times \mathbf{v})\sqrt{\|\mathbf{m}'\|^2 - (\mathbf{m}'^\top \cdot \mathbf{v})^2 - r'^2}}{\|\mathbf{m}'\|^2 - (\mathbf{m}'^\top \cdot \mathbf{v})^2}. \tag{4.26}$$

Proposition 4.8. *The general contour curve* (4.26) *of the canal surface defined by the medial axis transform* $\overline{\mathbf{m}} = (\mathbf{m}, r)^\top$ *is rational iff there exists a rational function* σ *such, that*

$$\|\mathbf{m}'\|^2 - (\mathbf{m}'^\top \cdot \mathbf{v})^2 - r'^2 = \sigma^2. \tag{4.27}$$

Moreover, since the unit normal vectors of the given canal surface along $\mathbf{c}_{\mathbf{v}}^{\pm}$ are of the form

$$\mathbf{n}_{\mathbf{v}}^{\pm} = \frac{\mathbf{c}_{\mathbf{v}}^{\pm} - \mathbf{m}}{\|\mathbf{c}_{\mathbf{v}}^{\pm} - \mathbf{m}\|} = -\frac{r'(\mathbf{m}' - \mathbf{v}(\mathbf{m}'^\top \cdot \mathbf{v})) \pm (\mathbf{m}' \times \mathbf{v})\sqrt{\|\mathbf{m}'\|^2 - (\mathbf{m}'^\top \cdot \mathbf{v})^2 - r'^2}}{\|\mathbf{m}'\|^2 - (\mathbf{m}'^\top \cdot \mathbf{v})^2} \tag{4.28}$$

the parameterization of the canal surface yields the associated Pythagorean normals, see the following proposition

Proposition 4.9. *The parameterizations* $\mathbf{s}^{\pm}$ *of the canal surface defined by* $\overline{\mathbf{m}} = (\mathbf{m}, r)^\top$ *computed by rotating the points of the contour curve* $\mathbf{c}_{\mathbf{v}}^{\pm}$ *around the tangents of* $\mathbf{m}$ *is PN iff there exists a rational function* σ *such, that condition* (4.27) *is satisfied.*

Example 4.10. The canal surface from Example 4.7 does not possess rational contour curves w.r.t. any direction of the coordinate axes. Nevertheless for the unit vector

$$\mathbf{v} = \left(-\frac{2}{3}, -\frac{1}{3}, \frac{2}{3}\right)^\top \tag{4.29}$$

we get

$$\|\mathbf{m}'\|^2 - (\mathbf{m}'^\top \cdot \mathbf{v})^2 - r'^2 = \left(2t^3 + t^2\right)^2, \tag{4.30}$$

and hence the associated general contour curve w.r.t. the vector $\mathbf{v}$ is rational, cf. (4.27).

Remark 4.11. Let us recall that for z-contour curves, i.e., for the contour curves w.r.t. the vector $\mathbf{e}_3$, condition (4.27) degenerates to the following MPH-condition in $\mathbb{R}^{2,1}$, see (4.10)

$$m_1'^2 + m_2'^2 - r'^2 = \sigma^2. \tag{4.31}$$

Using explicit formula (4.28) for the unit normal vectors of the given canal surface along $\mathbf{c}_{\mathbf{v}}^{\pm}$ we can immediately write down a parameterization of the given canal surface derived from quaternion formula (2.30) in the form

$$\mathbf{s}^{\pm} = \mathbf{m} + r\frac{\rho^2\mathbf{n}_{\mathbf{v}}^{\pm} + 2\rho\,(\mathbf{m}' \times \mathbf{n}_{\mathbf{v}}^{\pm}) + \mathbf{m}' \times (\mathbf{m}' \times \mathbf{n}_{\mathbf{v}}^{\pm}) - r'\mathbf{m}'}{\|\mathbf{m}'\|^2 + \rho^2}. \tag{4.32}$$

Remark 4.12. The curves in $\mathbb{R}^{3,1}$ satisfying condition (4.27) are the Pythagorean hodograph (PH) curves in 4-dimensional space w.r.t. the inner product defined by the matrix

$$\mathbf{A} = \begin{pmatrix} \mathbf{I} - \mathbf{v}\cdot\mathbf{v}^{\top} & \mathbf{o} \\ \mathbf{o}^{\top} & -1 \end{pmatrix}, \tag{4.33}$$

where $\mathbf{o} = (0,0,0)^{\top}$. Thus we can write

$$\overline{\mathbf{m}}'^{\top} \cdot \mathbf{A} \cdot \overline{\mathbf{m}}' = \|\mathbf{m}'\|^2 - (\mathbf{m}'^{\top} \cdot \mathbf{v})^2 - r'^2. \tag{4.34}$$

Remark 4.13. Condition (4.27) actually means that the projection $\pi_{\mathbf{v}}(\mathbf{m})$ of the spine curve $\mathbf{m}$ to the plane ν together with the radius function r form a rational MPH curve. This is satisfied if r is a rational function and the projection $\pi_{\mathbf{v}}(\mathbf{c}_{\mathbf{v}})$ of the contour curve $\mathbf{c}_{\mathbf{v}}$ is a rational PH curve.

Now, the natural question reads as follows: What the curves satisfying condition (4.27) look like? We will answer it at least for polynomial curves. From (2.24), the polynomial curves satisfying condition (4.27) w.r.t. the vector $\mathbf{e}_3$, i.e., the curves whose projection into the hyperplane $z = 0$ are MPH curves in $\mathbb{R}^{2,1}$, are of the form

$$\begin{aligned} x' &= p_1p_4 - p_2p_3; \\ y' &= p_1p_3 + p_2p_4; \\ z' &= p_5; \\ r' &= p_1p_3 - p_2p_4; \\ \sigma' &= p_2p_3 + p_1p_4, \end{aligned} \tag{4.35}$$

where $p_1(t), p_2(t), p_3(t), p_4(t), p_5(t) \in \mathbb{R}[t]$.

Now we describe a rotation, which transforms the vector $\mathbf{e}_3$ to the vector $\mathbf{v}$ – using matrix representation we have

$$\mathbf{B} = 2\frac{(\mathbf{v}+\mathbf{e}_3)\cdot(\mathbf{v}+\mathbf{e}_3)^{\top}}{\|(\mathbf{v}+\mathbf{e}_3)\|^2} - \mathbf{I} \tag{4.36}$$

Then rotating $(x', y', z')^{\top}$ from (4.35) with the help of matrix (4.36) yields the explicit formulas for the hodograph of all polynomial curves satisfying condition (4.27)

$$\begin{aligned} x' &= \left(\frac{a^2}{c+1} - 1\right)(p_1p_4 - p_2p_3) + \frac{ab}{c+1}(p_1p_3 + p_2p_4) + a\,p_5, \\ y' &= \frac{ab}{c+1}(p_1p_4 - p_2p_3) + \left(\frac{b^2}{c+1} - 1\right)(p_1p_3 + p_2p_4) + b\,p_5, \\ z' &= a(p_1p_4 - p_2p_3) + b(p_1p_3 + p_2p_4) + c\,p_5, \\ r' &= p_1p_3 - p_2p_4, \\ \sigma' &= p_2p_3 + p_1p_4, \end{aligned} \tag{4.37}$$

where $\mathbf{v} = (a, b, c)^\top \in \mathcal{S}^2$.

Although the main role in this chapter play canal surfaces with polynomial MATs the following example shows that the theory holds for the canal surfaces with rational MATs, in general.

Example 4.14. Let us consider the canal surface given by the rational quadratic MAT

$$\mathbf{m}(t) = \left(\frac{t^2 - t}{t^2 + 1}, \frac{2t}{t^2 + 1}, \frac{t^2 + 2t}{t^2 + 1}\right)^\top, \quad r(t) = \frac{t^2}{t^2 + 1}. \tag{4.38}$$

Then for the vector $\mathbf{v} = (-1/3, 2/3, 2/3)^\top$ we obtain

$$\|\mathbf{m}'\|^2 - (\mathbf{m}'^\top \cdot \mathbf{v})^2 - r'^2 = \left(\frac{4\sqrt{2}t}{(3t^2 + 1)^2}\right)^2. \tag{4.39}$$

Hence, the contour curve w.r.t. $\mathbf{v}$ is rational, i.e.,

$$\mathbf{c}_{\mathbf{v}}^{\pm}(t) = \left(\frac{-4\sqrt{2}t^2 + 7t^2 \mp 17t}{17\,(t^2 + 1)}, \frac{2\left(3\sqrt{2}t^2 + t^2 \mp 17t\right)}{17\,(t^2 + 1)}, \frac{2\left(2\sqrt{2}t^2 + 5t^2 \pm 17t\right)}{17\,(t^2 + 1)}\right)^\top, \tag{4.40}$$

and an exact rational parameterization of the corresponding canal surface can be obtained symbolically just by substituting to (2.30).

4.3 Computing the rational contour curves for canal surfaces with polynomial MATs

In this section, we will investigate the existence of rational general contour curves over reals for canal surfaces defined by the polynomial MATs. Let the spine curve $\mathbf{m} \in \mathbb{R}^3[t]$ and the radius function $r \in \mathbb{R}[t]$ be given. Then the problem is to find a unit vector $\mathbf{v} \in \mathcal{S}^2$ and a polynomial $\sigma \in \mathbb{R}[t]$ such that equation (4.27) is fulfilled. After denoting $\tau = \|\mathbf{m}'\|^2 - r'^2$ we have

$$\tau = (\mathbf{m}'^\top \cdot \mathbf{v})^2 + \sigma^2. \tag{4.41}$$

As the first consequence we see a necessary condition on $(\mathbf{m}, r)^\top$ – namely the polynomial τ must be PSD. So our goal is to find an SOS decomposition of $\tau = f_\varphi^2 + g_\varphi^2$ (cf. (2.47)) and a unit vector $\mathbf{v}$ such that

$$\mathbf{m}'^\top \cdot \mathbf{v} = g_\varphi, \tag{4.42}$$

which implies $\sigma = f_\varphi$ and therefore the associated contour curve is rational. We will write $\mathbf{p} = [p_0, \ldots, p_n]^\top$ for the coordinate vector of a polynomial $p = \sum_{i=0}^{n} p_i t^i$. With this notation, (4.42) can be rewritten as

$$\mathbf{M} \cdot \mathbf{v} = \mathbf{g}_\varphi, \tag{4.43}$$

where $\mathbf{M}$ is the matrix with the columns being the coordinate vectors of $\mathbf{m}'$ and $\mathbf{f}$ and $\mathbf{g}$ are the coordinate vectors of the polynomials from some particular SOS decomposition of τ. $\mathbf{M}$ is a matrix with $\deg \mathbf{m}' + 1 = \deg \mathbf{m}$ rows and 3 columns. Thus together with the parameter φ and the condition $\mathbf{v}^\top \cdot \mathbf{v} = 1$ we obtain $\deg \mathbf{m} + 1$ equations with 4 unknowns. From this, we can see that no solution can be generally expected for $\deg \mathbf{m} > 3$. In what follows the analysis of the low degree cases will be provided.

The canal surfaces with linear MATs are rotational surfaces, namely cylinders and cones. They contain rational contour curves w.r.t. all unit vectors (except the vector parallel to the axis of the cylinder or the cone) and the branches of these contour curves are straight lines.

The canal surfaces with quadratic and cubic MATs are more interesting, cf. Sections 4.3.1 and 4.3.2.

4.3.1 Canal surfaces with quadratic MATs

Firstly, we recall that the canal surfaces defined by quadratic MATs (i.e., their rational parameterizations of minimal degree, Bézier representations and implicit equations) were thoroughly studied in [53]. In this section we will focus only on properties dealing with the rationality of their general contour curves.

Since all quadratic polynomial curves are parabolas and the rationality of the contour curve does not obviously depend on isometries, scaling and reparamaterizations, we may assume w.l.o.g. that a real quadratic MAT is in the following canonical form

$$\overline{\mathbf{m}}(t) = \left(\frac{t^2}{2}, at, 0, \frac{b}{2}t^2 + ct + d \right)^\top, \tag{4.44}$$

where $a, b, c, d \in \mathbb{R}$. All the solutions of (4.43) are then given by

$$\mathbf{v}(\varphi, \psi) = \left(f_2 \cos\varphi + g_2 \sin\varphi, \frac{f_1 \cos\varphi + g_1 \sin\varphi}{a}, \psi \right)^\top, \tag{4.45}$$

where $\mathbf{f} = (f_1, f_2)^\top$, $\mathbf{g} = (g_1, g_2)^\top$ are the associated coordinate vectors of the decomposition of τ, $\varphi \in [0, 2\pi)$ and $\psi \in \mathbb{R}$. In order to find rational contour curves we need to identify all unit vectors in (4.45). Geometrically it is equivalent to find the intersection of the elliptic cylinder (4.45) with the unit sphere $\mathbf{v}^\top \cdot \mathbf{v} = 1$. We will show that the intersection consists of two great circles, i.e., the ellipse

$$\mathbf{e}(\varphi) = \left(f_2 \cos\varphi + g_2 \sin\varphi, \frac{f_1 \cos\varphi + g_1 \sin\varphi}{a} \right)^\top \tag{4.46}$$

has the unit semi-major axis. Implicitizing ellipse (4.46) and substituting the following decomposition of τ

$$f = \sqrt{1 - b^2} \left(t - \frac{bc}{1 - b^2} \right), \quad g = \frac{\sqrt{a^2 (1 - b^2) - c^2}}{\sqrt{1 - b^2}}, \tag{4.47}$$

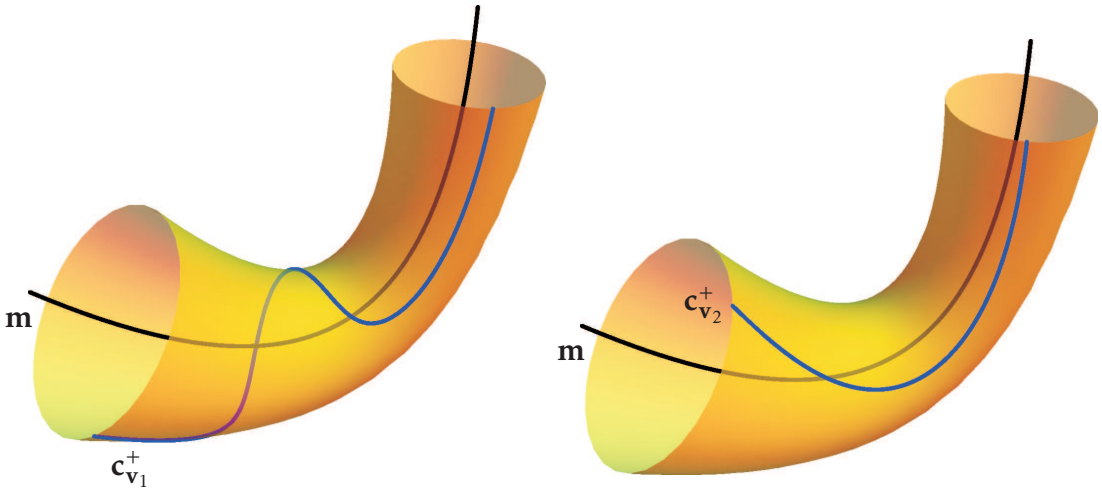

Figure 4.4: The plus branch of an arbitrary rational contour curve (blue), left and the plus branch of the rational contour curve with the minimal arc length (blue), right on a canal surface (yellow).

yields

$$(c^2-a^2)x^2-2abcxy+a^2(b^2-1)y^2-a^2(b^2-1)-c^2=0 \tag{4.48}$$

and the associated canonical form of (4.48) is

$$\frac{\lambda_1 x^2}{-a_{00}}+\frac{\lambda_2 y^2}{-a_{00}}=1, \tag{4.49}$$

where λ_1, λ_2 are the eigenvalues of the matrix of the quadratic terms

$$\begin{pmatrix} c^2-a^2 & -abc \\ -abc & a^2\left(b^2-1\right) \end{pmatrix}, \tag{4.50}$$

and $a_{00}=-a^2(b^2-1)-c^2$ is the absolute term in the equation (4.48). Hence, we arrive at the following canonical form of the ellipse (4.48)

$$\frac{x^2}{1}+\frac{y^2}{1-b^2-\frac{c^2}{a^2}}=1, \tag{4.51}$$

and we can immediately formulate:

Theorem 4.15. *For any canal surface $\mathcal{S}$ with a quadratic MAT satisfying $\tau=\|\mathbf{m}'\|^2-r'^2\geq 0$, there exists two 1-parameter families of vectors $\mathbf{v}$, corresponding to two great circles on the unit sphere, which yield rational contour curves $\mathcal{C}_{\mathbf{v}}$ on $\mathcal{S}$.*

For $b=c=0$ the canal surface becomes a pipe. In this case two great circles are coincident and all the solutions lie in the plane parallel to the plane of parabola.

Proposition 4.16. *For any pipe surface $\mathcal{S}$ with a quadratic spine curve $\mathbf{m}$ and radius r, there exists exactly one rational contour curve, namely*

$$\mathbf{c}^{\pm}_{\mathbf{v}}=\mathbf{m}\pm r\,\mathbf{n}, \tag{4.52}$$

where $\mathbf{n}$ is a unit vector perpendicular to the plane of the parabolic MAT.

Remark 4.17. Considering the 1-parameter family of vectors $\mathbf{v}$ (cf. Theorem 4.15), which yield corresponding rational contour curves $\mathbf{c}_{\mathbf{v}}^{\pm}$, one can require some additional extra criterion when choosing a particular $\mathbf{v}$. As a natural condition can be taken for instance the minimal arc length of the obtained contour curve since the contour curves with the minimal arc lengths do not wind too much around the canal surfaces. This guarantees a better distribution of the parameter lines on the canal surface. In Figure 4.4, the plus branch of some arbitrary rational contour curve (top) and the plus branch of a rational contour curve with the minimal arc length (bottom) on a given canal surface are shown.

We have already answered the question which unit vectors yield rational contour curves on a canal surface given by a quadratic MAT. In addition, another interesting question is which unit vectors give at least real contour curves (regardless of their rationality), i.e., for which $\mathbf{v} \in \mathcal{S}^2$ is the following condition satisfied?

$$\rho = \|\mathbf{m}'\|^2 - (\mathbf{m}'^{\top} \cdot \mathbf{v})^2 - r'^2 \geq 0. \tag{4.53}$$

Using canonical form (4.44) of a quadratic MAT and denoting $\mathbf{v} = (x, y, z)^{\top}$, we arrive at

$$\rho(t) = \rho_2 t^2 + \rho_1 t + \rho_0, \tag{4.54}$$

where

$$\rho_0 = a^2(1 - y^2) - c^2; \quad \rho_1 = -2(axy + bc); \quad \rho_2 = 1 - b^2 - x^2. \tag{4.55}$$

The necessary and the sufficient conditions of non-negativity of the quadratic polynomial ρ are the positivity of the coefficient of the quadratic term of ρ, i.e., $\rho_2 > 0$ and the non-positivity of the discriminant of ρ, i.e.,

$$D = (c^2 - a^2)x^2 - 2abcxy + a^2(b^2 - 1)y^2 - a^2(b^2 - 1) - c^2 \leq 0. \tag{4.56}$$

Hence the boundary curves enclosing the region on the unit sphere corresponding to the vectors giving the real contour curves are defined as

$$D = 0 \quad \text{and} \quad x^2 + y^2 + z^2 = 1, \tag{4.57}$$

which are exactly the curves on $\mathcal{S}^2$ corresponding to the vectors giving the rational contour curves, see (4.48). Then by parameterizing the ellipse $D = 0$ and substituting this parameterization to ρ_2 (only its x-coordinate is sufficient) we obtain the inequality of the form

$$\frac{p^2(s)}{(1 - b^2)q^2(s)} > 0, \tag{4.58}$$

where $p(s), q(s)$ are some polynomials in s. This condition is always satisfied since the positivity of $1 - b^2$ follows from condition (2.29) and it can be shown that for $1 - b^2$ being positive p (and thus also ρ_2) is never zero. Hence the condition $\rho_2 > 0$ is satisfied for all vectors satisfying the condition $D \leq 0$.

Theorem 4.18. *For any canal surface $\mathcal{S}$ with a quadratic MAT satisfying $\tau = \|\mathbf{m}'\|^2 - r'^2 \geq 0$, the great circles on the unit sphere $\mathcal{S}^2$ corresponding to the vectors giving the rational contour curves delimite the region on $\mathcal{S}^2$ corresponding to the vectors giving the real contour curves.*

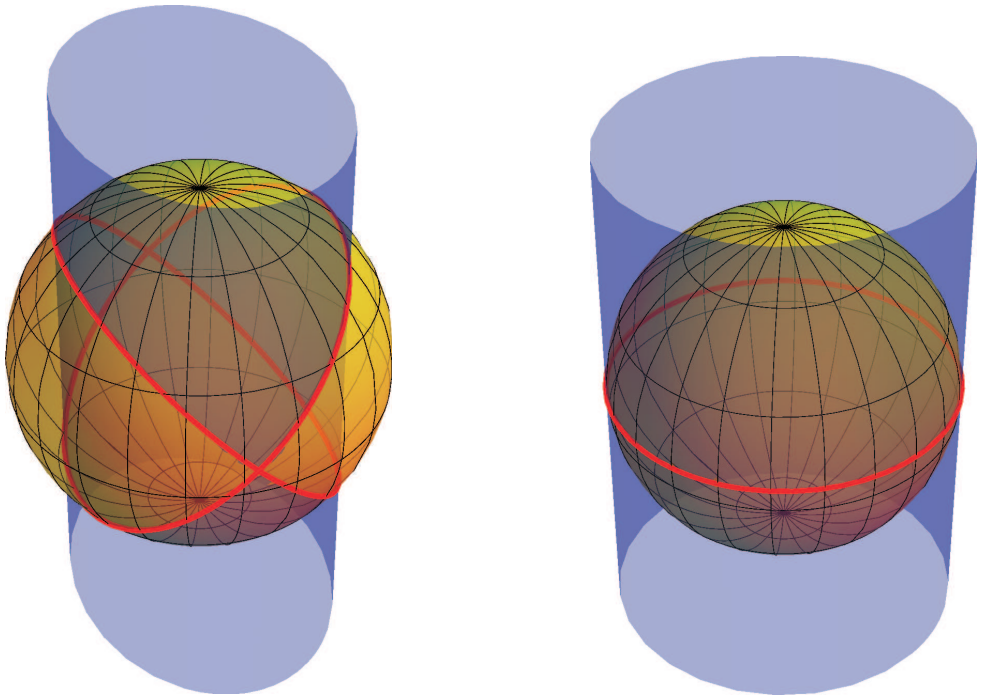

Figure 4.5: All possible unit vectors (red) giving a rational contour curve from Example 4.19 – for the canal surface (left), and for the pipe surface (right) .

Example 4.19. Let us consider the canal surface $\mathcal{S}$ defined by the quadratic MAT, where

$$\mathbf{m}(t) = (t^2, t, 0)^\top \quad \text{and} \quad r(t) = \frac{t^2}{2} + \frac{t}{2} + 1. \tag{4.59}$$

The canal surface fulfills non-degenerative condition (2.29), i.e., τ is PSD, and hence it contains two 1-parameter families of real rational contour curves corresponding to two great circles on the unit sphere, see Figure 4.5 (left). These great circles are simultaneously the boundary curves delimitating the region on $\mathcal{S}^2$ corresponding to the vectors giving the real contour curves – i.e., the parts of the sphere lying inside the cylinder. For the pipe surface defined by $\mathbf{m}$ from (4.59) and $r = \text{const.}$, there exists 1-parameter system of unit vectors corresponding to one great circle on the unit sphere all giving one rational contour curve, see Figure 4.5 (right) and of course all vectors from $\mathcal{S}^2$ give real contour curves.

4.3.2 Canal surfaces with cubic MATs

For a spatial cubic spine curve (we omit the planar case), the matrix $\mathbf{M}$ is 3×3 and regular. Hence, the solution of (4.43) has the form

$$\mathbf{v} = \mathbf{M}^{-1} \cdot \mathbf{g}_\varphi. \tag{4.60}$$

Moreover, as $\mathbf{v}$ is a unit vector we obtain

$$\mathbf{g}_\varphi^\top \cdot (\mathbf{M}^{-\top} \cdot \mathbf{M}^{-1}) \cdot \mathbf{g}_\varphi = 1. \tag{4.61}$$

The matrix $\mathbf{G} = \mathbf{M}^{-\top} \cdot \mathbf{M}^{-1}$ is regular and symmetric. Thus $\mathbf{x}^\top \cdot \mathbf{G} \cdot \mathbf{x} = 1$ describes a regular quadric in $\mathbb{R}^3$ with the center at the origin. So, we can transform (4.42) to the problem of intersection of the quadric $\mathbf{x}^\top \cdot \mathbf{G} \cdot \mathbf{x} = 1$ with a curve parameterized as $\mathbf{x}(\varphi) = \cos\varphi\, \mathbf{f} + \sin\varphi\, \mathbf{g}$, which is a conic section. For the sake of simplicity we denote $c := \cos\varphi$ and $s := \sin\varphi$. Thus, we solve the system

$$(c\,\mathbf{f} + s\,\mathbf{g})^\top \cdot \mathbf{G} \cdot (c\,\mathbf{f} + s\,\mathbf{g}) = 1, \quad c^2 + s^2 = 1, \tag{4.62}$$

which leads to the homogeneous quadratic equation

$$c^2(\mathbf{f}^\top \cdot \mathbf{G} \cdot \mathbf{f} - 1) + 2cs(\mathbf{f}^\top \cdot \mathbf{G} \cdot \mathbf{g}) + s^2(\mathbf{g}^\top \cdot \mathbf{G} \cdot \mathbf{g} - 1) = 0. \tag{4.63}$$

Denoting

$$\alpha := \mathbf{f}^\top \cdot \mathbf{G} \cdot \mathbf{f}, \;\; \beta := \mathbf{f}^\top \cdot \mathbf{G} \cdot \mathbf{g}, \;\; \gamma := \mathbf{g}^\top \cdot \mathbf{G} \cdot \mathbf{g} \tag{4.64}$$

we arrive at the following solution

$$c = \frac{\lambda}{\sqrt{\lambda^2 + 1}}, \quad s = \frac{1}{\sqrt{\lambda^2 + 1}}, \tag{4.65}$$

where

$$\lambda_{1,2} = \frac{-\beta \pm \sqrt{\beta^2 - (\alpha - 1)(\gamma - 1)}}{\alpha - 1}, \tag{4.66}$$

and

$$\mathbf{v} = \mathbf{M}^{-1} \cdot \frac{\lambda \mathbf{f} + \mathbf{g}}{\sqrt{\lambda^2 + 1}}. \tag{4.67}$$

Thus we can formulate

Theorem 4.20. *For a canal surface with the cubic MAT satisfying $\tau = \|\mathbf{m}'\|^2 - r'^2 \geq 0$, there exists a vector $\mathbf{v}$ such that $\mathbf{c}_\mathbf{v}$ is rational over reals iff at least for one (of two non-equivalent) decomposition of τ*

$$\beta^2 - (\alpha - 1)(\gamma - 1) \geq 0, \tag{4.68}$$

where α, β, γ are defined in (4.64).

Computing the vectors ensuring rational contour curves for canal surfaces with cubic MAT leads to two quadratic equations (corresponding to two non-equivalent decompositions of τ) and each of them possesses two (generally complex) solutions. Since the opposite vectors solve the problem as well (however give the same contour curve) we have at most 8 different (complex) vectors. In fact, the opposite vectors correspond to exchanging $\mathbf{f}$ and $\mathbf{g}$. So we can formulate the following proposition.

Proposition 4.21. *For a canal surface with the cubic MAT there exist at most 8 different real vectors ensuring the rationality of the corresponding contour curve.*

Now, let us focus on pipe surfaces. As in the quadratic case we can write a canonical representative of all cubically parameterized real polynomial spine curves (up to similarities and a reparameterization) in the form

$$\mathbf{m}(t) = \left(\frac{t^3}{3} + at, \frac{bt^2}{2} + ct, dt \right)^\top, \tag{4.69}$$

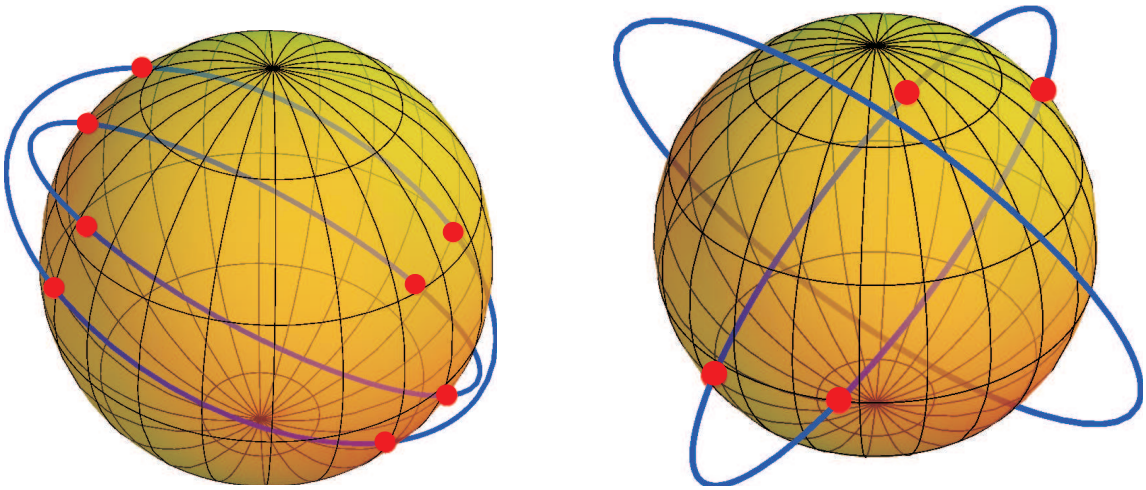

Figure 4.6: All possible unit vectors (red) giving a rational contour curve from Example 4.23 – for the canal surface (left), and for the pipe surface (right).

where $a, b, c, d \in \mathbb{R}$. Then the discriminants of (4.63) are of the form

$$D_1 = \frac{\left[(\beta-\delta)^2 - b^2\right]^2}{[(\alpha-\gamma)^2 + b^2][(\beta+\delta)^2 - b^2]}, \quad D_2 = \frac{\left[(\beta+\delta)^2 - b^2\right]^2}{[(\alpha-\gamma)^2 + b^2][(\beta-\delta)^2 - b^2]}, \tag{4.70}$$

where $\alpha \pm \beta i, \gamma \pm \delta i$ ($\alpha, \gamma \in \mathbb{R}$, $\beta, \delta \in \mathbb{R}^+$) are the roots of τ (for $r' = 0$), i.e.,

$$\begin{aligned}\tau(t) = t^4 + (2a + b^2)t^2 + 2bct + a^2 + c^2 + d^2 \\ = (t - \alpha - \beta i)(t - \alpha + \beta i)(t - \gamma - \delta i)(t - \gamma + \delta i).\end{aligned} \tag{4.71}$$

Hence the non-negativity of the discriminants D_1 and D_2 depends only on the polynomials

$$h_1 = (\beta+\delta)^2 - b^2, \quad h_2 = (\beta-\delta)^2 - b^2, \tag{4.72}$$

respectively. Solving (4.71) as a system of equations for coefficients of τ yields

$$\begin{aligned} a &= \frac{1}{2}\left(-2\alpha^2 - b^2 + \beta^2 + \delta^2\right); \\ c &= \frac{\alpha(\beta-\delta)(\beta+\delta)}{b}; \\ d &= \frac{\sqrt{-(4\alpha^2 + b^2)[(\beta+\delta)^2 - b^2][(\beta-\delta)^2 - b^2]}}{2b}, \end{aligned} \tag{4.73}$$

and since $\mathbf{m}$ possesses real coefficients

$$\left[(\beta+\delta)^2 - b^2\right]\left[(\beta-\delta)^2 - b^2\right] \tag{4.74}$$

have to be a non-positive polynomial. Hence h_1 is a non-negative and h_2 a non-positive polynomial, in general. We arrive at the following conclusion:

Proposition 4.22. *For any pipe surface with the cubic spine curve, there exists a real vector (at most 4 different vectors) ensuring the rationality of the corresponding contour curve.*

Example 4.23. Let us consider the canal surface $\mathcal{S}$ given by the cubic MAT, where

$$\mathbf{m}(t) = \left(3t^3 - 4t^2 - 4t, 3t^3 + 4t^2 + 4t, 3t - 5t^2\right)^\top, \tag{4.75}$$

and

$$r(t) = 3t^3 + 3t^2 - 5t. \tag{4.76}$$

Since condition (4.68) is satisfied for both non-equivalent classes of decomposition there exist 8 vectors yielding the rational contour curves on $\mathcal{S}$, see Figure 4.6 (left). For the pipe surface given by $\mathbf{m}$ from (4.75) and $r = \text{const.}$, there exist 4 vectors ensuring the rationality of the corresponding contour curves, see Figure 4.6 (right).

4.4 Blending by canal surfaces with rational contour curves

This section is devoted to presenting two simple methods for the computation of a blending canal surface between two prescribed canal surfaces based on the parameterizing contour curves. Such a blending surface shall smoothly join two given canal surfaces. Hence, if we consider the MAT representation of the given canal surfaces and the blending surface in $\mathbb{R}^{3,1}$ this problem can be transformed into the G^1/C^1 Hermite interpolation of data in 4-dimensional space.

Thus let us consider the MAT representation of two given canal surfaces $\mathcal{S}_1$ and $\mathcal{S}_2$ in the form

$$\overline{\mathbf{m}}_1(t) = (\mathbf{m}_1, r_1)^\top, \qquad \overline{\mathbf{m}}_2(t) = (\mathbf{m}_2, r_2)^\top. \tag{4.77}$$

Without loss of generality, we can suppose that both surfaces are defined for $t \in [0,1]$ since if not it could be fixed by linear reparameterization. Then we interpolate the following Hermite data in $\mathbb{R}^{3,1}$

$$\mathbf{p}_1 = \overline{\mathbf{m}}_1(1), \quad \mathbf{t}_1 = \overline{\mathbf{m}}_1'(1), \quad \mathbf{p}_2 = \overline{\mathbf{m}}_2(0), \quad \mathbf{t}_2 = \overline{\mathbf{m}}_2'(0), \tag{4.78}$$

by a curve $\overline{\mathbf{m}}(t) = (\mathbf{m}, r)^\top$, $t \in [0,1]$ with at least C^1/G^1 continuity and compute the rational parameterization of the corresponding blending surface.

The choice of the interpolation curve can make the computation of the parameterization of the corresponding blend easier. In Section 4.4.1 the blending method based on the MPH interpolation is designed and Section 4.4.2 is devoted to the blending method based on the SOS computations.

4.4.1 Blending based on the MPH interpolation.

In this section, we present a method for constructing a canal blending surface between two given canal surfaces based on interpolating by MPH curve in $\mathbb{R}^{2,1}$. We interpolate

Hermite boundary data (4.78) by a curve $\overline{\mathbf{m}}(t) = (m_1, m_2, m_3, r)^\top$ such that the first two coordinates together with the fourth coordinate $(m_1, m_2, r)^\top$ have a Pythagorean hodograph in $\mathbb{R}^{2,1}$. Now, we construct the corresponding boundary curve $\overset{\triangledown}{\mathbf{c}}(t) = (c_1, c_2)^\top$ in $\mathbb{R}^2$ and lift it back to space and obtain $\mathbf{c}(t) = (c_1, c_2, m_3)^\top$. Finally, rotating the points of $\mathbf{c}$ around the tangents of $\mathbf{m}(t) = (m_1, m_2, m_3)^\top$ yields a PN parameterization of the required blending canal surface.

Hence, we have to adapt the classical algorithms for Hermite interpolations by MPH curves such that we interpolate 4-dimensional data and obtain a curve whose first two coordinates together with the fourth coordinate possess the Pythagorean hodograph in the Minkowski space $\mathbb{R}^{2,1}$.

Our method is independent from a particular procedure for Hermite interpolation by planar MPH curves. And, obviously, this step can be easily replaced by a better or new technique. Nevertheless, we need some well-known testing procedure to present a functionality of the presented method. In our examples we have chosen a variant of the algorithm introduced in [47] however any arbitrary alternative method can be used – we recall e.g. [46, 48, 50, 51].

Let us emphasize that when a higher then G^1 continuity is needed it is enough to choose an interpolation method by MPH curves ensuring required continuity. Thus, the continuity of the blend surface depends only on the continuity of the MPH interpolant, i.e., it is independent of our "contour method".

Example 4.24. Let two canal surfaces be given by their MATs:

$$\begin{aligned} \overline{\mathbf{m}}_1(t) &= \left(2t-1, 4t^2-1, 4t^2-8t+4, t^2+\tfrac{1}{4}\right)^\top, \\ \overline{\mathbf{m}}_2(t) &= \left(4t^2, 4t^2+6t+2, 8t^3, \tfrac{4t^2}{3}+2t+1\right)^\top, \end{aligned} \tag{4.79}$$

where $t \in [0,1]$ for both curves. We compute the Hermite interpolation of boundary data (4.78), i.e.

$$\begin{aligned} \mathbf{p}_1 &= (1,3,0,\tfrac{5}{4})^\top, \qquad \mathbf{t}_1 = (2,8,0,2)^\top, \\ \mathbf{p}_2 &= (0,2,0,1)^\top, \qquad \mathbf{t}_2 = (0,6,0,2)^\top, \end{aligned} \tag{4.80}$$

such that the first two coordinates together with the fourth coordinate form an MPH curve, compute its corresponding contour curve and rotating its points around the tangents of the spine curve yields a PN parameterization of the blend between the given canal surfaces, see Figure 4.7 (left).

Example 4.25. Let us consider the cylinder $\mathcal{C}_1$ given by

$$2x^2 - 2xy - 2xz + 2y^2 - 2yz + 2z^2 - 3 = 0 \tag{4.81}$$

and the cone $\mathcal{C}_2$ defined by the equation

$$7x^2 - 4xy + 4xz - 20x + 4y^2 + 8yz - 24y + 4z^2 - 24z + 36 = 0. \tag{4.82}$$

We want to construct a blending surface $\mathcal{B}$ between $\mathcal{C}_1$ and $\mathcal{C}_2$ joining the given canal surfaces along the circles in the planes described by the linear equations

$$x + y + z = 0 \quad \text{and} \quad x + 2y - 2z - 8 = 0, \tag{4.83}$$

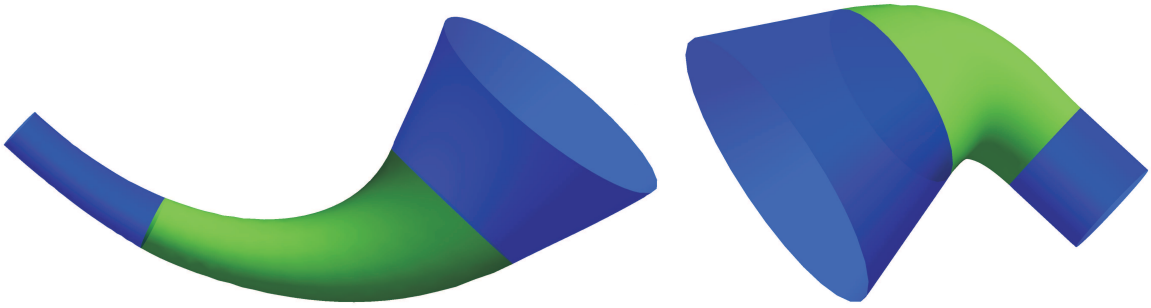

Figure 4.7: PN blending canal surface (green) between two given canal surfaces (blue) from Example 4.24, left and from Example 4.25, right.

respectively. This can be easily reduced to the problem of interpolating the following data:

$$\begin{aligned} \mathbf{p}_1 &= (0,0,0,1)^\top, \quad & \mathbf{v}_1 &= (1,1,1,0)^\top, \\ \mathbf{p}_2 &= (2,3,0,2)^\top, \quad & \mathbf{v}_2 &= (1,2,-2,1)^\top. \end{aligned} \tag{4.84}$$

Our solution is presented in Figure 4.7 (right).

4.4.2 Blending based on the SOS decomposition

This section is devoted to presenting two simple algorithms for the computation of a blending canal surface with the polynomial MAT of degree 2 and 3 between two prescribed canal surfaces. We simply interpolate Hermite data (4.78) by a quadratic biarc or Ferguson's cubic and compute the corresponding rational contour curve if exists.

To have guaranteed the PSD property of the polynomial τ associated to a quadratic or cubic MAT of the constructed blending canal surface, which is a necessary condition for using SOS decompositions, we will assume in what follows that the given Hermite data $\{\mathbf{p}_1, \mathbf{p}_2; \mathbf{t}_1, \mathbf{t}_2\}$ span a hyperplane $\zeta = \langle \mathbf{p}_1; \mathbf{p}_2 - \mathbf{p}_1, \mathbf{t}_1, \mathbf{t}_2 \rangle$ such that the angle between this hyperplane ζ and the coordinate hyperplane $r = 0$ is less than or equal to $\pi/4$. Then the angle between all lines in ζ, including the tangents of the constructed MAT, and the hyperplane $r = 0$ is also less than or equal to $\pi/4$, which implies condition (2.29). These input data are called *admissible data*. To decide if the input Hermite data $\{\mathbf{p}_1, \mathbf{p}_2; \mathbf{t}_1, \mathbf{t}_2\}$ are admissible it is enough to consider the normal vector $\mathbf{n}_\zeta$ of the hyperplane ζ which must be non-space-like, i.e., it must hold

$$\langle \mathbf{n}_\zeta, \mathbf{n}_\zeta \rangle \leq 0, \quad \text{where} \quad \mathbf{n}_\zeta = (\mathbf{p}_2 - \mathbf{p}_1) \times \mathbf{t}_1 \times \mathbf{t}_2. \tag{4.85}$$

Remark 4.26. Quadratic MATs (i.e., parabolas) are planar and cubic MATs are lying in 3D space. Hence the requirement that the given Hermite data are admissible (in our sense) guarantees that the constructed interpolating parabolas/cubics (contained in ζ) satisfy the PSD property. Of course, working only with the admissible data is condition which is satisfactory but not necessary. However, our tests showed that in the majority of practical situations given data are of this type.

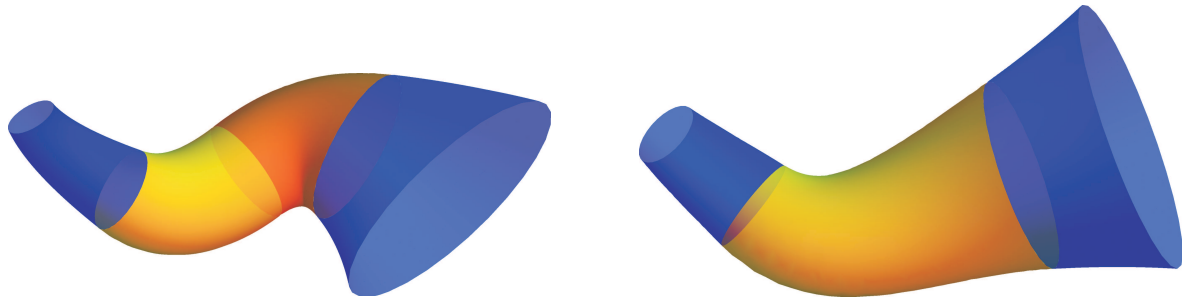

Figure 4.8: PN blending canal surface composed of two parts (yellow and orange) between two given canal surfaces (blue) from Example 4.27, left and PN blending canal surface (yellow) between two given canal surfaces (blue) from Example 4.28, right.

In Section 4.3.1 we showed that for a quadratic MAT (satisfying the PSD property of the polynomial τ) there always exist two 1-parameter families of vectors yielding the rational contour curves. Hence we design a method for constructing a blending canal surface having quadratic MAT between two other canal surfaces. Since parabolas can interpolate only planar data we have to use quadratic biarc which can interpolate spatial C^1 data. In particular, for the points $\mathbf{p}_1, \mathbf{p}_2$ and the tangent vectors $\mathbf{t}_1, \mathbf{t}_2$ at these points ($\{\mathbf{p}_1, \mathbf{p}_2; \mathbf{t}_1, \mathbf{t}_2\}$ are admissible data), we construct two Bézier quadratic curves (parabolas)

$$\begin{aligned} \overline{\mathbf{a}}(t) &= \sum_{i=0}^{2} \mathbf{a}_i B_i^3\left(\frac{t}{\tau}\right), \qquad t \in [0, \tau], \\ \overline{\mathbf{b}}(t) &= \sum_{i=0}^{2} \mathbf{b}_i B_i^3\left(\frac{t-\tau}{1-\tau}\right), \quad t \in [\tau, 1], \end{aligned} \tag{4.86}$$

where $\mathbf{a}_i$ and $\mathbf{b}_i$, $i = 0, 1, 2$ are the control points and

$$B_i^n(t) = \binom{n}{i} t^i (1-t)^{n-i}, \quad i = 0, 1, \ldots, n, \tag{4.87}$$

are the Bernstein basis polynomials. To interpolate the input data the conditions $\overline{\mathbf{a}}(0) = \mathbf{p}_1$, $\overline{\mathbf{a}}'(0) = \mathbf{t}_1$, $\overline{\mathbf{b}}(1) = \mathbf{p}_2$ and $\overline{\mathbf{b}}'(1) = \mathbf{t}_2$ must be satisfied. Hence we arrive at

$$\mathbf{a}_1 = \mathbf{p}_1, \quad \mathbf{a}_2 = \mathbf{p}_1 + \frac{\tau}{2}\mathbf{t}_1, \quad \mathbf{b}_2 = \mathbf{p}_2 - \frac{1-\tau}{2}\mathbf{t}_2, \quad \mathbf{b}_3 = \mathbf{p}_2. \tag{4.88}$$

In addition, to guarantee the C^1 continuity at the join point ($\overline{\mathbf{a}}(\tau) = \overline{\mathbf{b}}(\tau)$ and $\overline{\mathbf{a}}'(\tau) = \overline{\mathbf{b}}'(\tau)$) we have

$$\mathbf{a}_3 = \mathbf{b}_1 = (1-\tau)\mathbf{p}_1 + \tau\mathbf{p}_2 + \frac{\tau(1-\tau)}{2}(\mathbf{t}_1 - \mathbf{t}_2). \tag{4.89}$$

Example 4.27. Let us consider two canal surfaces given by the following MATs:

$$\begin{aligned} \overline{\mathbf{m}}_1(t) &= \left(\frac{1}{3}(2t+1), \frac{1}{9}(2t+1)^2 - 3, -\frac{1}{9}(2t+1)^2, \frac{1}{18}\left(2t^2 + 2t + 5\right)\right)^\top, \\ \overline{\mathbf{m}}_2(t) &= \left(4t^2, 2t(2t+3), 8t^3 - 3, 4t^2 + 2t + 1\right)^\top. \end{aligned} \tag{4.90}$$

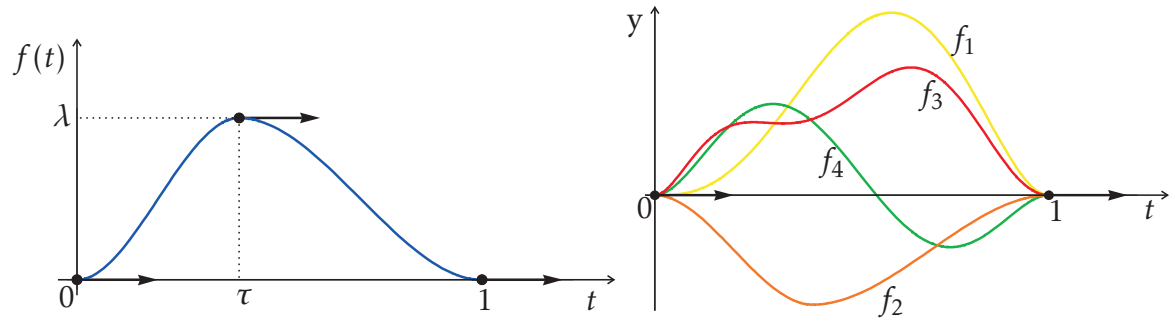

Figure 4.9: One dimensional non-zero Ferguson's distance function (composed of two parts) having zero values and derivatives at $t = 0$ and $t = 1$, left and different distance functions used for the construction of the adaptive blends shown in Figure 4.1, right.

We interpolate the admissible Hermite C^1 data (4.78) in $\mathbb{R}^{3,1}$ by a quadratic biarc $\overline{\mathbf{h}}_i$, $i = 1, 2$ and for each $\overline{\mathbf{h}}_i$ we compute the vector $\mathbf{v}_i$ ensuring the rationality of the corresponding contour curve $\mathbf{c}_i$. Rotating the points of $\mathbf{c}_i$ around the tangents of $\mathbf{h}_i$ yields a piecewise PN parameterization of the blending surface (composed of two parts) between the given canal surfaces, see Figure 4.8, left.

In Section 4.3.2, it was shown that for a real canal surface defined by the cubic MAT the rational contour curve exists if condition (4.68) is fulfilled. Hence in such cases we can use canal surfaces with cubic MAT for the blending process – it is enough to interpolate hermite data (4.78) by Ferguson's cubic and rotate the corresponding rational contour curve around the tangents of the spine curve.

Example 4.28. We construct a blending canal surface with a cubic MAT between two non-rational canal surfaces defined as

$$\begin{aligned} \overline{\mathbf{m}}_1(t) &= \left(\sin\left(\frac{t+1}{2}\right) - 1, \cos\left(\frac{t+1}{2}\right), e^{\frac{t+1}{2}} - 3, 2^{\frac{t-3}{2}}\right)^\top, \\ \overline{\mathbf{m}}_2(t) &= \left(\tan(3t), -12t, \sin(3t) - 1, 27^t\right)^\top. \end{aligned} \tag{4.91}$$

Thus we compute the Ferguson's cubic $\overline{\mathbf{h}}$ matching the admissible Hermite C^1 data (4.78). Since condition (4.68) is fulfilled we can compute the rational contour curve $\mathbf{c}_{\mathbf{v}}^{\pm}$ w.r.t. a suitable vector $\mathbf{v}$. Finally, by rotating the points of e.g. $\mathbf{c}_{\mathbf{v}}^{+}$ around the tangents of $\mathbf{h}$ we arrive at the PN parameterization of the blending surface, see Figure 4.8, right.

4.4.3 Blends bypassing the obstacles

In this subsection we deal with the problem of constructing a blending surface between two given canal surfaces which satisfies a certain constraint, in particular if it is required that the constructed blend shall bypass some obstacle(s). We will see an advantage of the contour method which allows us to generate at once a whole family of rational canal surfaces having the same projection of the contour curve (the silhouette) w.r.t. some vector $\mathbf{v}$, see Figure 4.1.

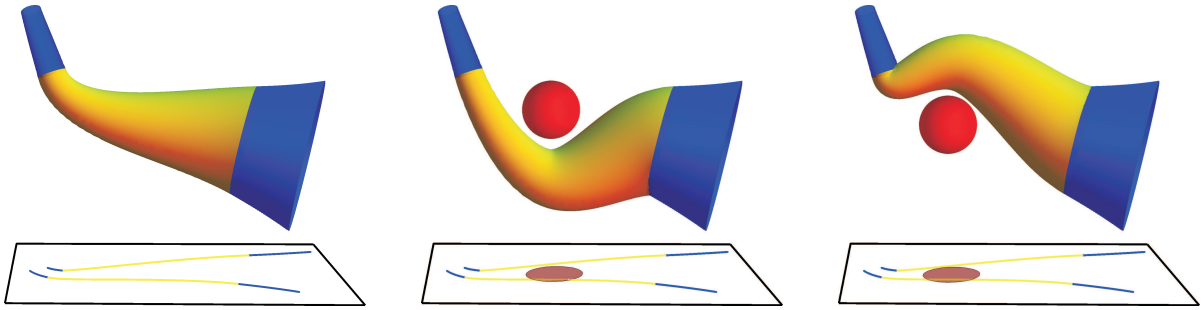

Figure 4.10: A blending surface (yellow) between two canal surfaces (blue) without an obstacle (left) and with an obstacle (middle and right).

Firstly, we construct a classical blending surface, see Sections 4.4.1 and 4.4.2 – we obtain a blending canal surface that is described by a medial axis transform $\overline{\mathbf{m}} = (\mathbf{m}, r)^\top$ and the rationality of its contour curve $\mathbf{c}_\mathbf{v}$ w.r.t. the vector $\mathbf{v}$ is generally guaranteed. Then we construct a new spine curve and a new contour curve in the form

$$\mathbf{m}^* = \mathbf{m} + \mathbf{v}f, \qquad \mathbf{c}_\mathbf{v}^* = \mathbf{c}_\mathbf{v} + \mathbf{v}f, \tag{4.92}$$

obtained from the original spine curve $\mathbf{m}$ and the original contour curve $\mathbf{c}_\mathbf{v}$ using some suitable rational *distance function* f continuous on $(0,1)$ and satisfying the conditions

$$f(0) = 0, \quad f'(0) = 0, \quad f(1) = 0, \quad f'(1) = 0. \tag{4.93}$$

The distance function f enables to modify the blending canal surface in the $\mathbf{v}$-direction and thus to satisfy the constraints. We emphasize that the original and also the new canal surfaces possess the same projection w.r.t. the direction $\mathbf{v}$, both have the contour curve being rational w.r.t. the direction $\mathbf{v}$, and both are blending the given canal surfaces.

The natural question reads how to choose the aforementioned distance function f. A suitable non-zero function of the lowest degree satisfying (4.93) and one extra-condition $f(\tau) = \lambda$ can be e.g. the following function of degree 4

$$f(t) = \frac{\lambda}{(\tau-1)^2\tau^2}(t-1)^2t^2. \tag{4.94}$$

However in what follows we will use a different function composed of the two parts which is of degree 3 only. Moreover, it is ensured that $[\tau, \lambda]$ is an extreme of f, see Figure 4.9, left

$$f(t) = \begin{cases} \frac{\lambda}{\tau^3}t^2(3\tau - 2t), & t \in [0,\tau]; \\ \frac{\lambda}{(1-\tau)^3}(t-1)^2(2t - 3\tau + 1), & t \in [\tau, 1]. \end{cases} \tag{4.95}$$

Remark 4.29. For the modification of the adaptive blends presented in Figure 4.1 we have used the distance functions f_1, f_2, f_3, f_4 whose graphs are shown in Figure 4.9, right.

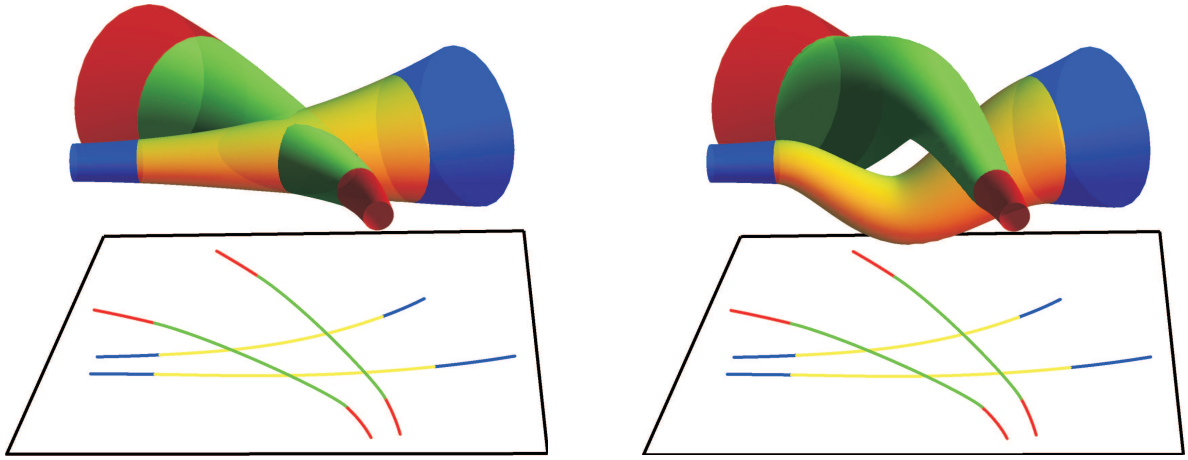

Figure 4.11: Two blending surfaces (yellow and green) between the given canal surfaces (blue and red) – intersecting (left) and after modification bypassing (right).

Example 4.30. A rational blending canal surface between two given canal surfaces was computed by the designed contour method, see Figure 4.10 (left). Hence, its spine curve $\mathbf{m}$, the radius function r and the rational contour curve $\mathbf{c}_\mathbf{v}$ are known. Now, the task is to modify this blending surface such that it bypasses a sphere which is given by its center $\mathbf{x}$ and the radius R. We construct a new blending surface (bypassing the given sphere) with the same silhouette, see Figure 4.10 (middle, right). This can be simply done by computing a new spine curve $\mathbf{m}^*$ and the corresponding contour curve $\mathbf{c}_\mathbf{v}^*$ according to (4.92), where the function f is chosen as in (4.95). A right choice of the values τ and λ shall guarantee that the new blending surface does not intersect the given sphere – in particular it must hold for all $t \in [0,1]$

$$\|\mathbf{m}(t) - \mathbf{x}\| > r(t) + R. \tag{4.96}$$

Example 4.31. In this example we consider the problem of constructing two different blending surfaces between two pairs of given canal surfaces such that the constructed blends bypass each other, i.e., they do not intersect. Using the contour method we can easily (and independently) construct the blending surfaces $\mathcal{B}_1$ and $\mathcal{B}_2$ and then we modify them suitably (to ensure that they do not intersect), see Figure 4.11. The non-intersection of the constructed canal surfaces can be verified e.g. by the methods form [60].

Remark 4.32. Let us discuss one detail of the above presented approach. When using the quadratic-biarc-method for the computation of the blend avoiding a given obstacle we have to, in fact, compute rational parameterizations of two canal surfaces (since the blend is composed of the two parts). Hence for each part we have to find a vector giving the rational contour curve. Nevertheless, when modifying the double-blend to bypass the given obstacle it must be satisfied that the both parts possess the rational contour curve with respect to the same direction. However, this can be always done since for each canal surface with the quadratic MAT there exist two one-parameter families of vectors corresponding to the two great circles on the unit sphere giving the rational contour curves. And the great circles always intersect in the real points.

Chapter 5

Modelling with rational ringed surfaces

In this chapter we will focus on modelling with the ringed surfaces. Firstly we study the question of the rationality of those surfaces – in particular we show which ringed surface are rational and how their rational parameterizations can be computed. Then we design a blending method based on interpolation by Pythagorean curves in the plane and show how this method can be modified to satisfy some constraints, e.g. to avoid obstacles or bypass other objects. Another modification of the method enables to construct n-ways blending surfaces between n ringed surfaces. We also design a method for approximating the implicitly given blends by rational ring surfaces based on approximation of contour curves. The paper in which the author of the thesis participated and which contain the author's main contribution to this topic is – [12].*

5.1 Rationality of ringed surfaces

In what follows, we will consider the ringed surface $\mathcal{R} : (\mathbf{d}, \mathbf{n}, \rho)$ given by a rational directrix $\mathbf{d}$, rational radius function ρ and rational orientation function $\mathbf{n}$. As discussed in Section 2.4, to compute a rational parameterization of $\mathcal{R}$ it is enough to find a rational curve

$$\mathbf{f}(t) = \frac{\mathbf{n}^\perp}{\|\mathbf{n}^\perp\|}, \tag{5.1}$$

associated to $\mathbf{n}$. This is a curve lying on the unit sphere $\mathcal{S}^2$ whose parameterization $\mathbf{f}$ satisfies the conditions

$$\mathbf{n} \cdot \mathbf{f} \equiv 0, \quad \mathbf{f} \cdot \mathbf{f} \equiv 1. \tag{5.2}$$

5.1.1 Rationality of special classes of ringed surfaces

Before we show a general result on the rationality of the ringed surfaces we present some special cases. These cases are mentioned and discussed especially because of their straightforward application potential in geometric modelling (blending, approximate parameterizations, etc.) – see the subsequent sections.

In [34] the so called polynomial *Pythagorean curves* (shortly *P-curves*) were introduced as polynomial curves $\mathbf{x}$ in $\mathbb{R}^3$ satisfying the defining condition

$$\mathbf{x}' \cdot \mathbf{x}' = \sigma^2 \tag{5.3}$$

for some polynomial $\sigma \in \mathbb{R}[t]$. This approach can be directly generalized to any dimension and also to rational curves.

P-curves possess a distinguished feature suitable for our construction, i.e., they enable to find immediately an associated polynomial/rational curve $\mathbf{x}^\perp$ with the same polynomial/rational norm σ and fulfilling the property $\mathbf{x}' \cdot \mathbf{x}^\perp \equiv 0$. In particular, all polynomial P-curves can be written in the form:

$$\mathbf{x} = \left(x_0^2 + x_1^2 - x_2^2 - x_3^2, 2(x_1x_2 - x_0x_3), 2(x_0x_2 + x_1x_3)\right)^\top \tag{5.4}$$

and

$$\sigma = x_0^2 + x_1^2 + x_2^2 + x_3^2, \tag{5.5}$$

where $x_i \in \mathbb{R}[t]$. Then there exist curves $\mathbf{x}_1^\perp$ and $\mathbf{x}_2^\perp$ such that $\|\mathbf{x}'\|^2 = \|\mathbf{x}_1^\perp\|^2 = \|\mathbf{x}_2^\perp\|^2 = \sigma^2$ and $\mathbf{x}' \cdot \mathbf{x}_1^\perp = \mathbf{x}' \cdot \mathbf{x}_2^\perp = \mathbf{x}_1^\perp \cdot \mathbf{x}_2^\perp = 0$ and are of the following form, see [90]

$$\mathbf{x}_1^\perp = \left(2(x_1x_2 + x_0x_3), x_0^2 - x_1^2 + x_2^2 - x_3^2, 2(x_2x_3 - x_0x_1)\right)^\top \tag{5.6}$$

and

$$\mathbf{x}_2^\perp = \left(2(x_1x_3 - x_0x_2), 2(x_0x_1 + x_2x_3), x_0^2 - x_1^2 - x_2^2 + x_3^2\right)^\top. \tag{5.7}$$

Hence, if the orientation function $\mathbf{n}$ of some ringed surface $\mathcal{R}$ is a P-curve we can easily find a spherical curve $\mathbf{f}$ in the form (5.1) by choosing some $\phi \in [0, 2\pi)$ and setting

$$\mathbf{f} = \frac{\cos(\phi)\mathbf{n}_1^\perp + \sin(\phi)\mathbf{n}_2^\perp}{\sigma}, \tag{5.8}$$

where $\mathbf{n}_i^\perp$ have the meaning of $\mathbf{x}_i^\perp$ for $\mathbf{x} := \mathbf{n}$. Consequently, we compute a rational parameterization of $\mathcal{R}$ using this $\mathbf{f}$ (and from it derived $\mathbf{c}$).

Proposition 5.1. *Let be given a ringed surface $\mathcal{R} : (\mathbf{d}, \mathbf{n}, \rho)$ such that the orientation function describes a spatial polynomial P-curve. Consider a spherical curve $\mathbf{f}$ associated to $\mathbf{n}$ in the form* (5.8) *and the corresponding curve $\mathbf{c}$ on the ringed surface $\mathcal{R}$ in the form* (2.38)*. Then parameterization* (2.37) *is rational.*

Example 5.2. If $\mathbf{n}$ is a constant orientation function then it is obviously a P-curve. Hence all ringed surfaces of this type can be parameterized rationally using the above approach.

Next, we will assume that $\mathbf{n}$ does not have to be a spatial P-curve but the projection of $\mathbf{n}$ to a plane going through the origin and having the unit normal vector $\mathbf{v}$, i.e.,

$$\pi_{\mathbf{v}}(\mathbf{n}) = \mathbf{n} - (\mathbf{n} \cdot \mathbf{v})\mathbf{v}, \tag{5.9}$$

is a planar P-curve. So it holds

$$\pi_{\mathbf{v}}(\mathbf{n}) \cdot \pi_{\mathbf{v}}(\mathbf{n}) = \mathbf{n} \cdot \mathbf{n} - (\mathbf{n} \cdot \mathbf{v})^2 = \sigma^2. \tag{5.10}$$

In this case we can take

$$\mathbf{f} = \frac{\mathbf{n} \times \mathbf{v}}{\sigma} \tag{5.11}$$

since this choice ensures that $\mathbf{f} \cdot \mathbf{n} = 0$ and moreover

$$\|\mathbf{f}\|^2 = \frac{\|\mathbf{n}\|^2 - (\mathbf{n} \cdot \mathbf{v})^2}{\sigma^2} = 1. \tag{5.12}$$

Proposition 5.3. *Let be given a ringed surface* $\mathcal{R} : (\mathbf{d}, \mathbf{n}, \rho)$ *such that the projection* $\pi_{\mathbf{v}}(\mathbf{n})$ *of the orientation function, see* (5.9)*, is a planar P-curve. Consider a spherical curve* $\mathbf{f}$ *associated to* $\mathbf{n}$ *in the form* (5.11) *and the corresponding curve* $\mathbf{c}$ *on the ringed surface* $\mathcal{R}$ *in the form* (2.38)*. Then parameterization* (2.37) *is rational.*

Example 5.4. If $\mathbf{n}$ is linear, i.e., $\mathbf{n}(t) = \mathbf{n}_1 + \mathbf{n}_2 t$, then the projection of $\mathbf{n}$ to the plane (going through the origin) with the normal vector equal to $\mathbf{n}_2$ ($\mathbf{n}_2$ is a unit vector) is a constant vector function and therefore it describes a P-curve. Hence all ringed surfaces of this type can be parameterized rationally using the above approach.

In addition, as the coordinate vectors $\mathbf{n}_1, \mathbf{n}_2$ of $\mathbf{n}$ span the plane and the normal vector of this plane is orthogonal to $\mathbf{n}$ we can directly set

$$\mathbf{f} = \frac{\mathbf{n}_1 \times \mathbf{n}_2}{\|\mathbf{n}_1 \times \mathbf{n}_2\|}. \tag{5.13}$$

Example 5.5. If $\deg(\mathbf{n}) \geq 2$ then the coordinate vectors of $\mathbf{n}$ do not lie in one plane in general and hence there does not exist a constant vector $\mathbf{f}$ orthogonal to $\mathbf{n}$. We will try to find a rational curve $\mathbf{f}$ on the unit sphere at least for the case of a quadratic orientation function.

To ensure the orthogonality we choose

$$\mathbf{f} = \frac{\mathbf{n} \times \mathbf{v}}{\|\mathbf{n} \times \mathbf{v}\|}. \tag{5.14}$$

As $\mathbf{f}$ is supposed to be rational $\|\mathbf{n} \times \mathbf{v}\|$ has to be a polynomial. Hence, the question reads as follows: Is there for a given $\mathbf{n}$ a vector $\mathbf{v} \in \mathcal{S}^2$ such that

$$\|\mathbf{v} \times \mathbf{n}\|^2 = \sigma^2? \tag{5.15}$$

After rewriting we get the conditions

$$\|\mathbf{n}\|^2 - (\mathbf{n} \cdot \mathbf{v})^2 = \sigma^2, \quad \|\mathbf{v}\| = 1. \tag{5.16}$$

In Chapter 4, the similar conditions to (5.16) appeared. In more detail, the existence of a rational contour curve on the canal surface with the spine curve $\mathbf{m}$ and the radius function r depends on the existence of a real solution of equation (4.27). In Section 4.3 it was proved that (4.27) possesses a real solution for all pipe surfaces (r = const.) when $\deg(\mathbf{m}) \leq 3$. This implies that equation (5.16) has a real solution for all quadratic orientation functions.

Remark 5.6. In other words, Example 5.5 shows that for any quadratic curve a plane going through the origin such that the projected curve to this plane is a planar P-curve exist.

5.1.2 Rationality of general ringed surfaces

In this section we will present how the curve $\mathbf{f}$ can be found for a general $\mathcal{R} : (\mathbf{d}, \mathbf{n}, \rho)$. In [56] and [68] a similar equation to (5.2), which is a crucial step for the computation of a rational parameterization of pipe/canal and normal ringed surfaces, is solved and discussed. Here, we exploit the idea introduced in [68]. The solution of (5.2) is a curve $\mathbf{f}$ such that for each $t \in \mathbb{R}$ the point $\mathbf{f}(t)$ lies on the unit circle $c(t)$ centered at the origin and lying in the plane having the normal vector $\mathbf{n}(t)$. When projecting the circles $c(t)$ via the stereographic projection $\delta : S^2 \to \nu$ (where ν denotes the plane $z = 0$) with the center $(0, 0, 1)^\top$, we obtain the circles in ν having the centers $\mathbf{s}(t)$ and radii $\rho(t)$

$$\mathbf{s} = -\frac{(n_1, n_2, 0)^\top}{n_3}, \quad \rho = -\frac{\|\mathbf{n}\|}{n_3}. \tag{5.17}$$

Remark 5.7. It is obvious that when $n_3 = 0$, i.e., the circle c contains the center $(0, 0, 1)^\top$, the projection $\delta(c)$ is a straight line going through the origin and having $(n_2, -n_1, 0)^\top$ as its direction vector.

Now, it is enough to find some rational curve $\mathbf{h}$ such that for each $t \in \mathbb{R}$ the point $\mathbf{h}(t)$ lies on the circle $\delta(c(t))$ Since the radius function ρ is not rational in general, we compute the sum of squares (SOS) decomposition of ρ^2. In particular, if $\mathbf{g} = (g_1, g_2, 0)^\top$ is a planar curve satisfying

$$\|\mathbf{n}\|^2 = g_1^2 + g_2^2 \tag{5.18}$$

then the curve $\mathbf{h}$ can be written as follows:

$$\mathbf{h} = \mathbf{s} + \frac{\mathbf{g}}{n_3}. \tag{5.19}$$

Finally the inverse projection $\delta^{-1} : \nu \to S^2$ yields the curve $\mathbf{f}$ solving equation (5.2).

$$\mathbf{f} = \frac{(2h_1, 2h_2, \|\mathbf{h}\|^2 - 1)^\top}{\|\mathbf{h}\|^2 + 1}. \tag{5.20}$$

Hence we can formulate the following theorem.

Theorem 5.8. *Any ringed surface $\mathcal{R} : (\mathbf{d}, \mathbf{n}, \rho)$ with a rational directrix, radius and orientation function is rational.*

We have proved that all ringed surfaces with rational directrices, radius functions and orientation functions are rational. However, a natural question follows: Do exist other rational ring surfaces which are not given by rational $\mathbf{d}, \mathbf{n}, \rho$? And the answer is yes.

Consider a canal surface $\mathcal{S}$ (which belongs to the class of ringed surfaces) determined by a rational spine curve $\mathbf{m}$ and a rational (sphere) radius function r. Such a canal surface is rational, see [68]. Nevertheless, considering it as a ringed surface $\mathcal{R}$ and computing its directrix, radius function and orientation function according to (2.35), the (circle) radius function ρ is a square root of a non-negative rational function

$$\rho = \sqrt{r^2 \frac{\|\mathbf{m}'\|^2 - r'^2}{\|\mathbf{m}'\|^2}}. \tag{5.21}$$

So we will continue with our considerations further and prove that a general ringed surface $\mathcal{R} : (\mathbf{d}, \mathbf{n}, \rho = \sqrt{R})$ with a rational directrix, a rational orientation function and a radius function equal to the square root of some non-negative rational function is rational.

W.l.o.g. we can assume that $\mathbf{n}$ is a polynomial orientation function. Our goal is to find a rational curve $\mathbf{f}$ satisfying

$$\mathbf{n} \cdot \mathbf{f} \equiv 0 \quad \text{and} \quad \mathbf{f} \cdot \mathbf{f} \equiv R. \tag{5.22}$$

For such a curve $\mathbf{f}$ we can construct a corresponding rational curve on $\mathcal{R}$ in the form

$$\mathbf{c} = \mathbf{d} + \rho \frac{\mathbf{f}}{\|\mathbf{f}\|} = \mathbf{d} + \mathbf{f}. \tag{5.23}$$

Equation (5.22) describes a curve $\mathbf{f}$ with the property that for each $t \in \mathbb{R}$ it holds $\mathbf{f}(t) \in c(t)$, where c is the great circle of the sphere centered at the origin with the radius $\sqrt{R}$ and lying in the plane having the normal vector $\mathbf{n}$. Hence we seek $\mathbf{f}$ determined by a 1-parameter system of circles

$$c(t) : \ \mathbf{x} \cdot \mathbf{x} - R(t) = 0, \quad \mathbf{x} \cdot \mathbf{n}(t) = 0, \tag{5.24}$$

where $\mathbf{x} = (x, y, z)^\top$. Projecting c to the plane ν we obtain a 1-parameter system of ellipses

$$(n_1 x + n_2 y)^2 + n_3^2 \left(x^2 + y^2 - R \right) = 0 \tag{5.25}$$

and the lifting (the inverse of the above projection) is described by

$$z = -\frac{n_1 x + n_2 y}{n_3}. \tag{5.26}$$

Ellipses (5.25) have centers at the origin and the directions of their axes are

$$\mathbf{a}_1 = (-n_2, n_1)^\top, \quad \mathbf{a}_2 = (n_1, n_2)^\top. \tag{5.27}$$

Hence by transforming (5.25) via the transformation (composition of a rotation and a scaling)

$$x \to -n_2 x' + n_1 y', \quad y \to n_1 x' + n_2 y' \tag{5.28}$$

we get

$$\left(n_1^2+n_2^2\right)n_3^2\,x'^2+\left(n_1^2+n_2^2\right)\|\mathbf{n}\|^2\,y'^2-n_3^2R=0. \tag{5.29}$$

Now using the projective coordinates, multiplying equation (5.29) by $\left(n_1^2+n_2^2\right)$ and performing transformation

$$X'\to\frac{X''}{n_3\left(n_1^2+n_2^2\right)},\quad X'\to\frac{Y''}{n_1^2+n_2^2},\quad Z'\to\frac{Z''}{n_3} \tag{5.30}$$

we arrive at the following 1-parameter system of ellipses:

$$X''^2+\|\mathbf{n}\|^2\,Y''^2-\left(n_1^2+n_2^2\right)R\,Z''^2=0. \tag{5.31}$$

Equation (5.31) can be rationally transformed to the following one

$$A(t)\,X^2+B(t)\,Y^2+C(t)\,Z^2=0, \tag{5.32}$$

where A,B,C possess only complex 1-multiple roots and A,B neither B,C neither A,C do not have common roots. When τ is a real root of e.g. A, it has to be $2p$-multiple (since A is a PSD polynomial) and we can perform transformation $Y\to Y'/(t-\tau)^p$ which fixes the problem. By analogy the multiple roots can be handled. If τ is a common root of A and B, we can multiply whole equation (5.32) by $(t-\tau)(t-\overline{\tau})$ and perform the transformation $Y\to Y'/((t-\tau)(t-\overline{\tau}))$, $Z\to Z'/((t-\tau)(t-\overline{\tau}))$.

In [65] one particular rational solution of equation (5.32) is constructed. For the sake of completeness we recall the approach only shortly.

We start with constructing polynomials

$$X(t)=\sum_{i=0}^{(l+m)/2}x_it^i,\quad Y(t)=\sum_{i=0}^{(k+m)/2}y_it^i,\quad Z(t)=\sum_{i=0}^{(k+l)/2}z_it^i, \tag{5.33}$$

where $k=\deg(A)$, $l=\deg(B)$ and $m=\deg(C)$.

Now for a root τ of A we obtain equation

$$B(\tau)Y^2(\tau)+C(\tau)Z^2(\tau)=0, \tag{5.34}$$

which can be factorized as

$$\left(\sqrt{B(\tau)}Y(\tau)+\sqrt{C(\tau)}Z(\tau)\right)\left(\sqrt{B(\tau)}Y(\tau)-\sqrt{C(\tau)}Z(\tau)\right)=0, \tag{5.35}$$

or

$$\left(\sqrt{B(\tau)}Y(\tau)+i\sqrt{C(\tau)}Z(\tau)\right)\left(\sqrt{B(\tau)}Y(\tau)-i\sqrt{C(\tau)}Z(\tau)\right)=0 \tag{5.36}$$

according to the signs of $B(\tau)$ and $C(\tau)$. Then for a complex conjugate par of roots $(\tau,\overline{\tau})$ we can choose two complex linear factors from factorizations (5.35) or 5.36 such that adding and subtracting them yields two linear equations with real coefficients. Performing this algorithm for all roots of A,B and C yields $k+l+m$ real linear equations which have 3-parametric solution since $X(t),Y(t)$ and $Z(t)$ have $k+l+m+3$ coefficients.

By substituting the 3-parametric solution to equation (5.32) and setting $t = 0$ we obtain a homogeneous implicit equation of a conic with the three parameters as its variables. Now it remains to choose the remaining three parameters such that the resulting equation gives a real point on the conic which certainly contains real points since it is the linearly transformed conic (5.32) for $t = 0$, for more details see [65].

Finally we transform the solution $X(t), Y(t), Z(t)$ of (5.31) back and obtain

$$\mathbf{f}(t) = \left(\frac{-n_2 X + n_1 n_3 Y}{\left(n_1^2 + n_2^2\right) Z}, \frac{n_1 X + n_2 n_3 Y}{\left(n_1^2 + n_2^2\right) Z}, -\frac{Y}{Z} \right)^\top . \tag{5.37}$$

Clearly, this approach can be generalized for rational $\mathbf{n}$ and R. We simply multiply equation (5.31) by the denominators of $\|\mathbf{n}\|^2$ and $(n_1^2 + n_2^2)R$ and obtain an equation which could be also rationally transformed to (5.32). Hence, we can formulate the following theorem.

Theorem 5.9. *Any ringed surface $\mathcal{R} : (\mathbf{d}, \mathbf{n}, \rho = \sqrt{R})$ with a rational directrix, rational radius function and orientation function equal to the square root of a non-negative rational function is rational.*

5.2 Blending by ringed surfaces

Consider two ringed surfaces $\mathcal{R}_1$ and $\mathcal{R}_2$ given by their directrices, radius functions and orientation functions, i.e.,

$$\mathcal{R}_1 : (\mathbf{d}_1, \mathbf{n}_1, \rho_1)(t), \quad \mathcal{R}_2 : (\mathbf{d}_2, \mathbf{n}_2, \rho_2)(t), \qquad t \in [0, 1]. \tag{5.38}$$

Our goal is to construct a blending ringed surface $\mathcal{B}$ between $\mathcal{R}_1$ and $\mathcal{R}_2$. When interpolating given Hermite data in $\mathbb{R}^7$

$$\begin{aligned} \mathbf{p}_1 &= (\mathbf{d}_1, \mathbf{n}_1, \rho_1)^\top(1), & \mathbf{t}_1 &= (\mathbf{d}_1', \mathbf{n}_1', \rho_1')^\top(1) \\ \mathbf{p}_2 &= (\mathbf{d}_2, \mathbf{n}_2, \rho_2)^\top(0), & \mathbf{t}_2 &= (\mathbf{d}_2', \mathbf{n}_2', \rho_2')^\top(0) \end{aligned} \tag{5.39}$$

by a curve $\mathbf{b}(t) = (\mathbf{d}, \mathbf{n}, \rho)(t)^\top$, $t \in [0, 1]$, with C^1/G^1 continuity we obtain a blending surface $\mathcal{B}$ which will join $\mathcal{R}_1$ and $\mathcal{R}_2$ with C^1/G^1 continuity, too.

In the previous section it was shown that an arbitrary rational curve $\mathbf{b} = (\mathbf{d}, \mathbf{n}, \rho)^\top$ describes a rational ring surface $\mathcal{B} : (\mathbf{d}, \mathbf{n}, \rho)$ and its rational parameterization can be computed by the SOS decomposition (which is solvable only numerically. in general). However, as indicated in Propositions 5.1 and 5.3, using some special curves (when interpolating (5.39)) will make the computation of the parameterization of the corresponding blending ringed surface considerably easier as it allows to avoid the SOS decomposition. Let us discuss this way in more detail.

When interpolating Hermite data sampled from the orientation functions, i.e., $\{\mathbf{n}_1(1), \mathbf{n}_1'(1); \mathbf{n}_2(0), \mathbf{n}_2'(0)\}$, by a P-curve we immediately obtain a curve with the polynomial

norm and fulfilling the condition on orthogonality. So we will focus on this part of the interpolation. The interpolation by polynomial P-curves is based on solving quadratic quaternion equations as in the case of spatial PH curves, see [34]. Consequently, Hermite data sampled from the directrices together with radius functions, i.e., $\{\mathbf{d}_1(1),\ \rho_1(1),\ \mathbf{d}_1'(1),\ \rho_1'(1);\ \mathbf{d}_2(0),\ \rho_2(0),\ \mathbf{d}_2'(0),\ \rho_2'(0)\}$, can be interpolated by an arbitrary rational curve. To sum up, we will interpolate

$$\begin{aligned} \mathbf{p}_1^1 &= (\mathbf{d}_1, \rho_1)^\top(1), \qquad \mathbf{t}_1^1 = (\mathbf{d}_1', \rho_1')^\top(1) \\ \mathbf{p}_2^1 &= (\mathbf{d}_2, \rho_2)^\top(0), \qquad \mathbf{t}_2^1 = (\mathbf{d}_2', \rho_2')^\top(0) \end{aligned} \tag{5.40}$$

by a suitable rational curve (e.g. Ferguson's cubic) and

$$\begin{aligned} \mathbf{p}_1^2 &= \mathbf{n}_1(1), \qquad \mathbf{t}_1^2 = \mathbf{n}_1'(1) \\ \mathbf{p}_2^2 &= \mathbf{n}_2(0), \qquad \mathbf{t}_2^2 = \mathbf{n}_2'(0) \end{aligned} \tag{5.41}$$

by a suitable spatial rational P-curve (e.g. spatial P-curve of degree 6, see [34] for more details). Then the assumptions of Proposition 5.1 are satisfied and we can construct a rational parameterization of $\mathcal{B}$.

Nevertheless, Proposition 5.3 offers even an easier way. It is enough to interpolate 2-dimensional data (sampled from the projection of the orientation functions to a coordinate plane) by a planar P-curve. This can be done by solving "only" complex quadratic equations. The remaining coordinate of the orientation function together with the directrix and the radius function will be obtained via the interpolation by some rational curve. Thus, we will interpolate

$$\begin{aligned} \mathbf{p}_1^1 &= (\mathbf{d}_1, n_1^3, \rho_1)^\top(1), \qquad \mathbf{t}_1^1 = (\mathbf{d}_1', {n_1'}^3, \rho_1')^\top(1) \\ \mathbf{p}_2^1 &= (\mathbf{d}_2, n_2^3, \rho_2)^\top(0), \qquad \mathbf{t}_2^1 = (\mathbf{d}_2', {n_2'}^3, \rho_2')^\top(0) \end{aligned} \tag{5.42}$$

by a suitable rational curve (e.g. Ferguson's cubic) and

$$\begin{aligned} \mathbf{p}_1^2 &= (n_1^1, n_1^2)^\top(1), \qquad \mathbf{t}_1^2 = ({n_1'}^1, {n_1'}^2)^\top(1) \\ \mathbf{p}_2^2 &= (n_2^1, n_2^2)^\top(0), \qquad \mathbf{t}_2^2 = ({n_2'}^1, {n_2'}^2)^\top(0) \end{aligned} \tag{5.43}$$

by a suitable planar rational P-curve (e.g. planar P-curve of degree 6).

Now, we show how the interpolation by a planar P-curve can be computed. As in the case of planar PH curves we use a complex representation of points/curves in the plane. Then the curve $\mathbf{x}(t)$ is a polynomial P-curve iff it can be written as

$$\mathbf{x}(t) = \mathbf{w}^2(t), \tag{5.44}$$

where $\mathbf{w}(t) = w_1(t) + \mathrm{i}\, w_2(t)$ is a polynomial with the complex coefficients, which can be described by the Bernstein-Bézier form

$$\mathbf{w}(t) = \sum_{i=0}^{n} \binom{n}{i} (1-t)^{n-i} t^i \mathbf{w}_i, \quad \mathbf{w}_i \in \mathbb{C}. \tag{5.45}$$

Conditions for C^1 Hermite interpolation

$$\mathbf{x}(0) = \mathbf{p}_1, \quad \mathbf{x}'(0) = \mathbf{t}_1, \quad \mathbf{x}(1) = \mathbf{p}_2, \quad \mathbf{x}'(1) = \mathbf{t}_2, \tag{5.46}$$

yield four complex quadratic equations which have a solution for $n \geq 3$. Hence, for $n = 3$ (i.e., the P-curves is of degree six) we obtain two distinct solutions:

$$\mathbf{w}_0 = \sqrt{\mathbf{p}_1}, \quad \mathbf{w}_1 = \frac{6\mathbf{p}_1 + \mathbf{t}_1}{6\sqrt{\mathbf{p}_1}}, \quad \mathbf{w}_2 = \pm\frac{6\mathbf{p}_2 - \mathbf{t}_2}{6\sqrt{\mathbf{p}_2}}, \quad \mathbf{w}_3 = \pm\sqrt{\mathbf{p}_2}. \tag{5.47}$$

As in the case of interpolating by planar PH quintics it can be shown that the "more suitable" interpolant is the one with + sign.

To sum up, the C^1 interpolation by planar P-curve is simple and straightforward since it is enough to substitute given Hermite data (in the form of the complex representation of points in the plain) to (5.47) and obtain the solution. A main drawback of this approach is that the resulting P-curve has degree 6, which could be for some applications considered as too high.

However, the degree of the interpolant can be reduced by using P-biarcs, which is a method successfully used for PH curves, [3, 6]. In particular we construct two quartic P-curves

$$\begin{aligned} \mathbf{x}_1(t) &= \left(\sum_{i=0}^{2}\binom{2}{i}(1-t)^{n-i}t^i\mathbf{w}_i\right)^2, \qquad t \in [0,\tau], \\ \mathbf{x}_2(t) &= \left(\sum_{i=0}^{2}\binom{2}{i}(1-t)^{n-i}t^i\mathbf{w}_{i+3}\right)^2, \quad t \in [\tau,1]. \end{aligned} \tag{5.48}$$

which have to satisfy the Hermite C^1 conditions:

$$\mathbf{x}_1(0) = \mathbf{p}_1, \quad \mathbf{x}_1'(0) = \mathbf{t}_1, \quad \mathbf{x}_2(1) = \mathbf{p}_2, \quad \mathbf{x}_2'(1) = \mathbf{t}_2 \tag{5.49}$$

and moreover these curves are joining with the C^1 continuity in a value $\tau \in (0,1)$ of the parameter t. This gives two additional conditions

$$\mathbf{x}_1(\tau) = \mathbf{x}_2(\tau), \quad \mathbf{x}_1'(\tau) = \mathbf{x}_2'(\tau). \tag{5.50}$$

Solving (5.49) and (5.50) yields three distinct solutions, however only two of them give a regular P-curve:

$$\begin{aligned} &\mathbf{w}_0 = \sqrt{\mathbf{p}_1}, \quad \mathbf{w}_1 = \frac{4\mathbf{p}_1 + \mathbf{t}_1}{4\sqrt{\mathbf{p}_1}}, \quad \mathbf{w}_2 = \frac{(\tau-1)\left(\pm\sqrt{\mathbf{p}_1}\mathbf{t}_2 + \sqrt{\mathbf{p}_2}(4\mathbf{p}_1 + \mathbf{t}_1)\right) \pm 4\sqrt{\mathbf{p}_1}\mathbf{p}_2}{4\sqrt{\mathbf{p}_1}\sqrt{\mathbf{p}_2}\tau}, \\ &\mathbf{w}_3 = \frac{\tau\left(-\sqrt{\mathbf{p}_2}\mathbf{t}_1 \pm \sqrt{\mathbf{p}_1}(4\mathbf{p}_2 - \mathbf{t}_2)\right) - 4\mathbf{p}_1\sqrt{\mathbf{p}_2}}{4\sqrt{\mathbf{p}_1}\sqrt{\mathbf{p}_2}(\tau-1)}, \quad \mathbf{w}_4 = \pm\frac{4\mathbf{p}_2 - \mathbf{t}_2}{4\sqrt{\mathbf{p}_2}}, \quad \mathbf{w}_5 = \pm\sqrt{\mathbf{p}_2}. \end{aligned} \tag{5.51}$$

And again, the "more suitable" interpolant is the one with + sign.

The whole method for the construction of a blending surface $\mathcal{B}$ between two ringed surfaces, described above, is summarized in Algorithm 4.

Example 5.10. Consider two ringed surfaces given by

$$\begin{aligned} &\mathbf{d}_1 = \left(2t - 6, 2t^2 - 5, t^3\right)^\top, \quad &&\mathbf{n}_1 = (1,t,t)^\top, \quad &&\rho_1 = \frac{t^2}{4} + 1, \\ &\mathbf{d}_2 = (3\sin(t), t, \log(t+1))^\top, \quad &&\mathbf{n}_2 = (4, \sin(t), t)^\top, \quad &&\rho_2 = t + 2. \end{aligned} \tag{5.52}$$

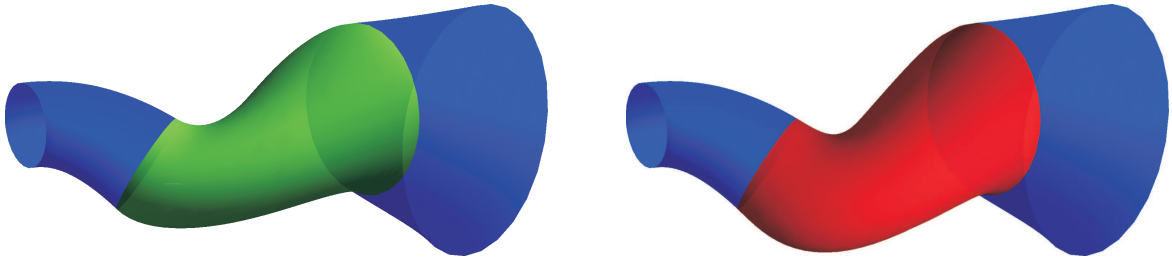

Figure 5.1: Blending ringed surface (green) and optimized blending (as much as possible normal) ringed surface (red) between two ringed surfaces (blue) from Example 5.10.

Algorithm 4 Blending by ringed surfaces

INPUT: Two ringed surfaces $\mathcal{R}_1$ and $\mathcal{R}_2$ given by directrices, orientation functions and radius functions, cf. (5.38).

1: Interpolate data (5.42) by a Ferguson's cubic $\mathbf{f}$;
2: Interpolate data (5.43) by a planar polynomial P-curve of degree six or by a P-biarc of degree four – obtain curve $\mathbf{g}$ with the norm equal to a polynomial σ;
3: Construct a curve $\mathbf{c} = (f_1, f_2, f_3)^\top + f_5 \frac{(g_2, -g_1, 0)^\top}{\sigma}$ on $\mathcal{B}$;
4: Using the curve $\mathbf{c}$ and formula (2.37) compute a rational parameterization of $\mathcal{B}$;

OUTPUT: The parameterization $\mathbf{s}(t, u)$ of the blending surface $\mathcal{B}$ between the given ringed surfaces $\mathcal{R}_1$ and $\mathcal{R}_2$.

According to Algorithm 4 we interpolate data (5.42) by the Ferguson's cubic and data (5.43) by the planar P-curve of degree six and compute the corresponding rational parameterization of the resulting ringed surface, see Figure 5.1, left.

Remark 5.11. We would like to emphasize that using ringed surfaces for the operation of blending significantly extends the family of surfaces (and their mutual positions) which can be blended. For instance, the surfaces from Example 5.10 have to be blended by (non-canal) ringed surface as they are not canal surfaces. Moreover, even when we want to construct blends between two specially situated canal surfaces it may occur a position which cannot be successfully solved by a canal-surface-blend but it is possible to find a suitable ringed-surface-blend, see Figure 5.2.

5.3 Adaptive blending and shape optimization

In Chapter 4, the contour curves on canal surfaces were investigated and used for constructing a whole family of canal surfaces sharing the same silhouette w.r.t. a parallel projection while only one SOS decomposition/MPH interpolation was necessary to be provided for the computation of their parameterizations. This approach is especially useful for constructing blends satisfying certain constrains, e.g. when avoiding obsta-

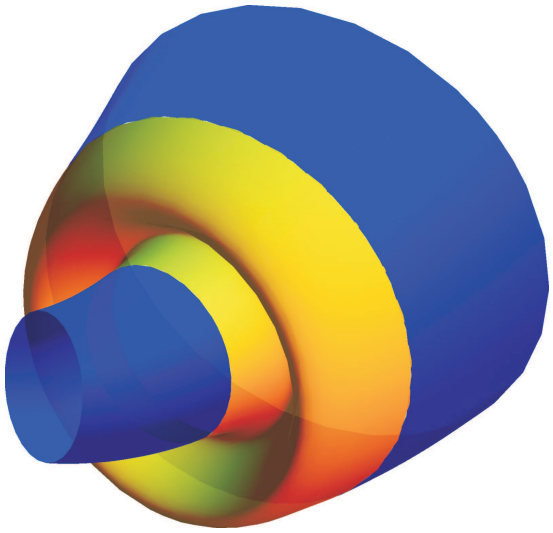

Figure 5.2: Blending ringed surface (yellow) between two canal surfaces (blue).

cles or bypassing other objects is required. The constructed blending surface can be easily modified only with the help of a certain distance function.

When using ringed surfaces for constructing blends with constraints, the situation is significantly easier. The key step of the computation of a parameterization of a curve on a ringed surface $\mathcal{R}$ (and thus also a parameterization of $\mathcal{R}$) is the computation of the unit rational vector field $\mathbf{f}$ orthogonal to the orientation function $\mathbf{n}$ of $\mathcal{R}$ (cf. (5.2)). This can be done by decomposing a polynomial/rational function into a sum of squares or by modelling with P-curves. However, this computation step does not depend on the directrix $\mathbf{d}$ and therefore $\mathbf{d}$ could be adjusted as the prescribed constraints require. In particular, we construct a new directrix

$$\mathbf{d}^* = \mathbf{d} + \mathbf{v}f, \tag{5.53}$$

obtained from the original directrix $\mathbf{d}$ by adding in a suitable direction $\mathbf{v}$ some (rational) distance function f. Analogously to Section 4.4.3 f should be continuous on $(0,1)$ and satisfying conditions (4.93). This distance function f enables to modify the blending ringed surface in the $\mathbf{v}$-direction. In examples presented in Figure 5.3, the following distance function w.r.t. the vector $\mathbf{v} = (0,0,\lambda)^\top$ for different values of τ and λ were applied

$$f(t,\tau) = \frac{(1-t)^2 t^2 (t(2-4\tau) + \tau(5\tau - 3))}{(1-\tau)^3 \tau^3}. \tag{5.54}$$

Example 5.12. Consider two normal ringed surfaces $\mathcal{R}_1$ and $\mathcal{R}_2$ defined by

$$\begin{aligned} \mathbf{d}_1 &= \left(\sin(t) - 4, \cos(t), 2^t - 5\right)^\top, & \rho_1 &= 2^{t-2}; \\ \mathbf{d}_2 &= (t, -t, \sin(t))^\top, & \rho_2 &= 3^{\frac{t}{2}}, \end{aligned} \tag{5.55}$$

and a prescribed sphere with the center at $(-1.4, -0.3, -1.2)^\top$ and the radius equal to 0.75 (taken as a obstacle). Firstly, we construct a blending ringed surface by Algorithm 4, see Figure 5.4, left. Then we adjust the blend so that it avoids the prescribed

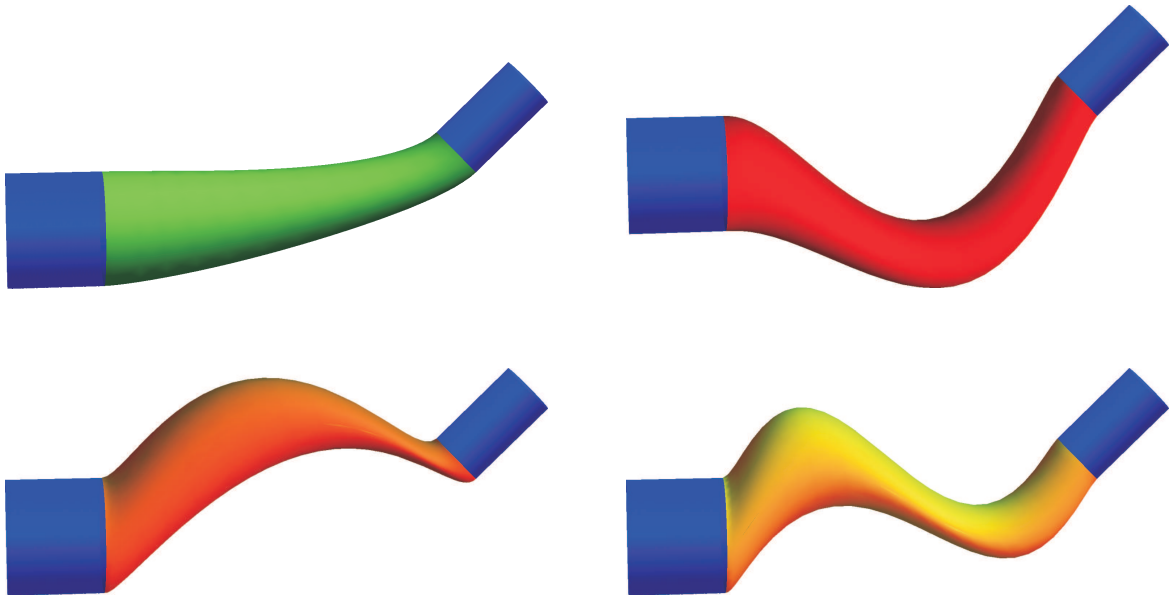

Figure 5.3: Adaptive blending ringed surface(s) (green, red, orange, yellow) between two cylinders (blue) differing only in the third coordinate of the directrices.

sphere, i.e., we modify its directrix according to (5.53). Analogously to canal surfaces, see condition (4.96), we use the following condition as the satisfying (not necessary) criterion for blending surface with the directrix $\mathbf{d}^*$ and the radius function ρ not intersecting the sphere centered at $\mathbf{s}$ and with the radius r:

$$\|\mathbf{d}^*(t) - \mathbf{s}\| > \rho(t) + r, \tag{5.56}$$

for all $t \in [0,1]$. We used the distance function (5.54) and

$$\mathbf{v} = \left(\frac{1}{5}, \frac{4}{5}, \frac{3}{5}\right)^\top \quad \text{and} \quad \tau = \frac{1}{2}. \tag{5.57}$$

The new constructed blend does not intersect the sphere (see Figure 5.4, right) since

$$\min_{t\in[0,1]} (\|\mathbf{d}^*(t) - \mathbf{s}\| - \rho(t) - r) \doteq 0.0228 > 0. \tag{5.58}$$

The shape variability (especially suitable for modelling purposes) of ringed surfaces can be used when e.g. one wants to optimize (in some sense) the shape of the already constructed blend. As a particular example, we choose a criterion that the shape of the modified blend is as close as possible to the shape of a normal ringed surface. This is a natural criterion from the point of view of practical applications as we would like to avoid the situations when the normals $\mathbf{n}$ differ too much from the tangents of $\mathbf{d}$.

The presented approach starts with the computation of a blending ringed surface, e.g. by Algorithm 4. So, we have the directrix $\mathbf{d}$, orientation function $\mathbf{n}$, radius function ρ and some function $\mathbf{f}$ satisfying (5.2). We construct the new directrix $\mathbf{d}^*$, cf. (5.53), where the distance function can be chosen as e.g. (5.54). We leave the vector $\mathbf{v}$ and

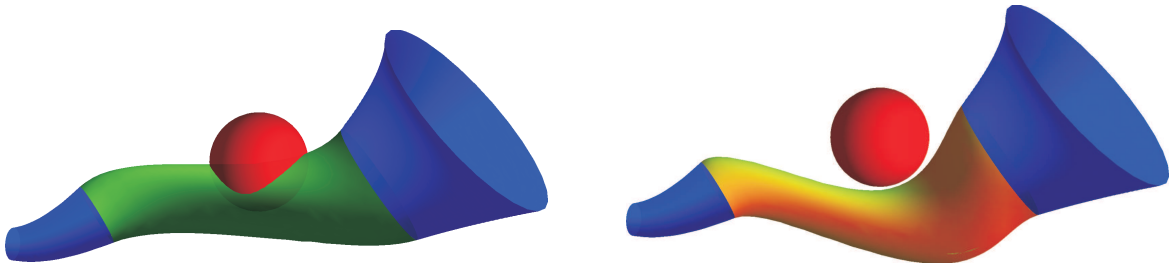

Figure 5.4: A blending ringed surface (green) intersecting the given obstacle (red) and a blending ringed surface (yellow) avoiding the given obstacle (red) between two ringed surfaces (blue) from Example 5.12.

the parameters of the distance function as free parameters and optimize the following objective function

$$\int_I \left(\frac{(\mathbf{f}\cdot(\mathbf{d}^*)')^2}{\|\mathbf{f}\|^2\|(\mathbf{d}^*)'\|^2} + \frac{((\mathbf{f}\times\mathbf{n})\cdot(\mathbf{d}^*)')^2}{\|\mathbf{f}\times\mathbf{n}\|^2\|(\mathbf{d}^*)'\|^2} \right) \mathrm{d}t, \tag{5.59}$$

which measures the deviance of the vectors $(\mathbf{d}^*)'$ from the vectors $\mathbf{n}$.

In Figure 5.1, right the blending surface from Example 5.10 modified by the previous approach to be as close as possible to a normal ringed surface is shown.

Example 5.13. Let be given two canal surfaces $\mathcal{S}_1$ and $\mathcal{S}_2$ defined by the cubic/quadratic mats

$$\begin{aligned} \overline{\mathbf{m}}_1 &= \left(0.3t-1.1, (1.1-0.3t)^2-1, (0.3t-1.1)^3, 0.03t^2-0.22t+0.736667\right)^\top, \\ \overline{\mathbf{m}}_2 &= \left(0.3t+2, 2(0.3t+1)^2, (0.3t+1)^2, 0.045t^2+0.3t+1\right)^\top. \end{aligned} \tag{5.60}$$

We consider them as ringed surfaces and compute their directrices, orientation functions and radius functions, cf. (2.35). Then we construct a blending ringed surface using Algorithm 4, see Figure 5.5, left. Finally involving the distance function (5.54) (where we set $\tau = 1/2$) and minimizing integral (5.59), we arrive at the vector

$$\mathbf{v} \doteq (-0.23824, -1.04859, 0.13459)^\top, \tag{5.61}$$

yielding a blending ringed surface which is "more normal" than the original one, see Figure 5.5, right.

5.4 Contour curves and approximate parameterizations of implicitly given blends.

We start with investigating contour curves on ringed surfaces and then we focus on computing approximate parameterizations of implicitly given ringed surfaces gained e.g. by some implicit blending techniques, cf. Section 3.1.

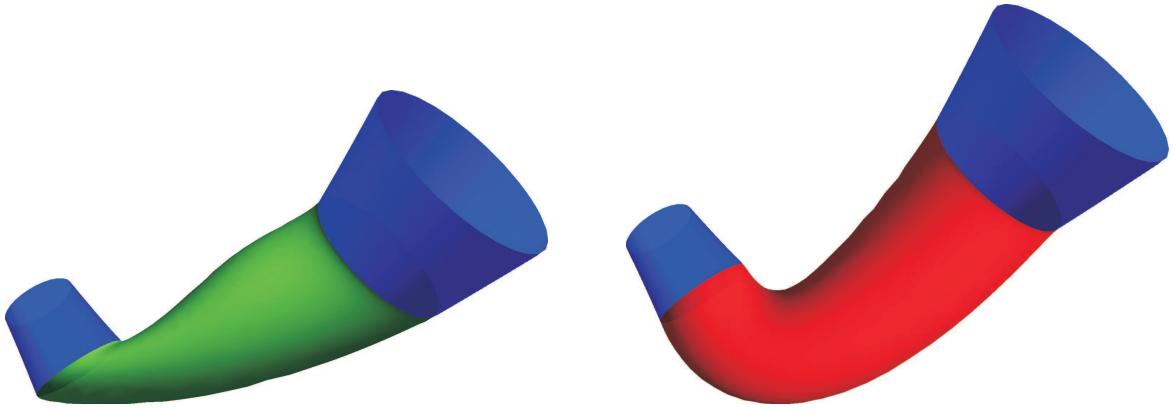

Figure 5.5: A blending ringed surface (green) and an optimized blending (almost normal) ringed surface (red) between two canal surfaces (blue) from Example 5.13.

As in the case of canal surfaces, a contour curve $\mathcal{C}_{\mathbf{v}}$ w.r.t. the vector $\mathbf{v}$ (a curve consisting of all the points at which the normals of $\mathcal{R}$ are orthogonal to $\mathbf{v}$) on a ringed surface corresponds to the silhouette of the given ringed surface when projecting it to the plane with the normal vector $\mathbf{v}$. We recall that studying projected contour curves (silhouettes) do not only help to create a first visual perception of the shape of the studied object but they have also many practical applications – for instance, in reconstruction of the 3D object from a 2D image, in rendering, in computing the visible area, when deleting invisible curves, see [7, 77, 83, 93].

Contrary to canal surfaces, the expression of contour curves for a general ringed surface is more complicated and contains even nested square roots. More precisely, a parameterization of the contour curve w.r.t. the vector $\mathbf{v}$ can be computed as the envelope of the family of ellipses obtained by projecting the family of sweeping circles

$$\|\mathbf{x}-\mathbf{d}\|^2-\rho^2=0, \quad (\mathbf{x}-\mathbf{d})\cdot\mathbf{n}=0 \tag{5.62}$$

in the projection $\pi_{\mathbf{v}}$, see (5.9).

Nonetheless, studying the resulting parametric expression in more detail is beyond the scope of this thesis. Here we only consider some special cases (special ringed surfaces) having the contour curves without nested square roots in their parametric expressions. One of the special situation occurs when the ellipses (projected characteristic circles in the projection $\pi_{\mathbf{v}}$) degenerate to line segments. This happens when the orientation function $\mathbf{n}$ is orthogonal to the direction $\mathbf{v}$ of the projection $\pi_{\mathbf{v}}$.

Consider a ringed surface $\mathcal{R}:(\mathbf{d},\mathbf{n},\rho)$ and a vector $\mathbf{v}$ for which the following condition holds

$$\mathbf{n}\cdot\mathbf{v}\equiv 0. \tag{5.63}$$

Then the orthogonal projection $\pi_{\mathbf{v}}$ sends the generating circles of $\mathcal{R}$ to the line segments and the contour curve of $\mathcal{R}$ w.r.t. $\mathbf{v}$ is of the form

$$\mathbf{c}_{\mathbf{v}}^{\pm}=\mathbf{d}\pm\rho\,\frac{\mathbf{n}\times\mathbf{v}}{\|\mathbf{n}\|}. \tag{5.64}$$

Thus we can formulate the following proposition.

Proposition 5.14. *Consider a vector* $\mathbf{v}$ *and a ringed surface* $\mathcal{R} : (\mathbf{d}, \mathbf{n}, \rho)$ *with the orientation function satisfying* (5.63). *Then* $\mathcal{R}$ *possesses a rational contour curve w.r.t.* $\mathbf{v}$ *iff the orientation function* $\mathbf{n}$ *corresponds to a P-curve.*

Corollary 5.15. *Any normal ringed surface with the directrix being a quadratic PH curve possesses a rational contour curve.*

The usefulness of the contour curves on ringed surfaces can be demonstrated on the problem of approximating implicitly given blends by a rational ringed surface.

Let us consider the problem formulated in Section 3.1, i.e., we want to approximate a blending surface $\mathcal{B}$ implicitly given by polynomial f between two normal ringed surfaces $\mathcal{R}_1$ and $\mathcal{R}_2$ (e.g. cones or cylinders of revolution) implicitly determined by polynomials f_1 and f_2, and bounded by planes $\mathcal{P}_1$ and $\mathcal{P}_2$ (perpendicular to their directrices) described by linear polynomials f_{10} and f_{20}, respectively.

In Chapter 3 the methods for computing approximate parameterizations of implicitly given canal surfaces based on approximating their contour curves by polynomial cubics were designed. The algorithm described in Section 3.4 starts with computing the polynomial cubic approximate parameterizations of three different contour curves of the given canal surface $\mathcal{S}$. From these parameterizations an approximation of the spine curve (also polynomial of degree 3) of $\mathcal{S}$ is reconstructed and consequently an approximate parameterization of $\mathcal{S}$ is computed.

An analogous approach can be used for computing approximate parameterizations of implicitly given ringed surfaces. We also (approximately) parameterize three different contour curves on the given ringed surface $\mathcal{B}$ and reconstruct an approximation of the directrix and the orientation function from these parameterizations.

In the case of canal surfaces the contour curves satisfy equality (2.33), which allows us to compute easily the parameterization of the spine curve from the parameterizations of three different contour curves, cf. (3.17). However, this advantageous equality is not satisfied for general ringed surfaces. So one can ask: Why to use the contour curves (in the case of ringed surfaces) while any arbitrary curves on $\mathcal{B}$ can be used instead with the same effect? Nonetheless the answer is simple: The contour curves on surfaces (not only ringed or canal) implicitly given by a polynomial f can be easily described as a complete intersection of two algebraic surfaces defined by (2.34).

We start with choosing three different contour curves $\mathcal{C}_{\mathbf{v}_1}$, $\mathcal{C}_{\mathbf{v}_2}$ and $\mathcal{C}_{\mathbf{v}_3}$ on $\mathcal{B}$. Then we compute the intersection points $\mathbf{p}_i^1, \ldots, \mathbf{p}_i^{k_i}$ of the plane $\mathcal{P}_1$ and the contour curves $\mathcal{C}_{\mathbf{v}_i}$, i.e., we solve the following system of equations

$$f_{10} = 0, \quad f = 0, \quad f_{\mathbf{v}_i} = 0, \quad i = 1, 2, 3. \tag{5.65}$$

Analogously by solving

$$f_{20} = 0, \quad f = 0, \quad f_{\mathbf{v}_i} = 0, \quad i = 1, 2, 3, \tag{5.66}$$

we obtain the intersection points $\mathbf{q}_i^1, \ldots, \mathbf{q}_i^{k_i}$ of the plane $\mathcal{P}_2$ and the contour curve $\mathcal{C}_{\mathbf{v}_i}$. Then we choose points $\mathbf{p}_i \in \{\mathbf{p}_i^1, \ldots, \mathbf{p}_i^{k_i}\}$ and $\mathbf{q}_i \in \{\mathbf{q}_i^1, \ldots, \mathbf{q}_i^{k_i}\}$ such that $\mathbf{p}_i\ \mathbf{q}_i$ lie on the

same branch of the contour curve $\mathcal{C}_{\mathbf{v}_i}$ – this can be done e.g. by considering a topology (constructing topological graphs) of the contour curves, for more details see Section 3.2.

From $\mathbf{p}_i$ and $\mathbf{q}_i$, $i = 1,2,3$, the centers of the characteristic circles $\mathbf{s}_1$ and $\mathbf{s}_2$ can be reconstructed. In particular the center of the circle passing through the points $\mathbf{p}_i$ is computed as follows

$$\mathbf{s} = \frac{\mathbf{p}_1 + \mathbf{p}_2}{2} + \frac{(\mathbf{a}\cdot\mathbf{b}) - \|\mathbf{b}\|^2}{2\|\mathbf{a}\times\mathbf{b}\|^2}\Big((\mathbf{a}\cdot\mathbf{b})\mathbf{a} - \|\mathbf{a}\|^2\mathbf{b}\Big), \tag{5.67}$$

where $\mathbf{a} = \mathbf{p}_2 - \mathbf{p}_1$ and $\mathbf{b} = \mathbf{p}_3 - \mathbf{p}_1$. Then we construct an auxiliary approximation $\overline{\mathbf{d}}$ of the directrix curve of $\mathcal{B}$ by interpolating points $\mathbf{s}_1$ and $\mathbf{s}_2$ with the tangent vectors being the normal vectors of the planes $\mathcal{P}_1$ and $\mathcal{P}_2$ by the Ferguson's cubic. The lengths of $\mathbf{n}_1$ and $\mathbf{n}_2$ can be chosen e.g. according to the distance of $\mathbf{s}_1$ and $\mathbf{s}_2$ – our tests have shown that using the lengths of $\mathbf{n}_1$ and $\mathbf{n}_2$ both equal to the distance of $\mathbf{s}_1$ and $\mathbf{s}_2$ works sufficiently.

Now we compute approximate parameterizations $\mathbf{c}_{\mathbf{v}_1}$, $\mathbf{c}_{\mathbf{v}_2}$ and $\mathbf{c}_{\mathbf{v}_3}$ of the particular branches of the contour curves $\mathcal{C}_{\mathbf{v}_1}$, $\mathcal{C}_{\mathbf{v}_2}$ and $\mathcal{C}_{\mathbf{v}_3}$ so that we construct the Ferguson's cubics joining the points $\mathbf{p}_i$ and $\mathbf{q}_i$ with the tangent vectors $\alpha_i\mathbf{t}_{\mathbf{p}_i}$ and $\beta_i\mathbf{t}_{\mathbf{q}_i}$ with the lengths α_i and β_i as free parameters, where

$$\mathbf{t}_{\mathbf{x}_i} = \frac{\nabla f(\mathbf{x}_i)\times\nabla f_{\mathbf{v}_i}(\mathbf{x}_i)}{\|\nabla f(\mathbf{x}_i)\times\nabla f_{\mathbf{v}_i}(\mathbf{x}_i)\|}. \tag{5.68}$$

Finally we compute the "optimal" values of the free parameters α_i and β_i by minimizing the following objective function

$$\Omega = \Phi(f, f_{\mathbf{v}_1}, \mathbf{c}_{\mathbf{v}_1}) + \Phi(f, f_{\mathbf{v}_2}, \mathbf{c}_{\mathbf{v}_2}) + \Phi(f, f_{\mathbf{v}_3}, \mathbf{c}_{\mathbf{v}_3}) + w\,\Psi(\overline{\mathbf{d}}, \mathbf{c}_{\mathbf{v}_1} - \mathbf{c}_{\mathbf{v}_2}, \mathbf{c}_{\mathbf{v}_1} - \mathbf{c}_{\mathbf{v}_3}), \tag{5.69}$$

where w is a suitable weight, the objective function

$$\Phi(f, g, \mathbf{c}) = \int_I \frac{f^2(\mathbf{c})}{\|\nabla f(\mathbf{c})\|^2} + \frac{g^2(\mathbf{c})}{\|\nabla g(\mathbf{c})\|^2}\,\mathrm{d}t \tag{5.70}$$

is responsible for the deviance of the approximate parameterization $\mathbf{c}$ from the implicit representation $f = g = 0$, cf. (2.42) and the objective function

$$\Psi(\mathbf{n}, \mathbf{a}, \mathbf{b}) = \int_I \frac{(\mathbf{a}\cdot\mathbf{n})^2}{\|\mathbf{a}\|^2\|\mathbf{n}\|^2} + \frac{(\mathbf{b}\cdot\mathbf{n})^2}{\|\mathbf{b}\|^2\|\mathbf{n}\|^2}\,\mathrm{d}t \tag{5.71}$$

measures the deviance of the approximation of the normal vector of the plane spanned by the vectors $\mathbf{a}$, $\mathbf{b}$ from the vector $\mathbf{n}$.

The whole method of computing an approximate parameterization of the implicitly given ringed surface is summarized in Algorithm 5.

Remark 5.16. When the blend, which shall be approximated, is of a more complex shape, then a refinement can be done to increase the accuracy. In particular we can

Algorithm 5 Approximate parameterization of implicitly given ringed surface.

INPUT: A ringed surface $\mathcal{B}$ (blend) given by the implicit equation $f = 0$ and two planes $\mathcal{P}_1$ and $\mathcal{P}_2$ (bounding $\mathcal{B}$) defined by the polynomials f_{10} and f_{20}.

1: Choose three different (unit) vectors $\mathbf{v}_i$, $i = 1,2,3$ and determine contour curves $\mathcal{C}_{\mathbf{v}_i}$, implicitly defined by polynomials $f, f_{\mathbf{v}_i}$, cf. (2.34);

2: Compute the intersection points $\mathbf{p}_i^1,\dots,\mathbf{p}_i^{k_i}$ of $\mathcal{C}_{\mathbf{v}_i}$ with $\mathcal{P}_1$, and $\mathbf{q}_i^1,\dots,\mathbf{q}_i^{k_i}$ of $\mathcal{C}_{\mathbf{v}_i}$ with $\mathcal{P}_2$, cf. (5.65) and (5.66);

3: Choose $\mathbf{p}_i \in \{\mathbf{p}_i^1,\dots,\mathbf{p}_i^{k_i}\}$ and $\mathbf{q}_i \in \{\mathbf{q}_i^1,\dots,\mathbf{q}_i^{k_i}\}$ such that couple $\mathbf{p}_i\mathbf{q}_i$ corresponds to the particular segment of $\mathcal{C}_{\mathbf{v}_i}$;

4: Compute the centers $\mathbf{s}_1$ and $\mathbf{s}_2$ of the circles going through $\mathbf{p}_i$ and $\mathbf{q}_i$, respectively, cf. (5.67);

5: Take the normal vectors $\mathbf{n}_j$, $j = 1,2$ of the planes $\mathcal{P}_j$, i.e., given by the coefficients of the linear terms of the polynomials f_{j0};

6: Construct the Ferguson's cubic $\overline{\mathbf{d}}$ interpolating the points $\mathbf{s}_1$ and $\mathbf{s}_2$ and the vectors $w_1\,\mathbf{n}_1$ and $w_2\,\mathbf{n}_2$, where w_1 and w_2 are chosen according to the distance of $\mathbf{s}_1$ and $\mathbf{s}_2$;

7: Construct the Ferguson's cubics $\mathbf{c}_{\mathbf{v}_i}$ interpolating the points $\mathbf{p}_i$ and $\mathbf{q}_i$ with the tangent vectors $\alpha_i\mathbf{t}_{\mathbf{p}_i}$ and $\beta_i\mathbf{t}_{\mathbf{q}_i}$ (see (5.68)) with the lengths α_i and β_i as free parameters;

8: Minimize the objective function (5.69) and set the obtained values of α_i and β_i to the parameterizations $\mathbf{c}_{\mathbf{v}_i}$;

9: Reconstruct the directrix $\mathbf{d}$ by computing the center of the 1-parameter family of circles going through $\mathbf{c}_{\mathbf{v}_i}$, see (5.67);

10: Reconstruct the orientation function $\mathbf{n} = (\mathbf{c}_{\mathbf{v}_1} - \mathbf{c}_{\mathbf{v}_2}) \times (\mathbf{c}_{\mathbf{v}_1} - \mathbf{c}_{\mathbf{v}_3})$;

11: Compute an approximate parameterization of $\mathcal{B}$ using one of the curves $\mathbf{c}_{\mathbf{v}_i}$ and formula (2.37);

OUTPUT: The approximate parameterization $\mathbf{s}(t,u)$ of the ringed surface $\mathcal{B}$.

modify Algorithm 5 analogously to Algorithms 2 and 3 such that we can consider the critical points of the contour curves when parameterizing them. Then the blending surface will be composed of more parts and each part will be approximated analogously as we discussed above. An easier way of providing a refinement (without computing the critical points) is to divide the input blending surface into a suitable number of parts by cutting it by planes $\mathcal{P}_{\tau_i}$, $\tau_i \in (0,1)$, where

$$\mathcal{P}_{\tau_i} : \overline{\mathbf{d}}'(\tau_i) \cdot (\mathbf{x} - \overline{\mathbf{d}}(\tau_i)) = 0. \tag{5.72}$$

Remark 5.17. Let us note that it is enough to use only two contour curves in the parameterization process. Since contour curves possess two real branches in general, we can work with the two real branches $\mathbf{c}_{\mathbf{v}_1}^{\pm}$ of one contour curve $\mathcal{C}_{\mathbf{v}_1}$ and one real branch $\mathbf{c}_{\mathbf{v}_2}^{+}$ of another contour curve $\mathcal{C}_{\mathbf{v}_2}$.

Example 5.18. We compute an approximate parameterization of the ringed surface $\mathcal{B}$ defined by the polynomial f, see Figure 5.6, obtained by the method from [39],

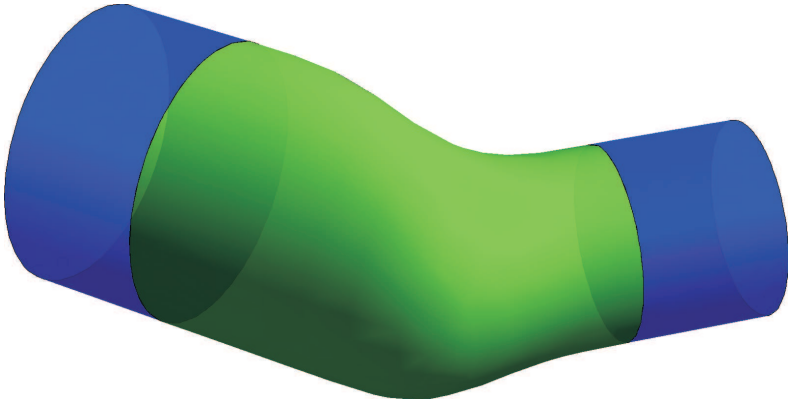

Figure 5.6: Implicit blending surface (green) between two cylinders (blue) from Example 5.18.

cf. (3.1), where we have set $\lambda = 1/2$ and $n = 2$, as an implicit blending surface between the cylinders given by

$$f_1 = y^2 + z^2 - 9, \quad f_2 = x^2 - 2xy - 12x + y^2 + 12y + 2z^2 + 28, \tag{5.73}$$

bounded by the planes

$$f_{10} = x = 0, \quad f_{20} = x + y = 10, \tag{5.74}$$

respectively. We start with computing approximate parameterizations of the contour curves w.r.t. the vectors

$$\mathbf{v}_1 = (0,0,1)^\top, \ \mathbf{v}_2 = (0,1,0)^\top, \ \mathbf{v}_3 = \left(0, \frac{1}{\sqrt{2}}, \frac{1}{\sqrt{2}}\right)^\top. \tag{5.75}$$

From these parameterizations we reconstruct the directrix $\mathbf{d}$ and the orientation function $\mathbf{n}$. Finally, we compute the approximate parameterization of $\mathcal{B}$ by using one of the curves $\mathbf{c}_{\mathbf{v}_i}$ and formula (2.37). The error of the approximation measured by integral (2.43) is less than $2.1 \cdot 10^{-2}$ when using parameterization of one part and $3.7 \cdot 10^{-4}$ when using parameterizations of two parts.

5.5 Blending three or more ringed surfaces

In this section, we will deal with the problem of constructing a blending surface between three or more ringed surfaces. The method is based on choosing an auxiliary sphere and separately constructing blending ringed surfaces between the given ringed surfaces and the sphere by the methods discussed in the previous sections.

Consider the (parts of the) three ringed surfaces $\mathcal{R}_i$, $i = 1,2,3$ given by

$$\mathcal{R}_i : (\mathbf{d}_i, \mathbf{n}_i, \rho_i)(t), \quad t \in [0,1]. \tag{5.76}$$

Firstly, we choose an auxiliary sphere $\mathcal{S}$ in a suitable position "between" $\mathcal{R}_i$ simultaneously not intersecting them – e.g., we can choose the center $\mathbf{s}$ of $\mathcal{S}$ on the line going

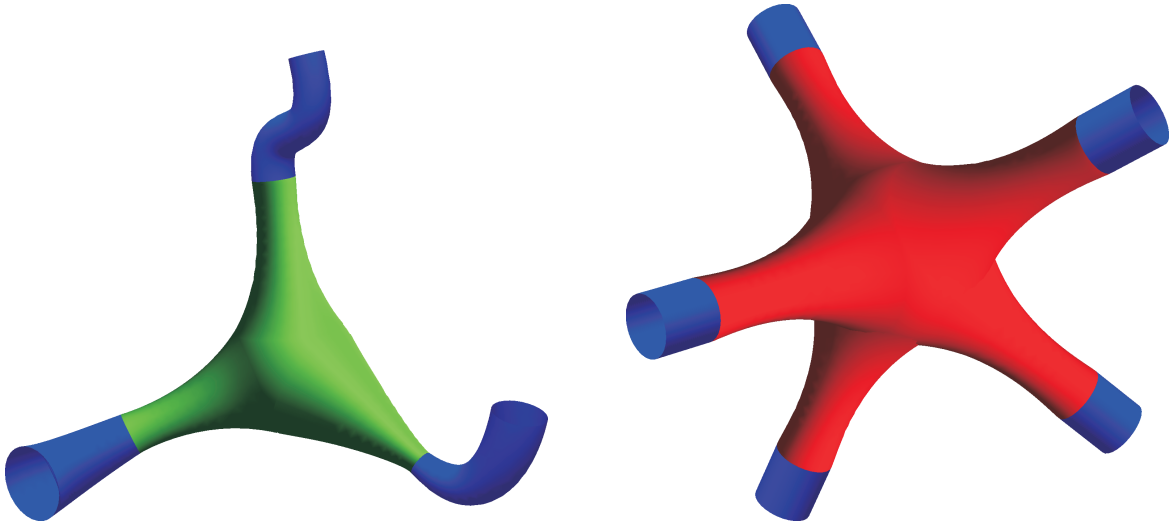

Figure 5.7: A blending surface (green) between three ringed surfaces (blue) from Example 5.20, left and a blending surface (red) between five ringed surfaces (blue), right.

through the center of the inscribed circle of the triangle joining points $\mathbf{d}_i(1)$ and having the direction vector perpendicular to the plane containing points $\mathbf{d}_i(1)$, i.e.,

$$\mathbf{s} = \mathbf{y}(1) + \alpha\left[(\mathbf{d}_1(1) - \mathbf{d}_2(1)) \times (\mathbf{d}_1(1) - \mathbf{d}_3(1))\right], \quad \alpha \in \mathbb{R}, \tag{5.77}$$

where

$$\mathbf{y}(t) = \mathbf{d}_1 + \frac{(\mathbf{d}_2 - \mathbf{d}_1)\|\mathbf{d}_3 - \mathbf{d}_1\| + (\mathbf{d}_3 - \mathbf{d}_1)\|\mathbf{d}_2 - \mathbf{d}_1\|}{\|\mathbf{d}_2 - \mathbf{d}_1\| + \|\mathbf{d}_3 - \mathbf{d}_1\| + \|\mathbf{d}_3 - \mathbf{d}_2\|}. \tag{5.78}$$

The parameter α is set to reflect the angle between $\mathbf{d}_i'(1)$ and the plane containing points $\mathbf{d}_i(1)$. The radius r of $\mathcal{S}$ has to be chosen so that $\mathcal{S}$ does not intersect any of $\mathcal{R}_i$, i.e.

$$r \in \left(0, \min_{i=1,2,3}\{\|\mathbf{p}_i - \mathbf{s}\|\}\right). \tag{5.79}$$

Next, for each ringed surface $\mathcal{R}_i$ we consider the sphere $\mathcal{S}$ as a ringed surface $\mathcal{S}_i$ given by

$$\begin{aligned} \mathbf{n}_i^* &= \frac{\mathbf{d}_i(1) - \mathbf{s}}{\|\mathbf{d}_i(1) - \mathbf{s}\|}, \\ \mathbf{d}_i^* &= \mathbf{s} - r\mathbf{n}_i^* + t(2r\mathbf{n}_i^*), \\ r_i^* &= \sqrt{r^2 - \|\mathbf{d}_i^* - \mathbf{s}\|^2} = 2r\sqrt{t(1-t)}. \end{aligned} \tag{5.80}$$

For each $i \in \{1,2,3\}$, this enables to describe the sphere $\mathcal{S}$ as a family of circles (denoted by $\mathcal{S}_i$) set coherently with the end circles of a particular $\mathcal{R}_i$

Now, for each $i \in \{1,2,3\}$ we compute a classical blending surface $\mathcal{B}_i$ between $\mathcal{R}_i$ and $\mathcal{S}_i$ (see Algorithm 4) such that we interpolate Hermite data

$$\begin{aligned} \mathbf{p}_i &= (\mathbf{d}_i, \mathbf{n}_i, \rho_i)^\top(1), \quad & \mathbf{v}_i &= (\mathbf{d}_i', \mathbf{n}_i', \rho_i')^\top(1) \\ \mathbf{p}_i^* &= (\mathbf{d}_i^*, \mathbf{n}_i^*, \rho_i^*)^\top(\lambda_i), \quad & \mathbf{v}_i^* &= \left(\left(\mathbf{d}_i^*\right)', \left(\mathbf{n}_i^*\right)', \left(\rho_i^*\right)'\right)^\top(\lambda_i), \end{aligned} \tag{5.81}$$

where $\lambda_i \in (0,1)$ corresponds to a particular selected circle $c_i \in \mathcal{S}_i$ at which $\mathcal{B}_i$ joins $\mathcal{S}_i$. Parameters λ_i have to be chosen so that the circles c_i, $i = 1,2,3$, do not intersect each other.

Remark 5.19. Let us note that in the construction of the multiple blends the position and the radius of the auxiliary sphere (and even the circles on the sphere at which the blend surfaces join it) can be chosen freely (only some natural criteria must be satisfied). Hence the multiple blends can be easily modified according to further prescribed requirements reflecting additional modelling conditions.

Example 5.20. We construct a blending surface between three given (normal) ringed surfaces $\mathcal{R}_1, \mathcal{R}_2$ and $\mathcal{R}_3$ given as follows:

$$\begin{aligned}
\mathbf{d}_1 &= \left(14t^3 - 23t^2 + 12t - 9, 4t - 7, 0\right)^\top, & \mathbf{n}_1 &= \mathbf{d}_1', \quad \rho_1 = \frac{1}{6}(t+4);\\
\mathbf{d}_2 &= \left(-4t^3 + 4t + 6, -2t^3 + 3t^2 + 4t - 8, 0\right)^\top, & \mathbf{n}_2 &= \mathbf{d}_2', \quad \rho_2 = \frac{1}{2}(2 - t^2);\\
\mathbf{d}_3 &= \left(0, 2t^3 - 5t^2 + 8, 2t^3 - 3t^2 + 4t - 8\right)^\top, & \mathbf{n}_3 &= \mathbf{d}_3', \quad \rho_3 = \frac{1}{6}(9 - 4t).
\end{aligned} \tag{5.82}$$

We have chosen the auxiliary spheres with the following center and radius

$$\mathbf{s} = (0.5, 0.3, -0.25)^\top, \qquad r = 2.6, \tag{5.83}$$

and all the parameters λ_i were set to 0.2, see Figure 5.7, left.

Analogously, we can construct general n-way blends between n ringed surfaces; Figure 5.7 (right) presents 5-way blend between five given ringed surfaces.

Chapter 6

Conclusion

In this thesis the techniques for computing exact/approximate parameterizations of canal and ringed surfaces was presented and studied. Firstly we focused on canal surfaces given implicitly – the designed approach is based on computing approximate topology-based parameterizations of spatial curves lying on the given canal surface. The method can be directly applied on the practical problem of parameterizing implicit blends consisting of parts of canal (or canal-surface-like) surfaces.

Then we studied a condition guaranteeing the rationality of contour curves on canal surfaces. These curves were then used for a computation of rational PN parameterizations of canal surfaces, where PN stands for Pythagorean normals. Our approach extends the results about rational spatial MPH curves and the associated planar PH curves and relates them with the contour curves of canal surfaces given by their medial axis transforms. In addition, methods for constructing (adaptive) rational offset blends between two canal surfaces were presented. A functionality of all these algorithms was demonstrated on several examples.

Finally we studied rational ringed surfaces which have been used for construction (adaptive) blends between two and more ringed surfaces. We also presented a method dealing with approximating implicitly given blends by rational ringed surfaces.

Bibliography

[1] Abhyankar, S., and Bajaj, C. Automatic parametrization of rational curves and surfaces ii: cubics and cubicoids. *Computer-Aided Design 19*, 9 (1987), 499 – 502.

[2] Altmann, S. L. *Rotations, quaternions, and double groups*. Dover Publications, 2005.

[3] Bastl, B., Bizzarri, M., Krajnc, M., Lávička, M., Slabá, K., Šír, Z., Vitrih, V., and Žagar, E. C1 hermite interpolation with spatial pythagorean-hodograph cubic biarcs. *Journal of Computational and Applied Mathematics 257* (Feb. 2014), 65–78.

[4] Bastl, B., Jüttler, B., Lávička, M., and Schulz, T. Blends of canal surfaces from polyhedral medial surface transform representations. *Computer-Aided Design Design 43*, 11 (2011), 1477–1484.

[5] Bastl, B., Jüttler, B., Lávička, M., Schulz, T., and Šír, Z. On the parameterization of rational ringed surfaces and rational canal surfaces. To appear in Mathematics in Computer Science, 2014.

[6] Bastl, B., Slabá, K., and Byrtus, M. Planar hermite interpolation with uniform and non-uniform tc-biarcs. *Computer Aided Geometric Design 30*, 1 (2013), 58 – 77. Recent Advances in Applied Geometry.

[7] Benichou, F., and Eiber, G. Output sensitive extraction of silhouettes from polygonal geometry. In *Computer Graphics and Applications, 1999. Proceedings. Seventh Pacific Conference on* (1999), pp. 60–69.

[8] Bizzarri, M., and Lávička, M. A symbolic-numerical method for computing approximate parameterizations of canal surfaces. *Computer-Aided Design 44*, 9 (2012), 846 – 857.

[9] Bizzarri, M., and Lávička, M. Parameterizing rational offset canal surfaces via rational contour curves. *Computer-Aided Design 45*, 2 (2013), 342–350.

[10] Bizzarri, M., and Lávička, M. A symbolic-numerical approach to approximate parameterizations of space curves using graphs of critical points. *Journal of Computational and Applied Mathematics 242* (2013), 107 – 124.

[11] Bizzarri, M., and Lávička, M. Approximation of implicit blends by canal surfaces of low parameterization degree. In *Mathematical Methods for Curves and Surfaces*, vol. 8177 of *Lecture Notes in Computer Science*. Springer Berlin Heidelberg, 2014, pp. 34–48.

[12] Bizzarri, M., and Lávička, M. On modelling with rational ringed surfaces. *submitted to Computer-Aided Design* (2014).

[13] Bizzarri, M., Lávička, M., and Vršek, J. Canal surfaces with rational contour curves and blends bypassing the obstacles. *submitted to Computer-Aided Design* (2014).

[14] Bloomenthal, J. Modeling the mighty maple. *SIGGRAPH Comput. Graph. 19*, 3 (July 1985), 305–311.

[15] Blum, R. Circles on surfaces in the Euclidean 3-space. In *Geometry and Differential Geometry*, vol. 792 of *Lecture Notes in Mathematics*. Springer Berlin / Heidelberg, 1980, pp. 213–221.

[16] Boudon, F., Meyer, A., and Godin, C. Survey on computer representations of trees for realistic and efficient rendering. Tech. Rep. RR-LIRIS-2006-003, LIRIS UMR 5205 CNRS/INSA de Lyon/Université Claude Bernard Lyon 1/Université Lumiére Lyon 2/École Centrale de Lyon, Feb. 2006.

[17] Brieskorn, E., and Knörer, H. *Plane Algebraic Curves*. Birkhäuser Basel, 1986.

[18] Cheng, J., Lazard, S., Peñaranda, L., Pouget, M., Rouillier, F., and Tsigaridas, E. On the topology of planar algebraic curves. In *Proceedings of the 25th annual symposium on Computational geometry* (New York, NY, USA, 2009), SCG '09, ACM, pp. 361–370.

[19] Cho, H., Choi, H., Kwon, S.-H., Lee, D., and Wee, N.-S. Clifford algebra, Lorentzian geometry and rational parametrization of canal surfaces. *Computer Aided Geometric Design 21* (2004), 327–339.

[20] Choi, H., and Lee, D. Rational parametrization of canal surface by 4 dimensional Minkowski Pythagorean hodograph curves. In *Proceedings of the Geometric Modeling and Processing 2000* (Washington, DC, USA, 2000), GMP '00, IEEE Computer Society, pp. 301–309.

[21] Choi, H. I., Han, C. Y., Moon, H. P., Roh, K. H., and Wee, N. S. Medial axis transform and offset curves by Minkowski Pythagorean hodograph curves. *Computer-Aided Design 31*, 1 (Jan. 1999), 59–72.

[22] Choi, M. D., Lam, T. Y., and Reznick, B. Sums of squares of real polynomials. *Proceedings of Symposia in Pure Mathematics 58* (1995), 103–126.

[23] Coolidge, J. *A Treatise on the Circle and Sphere*. Clarendon Press, 1916.

[24] Cox, D. A., Little, J., and O'Shea, D. *Ideals, Varieties, and Algorithms: An Introduction to Computational Algebraic Geometry and Commutative Algebra*. Springer-Verlag New York, Inc., Secaucus, NJ, USA, 2007.

[25] Daniels, R. W. *Introduction to Numerical Methods and Optimization Techniques*. Elsevier Science Ltd, 1978.

[26] Darboux, J. Sur le contact des courbes et des surfaces. *Bulletin des Sciences Mathématiques 2*, 4 (1880), 348–384.

[27] Dietz, R., Hoschek, J., and Jüttler, B. An algebraic approach to curves and surfaces on the sphere and on other quadrics. *Computer Aided Geometric Design 10*, 3-4 (1993), 211–229.

[28] Dohm, M., and Zube, S. The implicit equation of a canal surface. *J. Symb. Comput. 44* (February 2009), 111–130.

[29] Farin, G. *Curves and Surfaces for Computer-Aided Geometric Design*. Academic Press, 1988.

[30] Farin, G. *Curves and surfaces for CAGD: A practical guide*. Morgan Kaufmann Publishers Inc., San Francisco, CA, USA, 2002.

[31] Farin, G., Hoschek, J., and Kim, M.-S., Eds. *Handbook of Computer Aided Geometric Design*. Elsevier, 2002.

[32] Farouki, R. *Pythagorean-Hodograph Curves: Algebra and Geometry Inseparable*. Springer, 2008.

[33] Farouki, R., and Sakkalis, T. Pythagorean hodographs. *IBM Journal of Research and Development 34*, 5 (1990), 736–752.

[34] Farouki, R. T., and Giannelli, C. Spatial camera orientation control by rotation-minimizing directed frames. *Computer Animation and Virtual Worlds 20*, 4 (2009), 457–472.

[35] Farouki, R. T., and Pottmann, H. Polynomial and rational Pythagorean-hodograph curves reconciled. In *Proceedings of the 6th IMA Conference on the Mathematics of Surfaces* (New York, NY, USA, 1996), Clarendon Press, pp. 355–378.

[36] Goldman, R. Understanding quaternions. *Graphical Models 73* (March 2011), 21–49.

[37] Harris, J. *Algebraic Geometry: A First Course*. Springer-Verlag, 1992.

[38] Hartman, E. Blending of implicit surfaces with functional splines. *Computer-Aided Design 22* (October 1990), 500–506.

[39] Hartmann, E. G^n-continuous connections between normal ringed surfaces. *Computer Aided Geometric Design 18*, 8 (2001), 751 – 770.

[40] Hartmann, E. Implicit G^n-blending of vertices. *Computer Aided Geometric Design 18*, 3 (2001), 267 – 285.

[41] Heo, H.-S., Hong, S., Seong, J.-K., Kim, M.-S., and Elber, G. The intersection of two ringed surfaces and some related problems. *Graphical Models 63* (2001), 228–244.

[42] Hoffmann, C., and Hopcroft, J. Quadratic blending surfaces. *Computer-Aided Design 18*, 6 (1986), 301 – 306.

[43] Hoffmann, C., H. J. Automatic surface generation in computer aided design. *The Visual Computer 1*, 2 (1985), 92–100. cited By (since 1996) 16.

[44] Hoschek, J., and Lasser, D. *Fundamentals of computer-aided geometric design*. AK Peters, 1993.

[45] Johnstone, J. A new intersection algorithm for cyclides and swept surfaces using circle decomposition. *Computer Aided Geometric Design 10*, 1 (1993), 1 – 24.

[46] Kim, G.-I., and Ahn, M.-H. C^1 Hermite interpolation using MPH quartic. *Computer Aided Geometric Design 20* (2003), 469–492.

[47] Kosinka, J., and Jüttler, B. G^1 Hermite interpolation by Minkowski Pythagorean hodograph cubics. *Computer Aided Geometric Design 23* (2006), 401–418.

[48] Kosinka, J., and Jüttler, B. C^1 Hermite interpolation by Pythagorean hodograph quintics in Minkowski space. *Advances in Computational Mathematics 30* (2009), 123–140.

[49] Kosinka, J., and Lávička, M. On rational Minkowski Pythagorean hodograph curves. *Computer Aided Geometric Design 27*, 7 (2010), 514–524.

[50] Kosinka, J., and Lávička, M. A unified Pythagorean hodograph approach to medial axis transform and offset approximation. *Journal of Computational and Applied Mathematics 235*, 12 (2011), 3413–3424.

[51] Kosinka, J., and Šír, Z. C^2 Hermite interpolation by Minkowski Pythagorean hodograph curves and medial axis transform approximation. *Computer Aided Geometric Design In Press* (2010).

[52] Krasauskas, R., and Mäurer, C. Studying cyclides with Laguerre geometry. *Computer Aided Geometric Design 17*, 2 (2000), 101–126.

[53] Krasauskas, R., and Zube, S. Canal surfaces defined by quadratic families of spheres. In *Geometric Modeling and Algebraic Geometry*, B. Jüttler and R. Piene, Eds. Springer Berlin Heidelberg, 2008, pp. 79–92.

[54] Krasauskas, R., and Zube, S. Bézier-like parametrizations of spheres and cyclides using geometric algebra. In *9th International Conference on Clifford Algebras and their Applications in Mathematical Physics* (2011), K. Guerlebeck, Ed. `http://www.mif.vu.lt/~rimask/en/`.

[55] Kubota, K. Pythagorean triples in unique factorization domains. *American Mathematical Monthly 79* (1972), 503–505.

[56] Lü, W., and Pottmann, H. Pipe surfaces with rational spine curve are rational. *Computer Aided Geometric Design 13* (1996), 621–628.

[57] Landsmann, G., Schicho, J., and Winkler, F. The parametrization of canal surfaces and the decomposition of polynomials into a sum of two squares. *Journal of Symbolic Computation 32*, 1-2 (2001), 119 – 132.

[58] Lávička, M., and Bastl, B. Rational hypersurfaces with rational convolutions. *Computer Aided Geometric Design 24*, 7 (2007), 410–426.

[59] Lü, W., and Pottmann, H. Pipe surfaces with rational spine curve are rational. *Computer Aided Geometric Design 13*, 7 (Oct. 1996), 621–628.

[60] Ma, Y., Tu, C., and Wang, W. Distance computation for canal surfaces using cone-sphere bounding volumes. *Comput. Aided Geom. Des. 29*, 5 (June 2012), 255–264.

[61] Marshall, M. *Positive Polynomials and Sums of Squares*. Mathematical surveys and monographs, v. 146. Amer Mathematical Society, 2008.

[62] Moon, H. Minkowski Pythagorean hodographs. *Computer Aided Geometric Design 16* (1999), 739–753.

[63] Neumaier, A. *Introduction to Numerical Analysis*. Cambridge University Press, 2001.

[64] Peternell, M. Rational families of conics and quadrics. In *The Mathematics of Surfaces* (1998), vol. VIII, Information Geometers, pp. 369–382.

[65] Peternell, M. Rational families of conics and quadrics. *The Mathematics of Surfaces 8* (1998), 369–382.

[66] Peternell, M., and Manhart, F. The convolution of a paraboloid and a parametrized surface. *Journal for Geometry and Graphics 7*, 2 (2003), 157–171.

[67] Peternell, M., and Odehnal, B. Convolution surfaces of quadratic triangular Bézier surfaces. *Computer Aided Geometric Design 25* (2008), 116–129.

[68] Peternell, M., and Pottmann, H. Computing rational parametrizations of canal surfaces. *Journal of Symbolic Computation 23* (February 1997), 255–266.

[69] Peternell, M., and Pottmann, H. A Laguerre geometric approach to rational offsets. *Computer Aided Geometric Design 15* (1998), 223–249.

[70] Pottmann, H. Rational curves and surfaces with rational offsets. *Computer Aided Geometric Design 12*, 2 (1995), 175–192.

[71] Pottmann, H., and Peternell, M. Applications of Laguerre geometry in CAGD. *Computer Aided Geometric Design 15* (1998), 165–186.

[72] Pottmann, H., Shi, L., and Skopenkov, M. Darboux cyclides and webs from circles. *Computer Aided Geometric Design 29*, 1 (2012), 77 – 97.

[73] Rockwood, A. P. Displacement method for implicit blending surfaces in solid models. vol. 8, pp. 279–297. cited By (since 1996) 32.

[74] Rupprecht, D. An algorithm for computing certified approximate gcd of n univariate polynomials. *Journal of Pure and Applied Algebra 139*, 1-3 (1999), 255 – 284.

[75] Ryaben'kii, V. S., and Tsynkov, S. V. *A Theoretical Introduction to Numerical Analysis*. Chapman and Hall/CRC, 2006.

[76] Sampoli, M. L., Peternell, M., and Jüttler, B. Rational surfaces with linear normals and their convolutions with rational surfaces. *Computer Aided Geometric Design 23*, 2 (2006), 179–192.

[77] Schein, S., and Elber, G. Adaptive extraction and visualization of silhouette curves from volumetric datasets. *The Visual Computer 20*, 4 (2004), 243–252.

[78] Schicho, J. On the choice of pencils in the parametrization of curves. *Journal of Symbolic Computation 14* (December 1992), 557–576.

[79] Schicho, J. Rational parametrization of surfaces. *Journal of Symbolic Computation 26*, 1 (1998), 1–29.

[80] Schicho, J. Proper parametrization of real tubular surfaces. *J. Symb. Comput. 30* (November 2000), 583–593.

[81] Sederberg, T., and Snively, J. Parametrization of cubic algebraic surfaces. In *Proceedings on Mathematics of surfaces II* (New York, NY, USA, 1988), Clarendon Press, pp. 299–319.

[82] Sendra, J., and Winkler, F. Symbolic parametrization of curves. *Journal of Symbolic Computation 12*, 6 (1991), 607–631.

[83] Seong, J.-K., Kim, K.-J., Kim, M.-S., and Elber, G. Perspective silhouette of a general swept volume. *Visual Computer 22*, 2 (2006), 109–116. cited By (since 1996)4.

[84] Shafarevich, I. *Basic algebraic geometry*. Springer Verlag, 1974.

[85] Shene, C.-K. Blending two cones with Dupin cyclides. *Computer Aided Geometric Design 15*, 7 (1998), 643 – 673.

[86] Smith, K. E., Kahanpää, L., Kekäläinen, P., and Traves, W. *An Invitation to Algebraic Geometry*. Springer, 2000.

[87] Szilágyi, I., Jüttler, B., and Schicho, J. Local parametrization of cubic surfaces. *Journal of Symbolic Computation 41* (January 2006), 30–48.

[88] Takeuchi, N. Cyclides. *Hokkaido Mathematical Journal 29*, 1 (2000), 119.

[89] van Hoeij, M. Rational parametrizations of algebraic curves using a canonical divisor. *Journal of Symbolic Computation 23* (1997), 209–227.

[90] Wagner, M. G., and Ravani, B. Curves with rational frenet-serret motion. *Computer Aided Geometric Design 15*, 1 (1997), 79 – 101.

[91] Walker, R. *Algebraic Curves*. Princeton University Press, 1950.

[92] Winkler, F. *Polynomial Algorithms in Computer Algebra*. Texts and Monographs in Symbolic Computation. Springer-Verlag, 1996.

[93] Xuejun, L., Jiaguang, S., and Changgui, Y. Extracting silhouette curves of NURBS surfaces by tracing silhouette points. *Tsinghua Science and Technology 3*, 2 (1998), 1005–1008.

[94] Zhou, P., and Qian, W.-H. Blending multiple parametric normal ringed surfaces using implicit functional splines and auxiliary spheres. *Graphical Models 73*, 4 (2011), 87 – 96.

List of publications

Publications in journals with impact factor

- Bastl, B., Bizzarri, M., Krajnc, M., Lávička, M., Slabá, K., Šír, Z., Vitrih, V., and Žagar, E. C^1 Hermite interpolation with spatial Pythagorean-hodograph cubic biarcs. *Journal of Computational and Applied Mathematics 257*, (2014), 65 – 78.
- Bizzarri, M., and Lávička, M. A symbolic-numerical approach to approximate parameterizations of space curves using graphs of critical points. *Journal of Computational and Applied Mathematics 242*, (2013), 107 – 124.
- Bizzarri, M., and Lávička, M. Parameterizing rational offset canal surfaces via rational contour curves. *Computer-Aided Design 45*, 2 (2013), 342 – 350.
- Bizzarri, M., and Lávička, M. A symbolic-numerical method for computing approximate parameterizations of canal surfaces. *Computer-Aided Design 44*, 9 (2012), 846 – 857.

Publications in journals (without impact factor) indexed on Scopus

- Bizzarri, M., and Lávička, M. Approximation of implicit blends by canal surfaces of low parameterization degree. In *Mathematical Methods for Curves and Surfaces*, vol. 8177 of *Lecture Notes in Computer Science*. Springer Berlin Heidelberg, 2014, 34 – 48.
- Bizzarri, M., and Lávička, M. Algorithm for the Parameterization of Rational Curves Revisited. *Journal for Geometry and Graphics 15*, (2011), 1 – 18.
- Bizzarri, M., and Lávička, M. A note on the rational parameterization of algebraic curves in Mathematica. *Journal of Interdisciplinary Mathematics 12*, (2009), 293 – 317.

Other publications

- Bizzarri, M., and Lávička, M. On Canal Surfaces with Polynomial MATs and Rational Contour Curves. In *Proceedings of the 33nd Conference on Geometry and Graphics*, (2013).
- Bizzarri, M., and Lávička, M. On Computing Approximate Parameterizations Of Algebraic Surfaces. *Journal of Applied Mathematics*, (2012), 347 – 357.
- Bizzarri, M., and Lávička, M. Rational approximation of implicit blends of canal-surface-type. In *Proceedings of the 32nd Conference on Geometry and Graphics*, (2012).
- Bizzarri, M., and Lávička, M. Symbolic Algorithm For Computing Approximate Parameterizations Over Rationals. *Journal of Applied Mathematics*, (2011), 629 – 638.
- Bizzarri, M., and Lávička, M. Approximate parameterizations of space algebraic curves. In *Proceedings of the 31nd Conference on Geometry and Graphics*, (2011).

Submitted papers

- Bastl, B., Bizzarri, M., Kovač, B., Krajnc, M., Lávička, M., Počkaj, K., Slabá, K., Šír, Z., and Žagar, E. C^2 Hermite interpolation by Pythagorean-hodograph quintic triarcs. Submitted to *Computer Aided Geometric Design*, (2014).
- Bizzarri, M., and Lávička, M. On modelling with rational ringed surfaces. Submitted to *Computer-Aided Design*, (2014).
- Bizzarri, M., Lávička, M., and Vršek, J. Canal surfaces with rational contour curves and blends bypassing the obstacles. Submitted to *Computer-Aided Design*, (2014).